

**Best Available  
Copy  
for all Pictures**

AD/A-003 408

INTEGRATED OPTICS

HUGHES RESEARCH LABORATORIES

PREPARED FOR

AIR FORCE CAMBRIDGE RESEARCH LABORATORIES

DEFENSE ADVANCED RESEARCH PROJECTS AGENCY

OCTOBER 1974

DISTRIBUTED BY:

**NTIS**

National Technical Information Service  
U. S. DEPARTMENT OF COMMERCE

ARPA Order No. 2074

Program Code No. 2D10

Contractor: Hughes Research Laboratories

Effective Date of Contract, 1 June 1972

Contract F19628-72-C-0322

Principal Investigator and Telephone No.

G. Sanjiv Kamath, (213) 456-6411, Ext. 210

Amnon Yariv, (213) 795-6841

AFCRL Project Scientist and Telephone No.

Dr. Freeman D. Shepherd, Jr. (617) 861-2225

Contract Expiration Date: 30 August 1974

ACCESSION for	
NTIS	Write Section <input checked="" type="checkbox"/>
DGC	Self Section <input type="checkbox"/>
UNANNOUNCED	<input type="checkbox"/>
JUSTIFICATION .....	
BY .....	
DISTRIBUTION/AVAILABILITY CODES	
Dist.	APPROL. and/or SPECIAL
A	

Qualified requesters may obtain additional copies from the Defense Documentation Center. All others should apply to the National Technical Information Service.

UNCLASSIFIED

SECURITY CLASSIFICATION OF THIS PAGE (When Data Entered)

AD/A 003 408

REPORT DOCUMENTATION PAGE		READ INSTRUCTIONS BEFORE COMPLETING FORM
1. REPORT NUMBER AFCRL-TR-74-0542	2. GOVT ACCESSION NO.	3. RECIPIENT'S CATALOG NUMBER
4. TITLE (and Subtitle) INTEGRATED OPTICS		5. TYPE OF REPORT & PERIOD COVERED Final Technical Report 1 June 1972-30 August 1974
		6. PERFORMING ORG. REPORT NUMBER
7. AUTHOR(s) G. Sanjiv Kamath Michael Barnoski Amnon Yariv Steven Jensen R.G. Hunsperger Viktor Evtuhov		8. CONTRACT OR GRANT NUMBER(s) F19628-72-C-0322
9. PERFORMING ORGANIZATION NAME AND ADDRESS Hughes Research Laboratories 3011 Malibu Canyon Road Malibu, California 90265		10. PROGRAM ELEMENT, PROJECT, TASK AREA & WORK UNIT NUMBERS 2074-N/A-N/A 61101D
11. CONTROLLING OFFICE NAME AND ADDRESS Air Force Cambridge Research Laboratories Hanscom AFB, Massachusetts 01731 Contract Monitor: F.D. Shepherd/LQD		12. REPORT DATE October 1974
		13. NUMBER OF PAGES 157
14. MONITORING AGENCY NAME & ADDRESS (if different from Controlling Office)		15. SECURITY CLASS. (of this report) Unclassified
		15a. DECLASSIFICATION DOWNGRADING SCHEDULE
16. DISTRIBUTION STATEMENT (of this Report) Approved for public release; distribution unlimited.		
17. DISTRIBUTION STATEMENT (of the abstract entered in Block 20, if different from Report) PRICES SUBJECT TO CHANGE		
18. SUPPLEMENTARY NOTES This research was sponsored by Defense Advanced Research Projects Agency, ARPA Order No. 2074.		
19. KEY WORDS (Continue on reverse side if necessary and identify by block number) Integrated Optics, $\text{Ga}_{(1-x)}\text{Al}_x\text{As}$ , Epitaxy, Optical Waveguides		
20. ABSTRACT (Continue on reverse side if necessary and identify by block number) The objectives of this program were to study and analyze the propagation, attenuation, modulation, and detection of coherent optical waves in thin film waveguides, in particular, epitaxial semiconductor structures at a wavelength of 8500 Å, to determine the parameters controlling the solution regrowth epitaxy of the $\text{Ga}_{(1-x)}\text{Al}_x\text{As}$ system to study the influence of the index discontinuity and semiconductor carrier concentration on optical properties, and to develop the elementary optical device elements. Early		

DD FORM 1473

JAN 73

EDITION OF 1 NOV 65 IS OBSOLETE

UNCLASSIFIED

SECURITY CLASSIFICATION OF THIS PAGE (When Data Entered)

UNCLASSIFIED

SECURITY CLASSIFICATION OF THIS PAGE(When Data Entered)

in the program we conducted theoretical and experimental studies to define the epilayer material and structure requirements for factors affecting waveguiding. It was determined from theoretical projections that the absolute Al concentration required to keep band-to-band absorption loss less than 3 dB/cm ranges from  $x \sim 40\%$  for light of wavelength  $\lambda = 0.85 \mu\text{m}$  to  $x \sim 20\%$  for  $\lambda = 1 \mu\text{m}$ . The accuracy of these projected values was later supported by experimental measurements of loss = 0.7 dB/cm at  $\lambda = 1.15 \mu\text{m}$  in  $\text{Ga}_{(1-x)}\text{Al}_x\text{As}$  waveguides with  $x \sim 30\%$ . It was also shown that an Al concentration difference between the guiding layer and the substrate of  $1.5\% \leq \Delta x \leq 3.5\%$  is required for single mode waveguides of thickness  $1.25 \mu\text{m}$  to  $2.5 \mu\text{m}$  for light of  $\lambda \approx 0.9 \mu\text{m}$ . Materials growth techniques were developed to produce  $\text{Ga}_{(1-x)}\text{Al}_x\text{As}$  layers meeting the various requirements. Single and double layer  $\text{Ga}_{(1-x)}\text{Al}_x\text{As}$  waveguides were epitaxially grown using both the limited melt, slidebar method and the infinite melt technique of liquid epitaxy. These waveguides were evaluated, and optimized waveguiding layers were grown. Losses in typical waveguides at  $\lambda = 1.15 \mu\text{m}$  were generally  $< 3 \text{ dB/cm}$ , and in the best samples were equal to 0.7 dB/cm (with Al concentration  $x = 30\%$ ). Extrapolation predicts a corresponding loss at  $\lambda = 0.85 \mu\text{m}$  of 2.2 dB/cm in the best samples. Thus it has been demonstrated that  $\text{Ga}_{(1-x)}\text{Al}_x\text{As}$  waveguides can be epitaxially grown with acceptably low loss for use in optical integrated circuits. The limited melt slidebar method is most useful for growing double layers of  $\text{Ga}_{(1-x)}\text{Al}_x\text{As}$ . However the layers grown by the infinite melt technique are better in that they have lower carrier concentration and more uniform Al concentration. Infinite melt samples were also grown in large area ( $4 \text{ cm}^2$ ) configurations for possible use as substrates for integrated optics applications. In the final phase of the program we studied device elements for which GaAs and  $\text{Ga}_{(1-x)}\text{Al}_x\text{As}$  are particularly suitable. Theoretical analyses were made of "leaky" waveguides and of periodic waveguide structures for filters or DFB lasers. The results of these analyses indicated that useful integrated optics devices can be fabricated using leaky waveguides provided the guide height is  $\geq 10 \mu\text{m}$  for a  $\lambda \approx 0.8 \mu\text{m}$ . Another conclusion was that there is a frequency range for corrugated dielectric waveguides within which there is strong coupling between the forward and backward traveling waves. Thus corrugated waveguides can be used as reflectors for filters or DFB lasers. In addition to the theoretical device studies monolithic waveguide/detectors formed by proton bombardment of  $\text{Ga}_{(1-x)}\text{Al}_x\text{As}$  waveguides were fabricated and analyzed. Photocurrent of  $\sim 1 \mu\text{A}$  was observed at  $\lambda = 1.15 \mu\text{m}$  in a  $\text{Ga}_{(1-x)}\text{Al}_x\text{As}$  waveguide with  $x = 10\%$ , demonstrating that the proton bombardment technique can be used to produce detectors for longer-than-band gap-wavelength in  $\text{Ga}_{(1-x)}\text{Al}_x\text{As}$ .

The results described in this report demonstrate that  $\text{Ga}_{(1-x)}\text{Al}_x\text{As}$  epitaxy is a practical means of producing low loss waveguides for integrated optics and that monolithic device elements can also be produced on the wafer. However some additional work is needed to fully optimize waveguide structures, and much work is required to develop practical monolithic device elements for optical integrated circuits.

UNCLASSIFIED

SECURITY CLASSIFICATION OF THIS PAGE(When Data Entered)

## TABLE OF CONTENTS

I.	INTRODUCTION AND SUMMARY . . . . .	9
A.	Establishment of Epilayer Material and Structure Requirements . . . . .	9
B.	Development of Materials Growth Techniques . .	11
C.	Materials Evaluation . . . . .	15
D.	Device Analysis and Fabrication Techniques . .	17
II.	DEFINITION OF EPILAYER MATERIAL AND STRUCTURE REQUIREMENTS . . . . .	21
A.	Requirements on the Aluminum Concentration Difference Between Guide and Substrate . . . .	21
B.	Absolute Aluminum Concentration Requirements . . . . .	22
C.	Limits on (GaAl)As Epilayer Impurity Concentrations . . . . .	30
III.	MATERIALS GROWTH PHASE I — DEVELOPMENT OF GROWTH TECHNIQUES AND SYSTEMS. . . . .	35
A.	Vapor Epitaxy. . . . .	35
B.	Limited Melt Liquid Epitaxy. . . . .	39
C.	Infinite Melt Liquid Epitaxy . . . . .	63
IV.	MATERIALS GROWTH PHASE II — GROWTH AND EVALUATION OF EPITAXIAL LAYERS FOR OPTICAL INTEGRATED CIRCUITS. . . . .	73
A.	Limited Melt Liquid Epitaxy. . . . .	73
B.	Infinite Melt Liquid Epitaxy . . . . .	80
V.	MATERIALS GROWTH PHASE III — OPTIMIZATION. . . . .	91
A.	Limited Melt Liquid Epitaxy. . . . .	91
B.	Double Layers of (GaAl)As. . . . .	97

C.	Infinite Melt Liquid Epitaxy . . . . .	97
D.	The Two Liquid Epitaxial Techniques: A Critique . . . . .	100
VI.	OPTICAL WAVEGUIDE EVALUATION . . . . .	105
VII.	DEVICE ANALYSIS AND FABRICATION TECHNIQUES . . . . .	123
A.	Proton Implanted Waveguide/Detectors in GaAs and (GaAl)As. . . . .	123
B.	Analysis of "Leaky" Waveguides . . . . .	130
C.	Analysis of Propagation Characteristics of Periodic Dielectric Waveguides . . . . .	137
VIII.	CONCLUSION AND RECOMMENDATIONS . . . . .	153
	REFERENCES . . . . .	157
	APPENDICES . . . . .	159

## LIST OF ILLUSTRATIONS

Fig. No.

II-1	Al concentration difference for single-mode propagation . . . . .	23
II-2	Index of refraction of $Ga_{1-x}Al_xAs$ as a function of Al concentration . . . . .	24
II-3	Refractive index difference as a function of Al concentration difference between two layers of $Ga_{1-x}Al_xAs$ for two values of absolute Al concentration. . . . .	25
II-4	Guide thickness to wavelength ratio as a function of Al concentration between layer and substrate. . . . .	26
II-5	Interband absorption as a function of wavelength and Al concentration. . . . .	28
II-6	Absorption in the long wavelength tail of the GaAs band edge . . . . .	29
III-1	Cross-sectional view of wafer. . . . .	37
III-2	GaAl As epilayer as received . . . . .	38
III-3	GaAs vapor epilayer grown on GaAlAs. . . . .	38
III-4	Solubility limit of arsenic in gallium versus temperature . . . . .	41
III-5	Variation of Al concentration through the epilayer film versus film thickness for particular values of the parameter $W_{melt}/A$ . . . . .	44
III-6	Growth rate, $d\lambda/dT$ and percentage change of Al concentration for an incremental change in film thickness versus $W_{melt}/A$ . . . . .	46
III-7	Schematic diagram of horizontal liquid epilayer system growth . . . . .	48
III-8	Horizontal liquid epilayer growth system . . . . .	49
III-9	Photograph of the graphite slidebar in which the epitaxial growth occurs. . . . .	51

Fig. No.

III-10	Surface of a (GaAl)As film . . . . .	54
III-11	Deviation in surface flatness of the film shown in Fig. III-10 . . . . .	54
III-12	Photomicrograph of the cleaved edge of a double layer of (GaAl)As on GaAs . . . . .	55
III-13	Sample 0040. GaAs with Ga <sub>0.95</sub> Al <sub>0.05</sub> As epilayer . . . . .	59
III-14	Sample 0042. Ga <sub>0.95</sub> Al <sub>0.05</sub> As epilayer on GaAs. .	60
III-15	Ga <sub>0.95</sub> Al <sub>0.05</sub> As layer on GaAs . . . . .	61
III-16	Ga <sub>0.95</sub> Al <sub>0.05</sub> As layer on GaAs . . . . .	62
III-17	Ga <sub>0.95</sub> Al <sub>0.05</sub> As layer on GaAs . . . . .	62
III-18	Reactor for liquid epitaxy . . . . .	67
III-19	Ga <sub>0.95</sub> Al <sub>0.95</sub> As layer grown by the infinite melt method . . . . .	70
III-20	Ga <sub>0.95</sub> Al <sub>0.95</sub> As grown by infinite melt method . .	71
IV-1	Limited melt liquid epi sample No. 122 . . . . .	75
IV-2	Electron microprobe profile of epitaxial layer surface - limited melt slide bar . . . . .	78
IV-3	Aluminum concentration profile in limited melt epitaxial layer on a 1° bevel in cross section. . . . .	79
IV-4	Waveguided light in a (GaAl)As layer with graded aluminum concentration. . . . .	81
IV-5	A double layer of Ga <sub>1-y</sub> Al <sub>y</sub> As/Ga <sub>1-x</sub> Al <sub>x</sub> As grown on GaAs. . . . .	82
IV-6	Aluminum concentration profile on ∞ melt LEPI layers (surface of epilayer). . . . .	87
IV-7	Aluminum concentration profile in ∞ melt liquid epitaxial layers on a 3° bevel in cross section (LEPI No. 41). . . . .	88

Fig. No.

V-1	Al concentration profile of graded (GaAl)As waveguide sample (0147) . . . . .	95
V-2	Al concentration profile of graded (GaAl)As waveguide sample (0175) . . . . .	96
V-3	Al concentration profile in double layer waveguide sample (0171) . . . . .	99
VI-1	Experimental setup for waveguide alignment and optical measurements. . . . .	106
VI-2	Experimental setup for laser/waveguide alignment and optical measurements. . . . .	107
VI-3	Waveguided light in a graded (GaAl)As layer . . . . .	109
VI-4	Micrometer adjusted alignment fixtures. . . . .	110
VI-5	Optical transmission of (GaAl)As waveguides from sample (0175). . . . .	111
VI-6	Index of refraction in (GaAl)As waveguide, sample (0147) . . . . .	113
VI-7	Index of refraction in (GaAl)As waveguide, sample (0175) . . . . .	114
VI-8	Experimentally determined mode profile for sample 0147 . . . . .	116
VI-9	Experimentally determined mode profile for sample 0175 . . . . .	117
VI-10	Index of refraction in (GaAl)As waveguide, sample 0171 . . . . .	120
VI-11	Optical mode profile for (GaAl)As layer grown by infinite melt technique. . . . .	121
VII-1	Proton-implanted integrated optical detector device geometry . . . . .	124

Fig. No.

VII-2	Principle of operation of integrated optical detector: upon the application of a reverse bias (V) electrons liberated by transitions labeled A and B are swept out of depletion layer d resulting in the flow of current . . .	126
VII-3	Diagram of double layer waveguide structure. .	132
VII-4	Schematic of thin film dielectric waveguide with a sinusoidal corrugation on one side of a guide . . . . .	138
VII-5	Asymptotic lines of dispersion diagram . . . .	141
VII-6	Dispersion diagrams for a corrugated and an uncorrugated waveguide. . . . .	142
VII-7	Enlarged dispersion diagram at the vicinity of a forbidden gap (TM mode) . . . . .	143
VII-8	(a) Unperturbed waveguide. (b) Waveguide with square wave perturbation. . . . .	145
VII-9	Normalized mode power flowing in the +z direction, and in the -z direction, as a function of z. . . . .	149
VII-10	Dispersion diagram for periodically perturbed waveguide in the region of the forbidden optical gap. . . . .	151
VII-11	The transmission and reflection characteristics of a corrugated section of length L as a function of $\Delta \cdot L$ drawn for $\kappa L = 1.84$ . . . . .	152

## I. INTRODUCTION AND SUMMARY

The objectives of this contract were to study and analyze the propagation, attenuation, modulation, and detection of coherent optical waves in thin film waveguides, in particular, epitaxial semiconductor structures at a wavelength of  $8500 \text{ \AA}$ , to determine the parameters controlling the solution regrowth epitaxy of the  $\text{Ga}_{1-x}\text{Al}_x\text{As}$  system, to study the influence of the index discontinuity and semiconductor carrier concentration on optical properties, and to develop the elementary optical device elements.

This final report covers the work accomplished during the entire contract period from 1 June 1972 to 31 July 1974.

The program may be viewed as consisting of four elements: (1) definition of epilayer material and structure requirements, (2) development of materials growth techniques, (3) materials evaluation, and (4) device analysis and fabrication techniques.

The work relating to elements (2) and (3) can be conveniently considered in three phases: (1) development of growth techniques and systems, substantially accomplished in the period prior to August 1973, (2) growth and evaluation of epitaxial layers for optical integrated circuits, August 1973 to January 1974, and (3) optimization, during the final seven months of the program.

### A. Definition of Epilayer Material and Structure Requirements

Consideration has been given to primarily three factors affecting waveguiding: absolute aluminum concentration required to minimize band-to-band absorption at various wavelengths, difference in aluminum concentration between the guiding layer and the substrate required to achieve single mode propagation, and free carrier absorption and its effect on propagation losses. The absolute level of aluminum concentration in the guiding layer was estimated by considering the spectral location and shape of the  $\text{Ga}_{1-x}\text{Al}_x\text{As}$  absorption edge as a function of aluminum concentration and assuming a value

for maximum allowable absorption due to interband transitions at wavelengths in the range  $1\text{ }\mu\text{m}$  to  $0.85\text{ }\mu\text{m}$ . Curves of  $\alpha$  versus wavelength for  $\text{Ga}_{(1-x)}\text{Al}_x\text{As}$  were plotted by taking available data for the GaAs absorption edge and shifting the edge to correspond to a particular  $x$  value. In this manner the ranges of absolute aluminum concentration have been computed to be  $x \sim 4\%$  to  $21\%$  (minimum) for the substrate and  $x \sim 0\%$  to  $17\%$  minimum for the guiding layer, depending on the source wavelength to be used, and assuming a maximum acceptable loss of  $\alpha = 2\text{ cm}^{-1}$  or  $8.6\text{ dB/cm}$ . Alternatively, if one assumes that the maximum acceptable loss is  $3\text{ dB/cm}$  or  $\alpha = 0.7\text{ cm}^{-1}$  the ranges of absolute aluminum concentration are  $x \sim 16\%$  to  $36\%$  for the substrate and  $x \sim 20\%$  to  $40\%$  for the guiding layer. It should be noted that the requirements that have been defined for the epitaxial layer are minimum requirements for single mode propagation with interband absorption losses less than some chosen level, which in practice would depend on the particular application. However, a loss of  $3\text{ dB/cm}$  is certainly acceptable for many applications employing a wafer size  $\sim 1$  or  $2\text{ cm}$ . Actual waveguides fabricated under this contract have exhibited total optical losses as low as  $\alpha = 0.17\text{ cm}^{-1}$  or  $0.7\text{ dB/cm}$  at  $\lambda = 1.15\text{ }\mu\text{m}$ . (Aluminum concentration in these samples was  $x = 30\%$ .) Extrapolation of these data to  $\lambda = 0.85\text{ }\mu\text{m}$  predicts a corresponding loss of  $2.2\text{ dB/cm}$ . This result is to be compared with the theoretically projected value for absorption loss, which is  $3.8\text{ dB/cm}$ . The comparison suggests that our projections of absorption loss in  $(\text{GaAl})\text{As}$  are conservatively large.

The aluminum concentration difference between the guiding layer and the substrate required for single mode propagation was determined by using the Sellmeier equation to relate the indices of refraction to the values of  $x$  for  $\text{Ga}_{1-x}\text{Al}_x\text{As}$  and substituting those results into the expressions for the threshold of propagation of the first and second order modes. By this procedure we determined that an aluminum concentration difference between the guiding layer and the substrate of  $1.5\% \leq \Delta x \leq 3.5\%$  is required for single mode waveguides of thickness  $1.25\text{ }\mu\text{m}$  to  $2.5\text{ }\mu\text{m}$  for light of  $\lambda \approx 0.9\text{ }\mu\text{m}$ .

Theoretical estimates of the expected free carrier absorption losses in thin film semiconductor waveguides have been made in order to determine the allowable free carrier concentration. The result for GaAs is that the theoretical attenuation constant is given by

$$\alpha = (7.7 \times 10^{-19} N) \text{ cm}^{-1}$$

where  $N$  is the maximum carrier concentration in the structure (substrate or epitaxial layer). However, experimental data suggest that this is a very optimistic estimate and a more realistic value is

$$\alpha \approx (5 \times 10^{-18} N) \text{ cm}^{-1}$$

Assuming that free carrier absorption losses of  $\alpha \leq 0.5 \text{ cm}^{-1}$  can be tolerated, we have obtained a criterion on the maximum allowable carrier concentration:

$$N < 10^{17} \text{ cm}^{-3} .$$

Experimental results described in this report show that carrier concentrations  $\leq 1 \times 10^{16} / \text{cm}^3$  can be repeatably produced in epitaxial layers grown by both the limited melt and infinite melt methods. Thus the above criterion can be met easily, and, in fact, exceeded to produce layers with free carrier absorption loss  $\alpha \leq 0.1 \text{ cm}^{-1}$ .

#### B. Development of Materials Growth Techniques

The program in materials growth can best be considered in three phases: (1) prior to August 1973, (2) August 1973 to January 1974, and (3) January 1974 to present.

During the first phase of the program we evaluated three different possible approaches to the growth of epitaxial layers of III V compounds for waveguide fabrication. These were vapor phase epitaxy and two solution growth techniques — limited melt graphite slide bar, and infinite melt. We were able to grow GaAs layers on (GaAl)As substrates using the vapor growth method and show that

these would waveguide. However the source of (GaAl)As substrates was found unreliable and the vapor growth of GaAs layers on (GaAl)As substrates poses severe problems because of the reactivity of aluminum. As a consequence, we decided to concentrate on the two liquid epitaxial techniques for the remainder of this program, especially since the ternary system offered the attractive option of varying the bandgap as well as the refractive index.

The crystal growth equipment was modified to grow epitaxial layers of (GaAl)As. This included the design of various graphite boats for the limited melt technique, as well as the choice of a suitable crucible material for the infinite melt. The growth chambers had to be tested afresh to eliminate all possible leaks, since the highly reactive aluminum would tend to form an oxide even in the presence of traces of oxygen or water vapor.

By August 1973 we had succeeded in growing a series of layers using the limited melt epitaxy and established the kinetics of growth. Correlation of the parameters of the starting solution, the growth temperature cycle and the layer grown were established. Layers of (GaAl)As with varying concentrations of Al were grown using the infinite melt technique. The layers were characterized and shown to be better than those from the limited melt, since they had lower carrier concentration ( $\sim 10^{14}$  or  $10^{15}/\text{cm}^2$  as compared to  $\sim 10^{16}/\text{cm}^3$ ) and higher mobility (typically  $> 4000 \text{ cm}^2/\text{V-s}$ ). They were also grown in large-area configurations ( $\sim 4 \text{ cm}^2$ ) for possible use as substrates for integrated optics applications.

The second phase covering August 1973 to January 1974 was devoted mainly to accumulating data on epitaxial layers both from the materials characterization and from the waveguide data. A significant achievement during this period was the progressive improvement of our understanding of the relationship between the layer growth parameters (such as the temperature cycle for growth, the surface preparation prior to epitaxy, and the role of supersaturation of the source melt) and the heterojunction characteristics. By studying the electron microprobe data on aluminum concentration in the epi layer,

we were able to optimize the growth parameters to produce a series of layers with aluminum concentrations ranging from 0 to 20% (atomic) in aluminum. Reproducibility of aluminum concentration from day to day was better than  $\pm 10\%$  of the desired value. Microprobe measurements of aluminum concentration profiles indicated that variation across the surface of the samples was generally within  $\pm 2$  to  $3\%$  of the nominal value and variation with depth from the surface was less than  $1\%$  for infinite melt grown layers as thick as  $50\text{ }\mu\text{m}$ . Limited melt grown samples exhibited surface variations of  $\pm 6\%$  and variation with depth less than  $5\%$  for thicknesses of 2 to  $3\text{ }\mu\text{m}$ . Thicker limited melt layers ( $\sim 5$  to  $10\text{ }\mu\text{m}$ ) had a variation of 10 to  $20\%$ . In parallel with achieving this control over composition, we also optimized the processing of the substrates to yield good, even heterojunctions and surfaces to permit efficient optical waveguiding. At the end of the second phase we were in a position to produce (GaAl)As epitaxial layers with attenuation coefficients of approximately  $1\text{ cm}^{-1}$  matching the state of the art in the literature.

In the third phase of the program we have succeeded in fine-tuning the epitaxial layer growth techniques to improve layer perfection and aluminum profile control to reduce the attenuation to less than  $0.2\text{ cm}^{-1}$  and produce large area layers that provide waveguides of larger dimensions to permit optical loss measurements to be made more accurately. For example, we have cleaved waveguides of length  $> 1\text{ cm}$  from samples that were  $1\text{ cm} \times 2\text{ cm}$  in size.

The major emphasis during the last seven months has been on improving the limited melt techniques. Three growth temperatures we have investigated to grow the (GaAl)As layers are  $880^{\circ}\text{C}$ ,  $840^{\circ}\text{C}$ , and  $800^{\circ}\text{C}$ .

It has been determined that the rate of the growth of the layer increases at the higher temperature and the aluminum concentration in the layer goes down. The aluminum concentration is affected by the segregation coefficient of aluminum from a gallium solution; the coefficient decreases between  $800^{\circ}$  and  $880^{\circ}$ , so that at the higher temperature the layers are  $\sim 50\%$  lower in aluminum concentration when the growth solutions have the same concentrations. The lower

temperature of growth has some advantages. First, the growth rates are slow and all reactivities, including that of Al, are lower; hence problems due to low level ambient impurities in the growth system are reduced. Second, spurious nucleation and dendritic growth in and around the substrates caused by high energy nucleation sites is reduced. As a result, the epitaxial growth can be restricted to the substrate. Because of these advantages, we have preferred to do most of our recent work at the low temperature.

Early in this optimization phase of our program we observed waveguiding in single layers of (GaAl)As grown on GaAs. Since they were grown on GaAs which has a higher refractive index, we had to assume that the confinement of the wave was due to the high aluminum concentration at the heterojunction. Therefore, we began a detailed investigation of the aluminum concentration in the cross section of the grown layer using the electron microprobe, paying particular attention to the concentration in the region of the GaAs-(GaAl)As interface. To observe the profile in detail, the layer was beveled at a  $1^{\circ}$  angle. The bevel was examined using an electron beam so that each step was effectively  $0.2 \mu\text{m}$  in layer cross section. These microprobe measurements have revealed that the aluminum concentration in the epilayer is graded with a peak occurring at the GaAs-(GaAl)As interface. Thus the layers are capable of optical waveguiding.

Since a single layer of (GaAl)As was sufficient to permit waveguiding, most of the waveguide experiments described in this report were conducted using single layers. However, we felt it would be desirable to grow some double layers with the second layer having higher aluminum concentration than the first. Such a procedure should permit the confinement of the wave between the high aluminum concentration region at the GaAs-(GaAl)As interface described before and the lower refractive index-high aluminum concentration top layer. We have determined that, when properly made, the top GaAs-(GaAl)As interface provides a better confining surface than a (GaAl)As-air interface leading to lower optical loss because of reduced scattering of light at the upper surface of the waveguiding layer.

Large area (GaAl)As layers of  $>4 \text{ cm}^2$  have been grown by the infinite melt liquid epitaxy technique with aluminum concentrations up to  $x \leq 0.5$  for integrated optics applications. The long range goal is to use these for substrates for monolithic integrated circuits. The quality and characteristics of the layers have been found to be eminently suitable for this application. Since the single layers grown by limited melt slide bar technique were found to be suitable for waveguiding, we felt it would be desirable to try similar experiments with out infinite melt layers. Cleaved pieces of the layers were fabricated accordingly. It has been shown that they are capable of guiding. This suggests new approaches which may simplify the technology for producing integrated optics devices in some cases. It may be unnecessary to grow a second layer of  $\text{Ga}_{(1-y)}\text{Al}_y\text{As}$  on a layer of a different Al concentration  $\text{Ga}_{(1-x)}\text{Al}_x\text{As}$  for several simple device assemblies. Instead by using alternative techniques of etching, masking, diffusion and ion implantation presently available, simple circuit assemblies can be fabricated on single layers of (GaAl)As that are easily grown by our infinite melt technique on GaAs substrates.

In summary we have grown (GaAl)As layers of GaAs by both limited melt and infinite melt epitaxy and demonstrated that both methods are capable of producing layers of adequate quality for integrated optics application. Single layers of (GaAl)As grown on GaAs are shown to provide good confinement and hence act as waveguides with acceptable characteristics for use in device fabrication, and a model has been postulated to explain the confinement in a single layer of (GaAl)As grown on GaAs.

### C. Materials Evaluation

In parallel with the growth programs we also developed characterization techniques such as Hall measurements of carrier concentration and mobility, and electron microprobe and photoluminescence measurements to determine aluminum concentration profiles; we also developed etching and processing techniques to allow us to study the layers and interfaces by optical examination to determine their crystal characteristics.

These measurements of the chemical and electrical properties of (GaAl)As layers grown under this program have demonstrated that the layers have aluminum concentration profiles and low carrier concentrations as desired for optical waveguides. However, the final test of their suitability lies in actually using them as waveguides for light of the desired wavelength. Therefore, the optical waveguiding properties of (GaAl)As layers grown under this program have been measured and evaluated with respect to mode shape and attenuation. Optical mode shape and attenuation have been measured for waveguides with a variety of thicknesses, produced by both the limited melt and the infinite melt methods. We have observed mode profiles of both the single mode and multimode types, depending on layer thickness and aluminum concentration profile. A theoretical model has been developed to describe the mode shape of light propagating in these layers with graded aluminum concentration. Measurements of optical attenuation in various samples have confirmed that loss is reduced when Al concentration is increased. For samples with aluminum concentration of 15% (atomic) the loss coefficient was measured to be  $\alpha = 0.17 \text{ cm}^{-1}$  or 0.7 dB/cm at a wavelength of 1.15  $\mu\text{m}$ . This value is close to the limit imposed by free carrier absorption for carrier concentration  $\approx 10^{16} / \text{cm}^3$ . It is significantly better (by a factor  $\approx 5$ ) than losses at  $\lambda = 1.15 \text{ } \mu\text{m}$  previously reported in the literature for semiconductor waveguides made by any means. Extrapolation predicts a corresponding loss at  $\lambda = 0.85 \text{ } \mu\text{m}$  of  $\alpha = 0.51 \text{ cm}^{-1}$  or 2.2 dB/cm. The fact that such low loss waveguides can be made by growing only a single layer of (GaAl)As on a GaAs substrate is highly significant with respect to the feasibility of making monolithic optical integrated circuits in the (GaAl)As system. The results of our work on these waveguides are described in a paper, "Low Loss Waveguides in Single Layers of  $\text{Ga}_{1-x}\text{Al}_x\text{As}$ ," by S. M. Jensen, M. K. Barnoski, R. G. Hunsperger, and G. S. Kamath, which will shortly be submitted for publication in the Journal of the Optical Society of America.

Loss coefficients were  $\leq 1 \text{ cm}^{-1}$  in most of the waveguiding layers that were evaluated. However,  $\alpha \sim 5$  to  $10 \text{ cm}^{-1}$  was measured in some samples. The major reason for the greater loss in these

samples was that they had an overgrowth while the low-loss samples did not. This overgrowth is an additional graded layer, several microns thick, caused by a fast freeze of refined melt due to insufficient wiping. Additional loss is introduced by the overgrowth layer because it reduces the index of refraction difference at the interface with the guiding layer from what it would be for air allowing light to penetrate into the rough, spotty, lossy overgrowth. The effect of the overgrowth was clearly demonstrated in the case of one sample which was only partially covered by an overgrowth. In the region which had no overgrowth losses were measured to be  $\alpha = 0.5 \text{ cm}^{-1}$ , while in the region where the overgrowth was present, losses were increased to  $\alpha = 5.0 \text{ cm}^{-1}$ . By eliminating the overgrowth problems and improving surface quality, low loss waveguides can be fabricated consistently.

#### D. Device Analysis and Fabrication Techniques

As part of the program of research and development under this contract we have considered device elements for which GaAs and  $\text{Ga}_{1-x}\text{Al}_x\text{As}$  are particularly suitable with the goal of establishing the relationship between device requirements and material and structure characteristics. Such components as waveguide bends and couplers, distributed feedback injection lasers, integrated detectors, modulators, and periodic optical filters have been considered. Optical filters have been analyzed theoretically. Computer results for the dispersion diagram of a periodically corrugated dielectric waveguide with typical parameters have been obtained. The behavior of the waveguide near the important Bragg regime, where the corrugation period is equal to one-half wavelength, was studied in detail. Periodic optical structures are expected to play an important role in applications such as optical filters, grating air-waveguide couplers, directional couplers, and distributed feedback lasers.

A theoretical analysis has also been made of the properties of "leaky" waveguides, or layers in which the index of refraction is lower in the guide than it is in the substrate. The results of this

analysis indicate that useful integrated optics devices can be fabricated using leaky waveguides provided the guide height is  $t \gtrsim 10 \mu\text{m}$  for a wavelength of  $\lambda = 0.8 \mu\text{m}$ . The losses due to leaks become  $< 1 \text{ cm}^{-1}$  for aluminum concentrations  $> 10\%$  (atomic).

Another device that we have paid particular attention to is the integrated waveguide/detector. A company-funded program to develop a method for forming integrated waveguide/detectors in GaAs has produced encouraging preliminary results. Proton bombardment has been used to create the required absorbing centers in the detector volume. Detectors have been fabricated with a quantum efficiency of 17% and a pulse response time less than 200 ns, and it is felt that further development of the technique will yield devices with significantly improved characteristics. We have performed a theoretical analysis of the proton implanted detector under this contract which indicates that the same basic fabrication methods used in GaAs should be applicable to (GaAl)As. Projections based on the GaAs data indicate that a (GaAl)As waveguide/detector operating at  $\lambda = 9000 \text{ \AA}$  with a GaAs LED or laser source is feasible. If a  $\text{Ga}_{0.93}\text{Al}_{0.07}\text{As}$  waveguide is used and the carrier concentration in the waveguide is  $\leq 1 \times 10^{16} / \text{cm}^3$  so that the detector volume can be completely depleted by the reverse biased Schottky diode, the estimated internal quantum efficiency is at least 60%.

In the final months of the contract period the proton bombardment technique was used for the first time to fabricate an integrated waveguide detector in a (GaAl)As single-layer waveguide. The Waveguide was a single layer of (GaAl)As on a silicon-doped GaAs substrate. The guiding layer had an aluminum concentration of 5% (atomic) and a thickness of  $13 \mu\text{m}$ . Optical loss measurements made on waveguides cleaved from the sample prior to proton bombardment indicated an absorption coefficient at  $\lambda = 1.15 \mu\text{m}$  of  $\alpha \approx 0.2 \text{ cm}^{-1}$ . A 3 mm long waveguide cleaved from this sample was bombarded over one third of its length with a dose of  $1 \times 10^{15} / \text{cm}^2$ , 300 keV protons. This bombardment produced a factor of 10 increase in absorption ( $\alpha = 2 \text{ cm}^{-1}$  at  $1.15 \mu\text{m}$ ) as compared to the loss observed in the nonbombarded region.

A Schottky barrier contact was formed on the surface of the bombarded region to form an integral waveguide/detector diode. When the device was reverse biased with a dc voltage of 20 V, and light from a He-Ne laser was focused onto the cleaved end face of the waveguide nearest the proton bombarded region a photocurrent  $\sim 1 \mu\text{A}$  was produced. Since the magnitude of the coupling loss at the cleaved end face is not known, it is impossible to determine a quantum efficiency for the device from these experiments. (The measurement of coupling loss is straightforward but was not performed for lack of time.) However, they have served to demonstrate that proton bombardment can be used to produce a monolithically coupled waveguide/detector in (GaAl)As as well as GaAs.

#### E. Report Organization

In the following sections of this report we describe the details of what has been summarized in the preceding paragraphs. The definition of epilayer material and structural requirements is presented in Section II. Sections III, IV, and V describe the three phases of the materials growth program — development of growth techniques, growth and evaluation of epitaxial layers for optical integrated circuits, and optimization. Optical waveguide evaluation is detailed in Section VI. Device analysis and fabrication techniques are described in Section VII. Finally, we summarize our conclusions and make recommendations for further study and applications in Section VIII.

## II. DEFINITION OF EPI-LAYER MATERIAL AND STRUCTURE REQUIREMENTS

Work on the establishment of the basic requirements imposed by the need to achieve efficient propagation in waveguides was performed under this contract. In the course of the program consideration was given to primarily three factors affecting waveguiding: free carrier absorption and its effect on propagation losses, difference in aluminum concentration between the guiding layer and the substrate required to achieve single mode propagation, and absolute aluminum concentration required to minimize band-to-band absorption at various wavelengths. The approximate ranges of absolute aluminum concentration for the substrate and the guiding layer for various source wavelengths also have been computed using the data available to date.

### A. Requirements on the Aluminum Concentration Difference Between Guide and Substrate

The aluminum concentration difference between the guiding layer and the substrate required for single mode propagation can be determined in a straightforward but somewhat approximate fashion by ignoring the slight nonlinearity in the dependence of the refractive index on aluminum concentration. We assumed in these calculations the following relationship between layer-substrate index difference ( $n_2 - n_3$ ) and aluminum concentration difference ( $\Delta x$ ):  $n_2 - n_3 \approx 0.4 \Delta x$ , where  $n_2$  and  $n_3$  are the guiding layer and the substrate indices of refraction, respectively. This approximate expression for  $\Delta x$  was empirically deduced from data available for (GaAl)As close confinement injection lasers.

The approximate condition for propagation of the first  $m$  modes at wavelength  $\lambda_0$  in a waveguide of height  $t$  is

$$(n_2^2 - n_3^2) \geq \left[ \frac{(2m - 1) \lambda_0}{4t} \right]^2, \quad m = 1, 2, 3, \dots$$

Relating  $(n_2 - n_3)$  to aluminum concentration difference  $\Delta x$  yields the condition for lowest order mode propagation

$$\frac{11.25}{n} \left( \frac{\lambda_0}{4t} \right)^2 > \Delta x > \frac{1.25}{n} \left( \frac{\lambda_0}{4t} \right)^2 ,$$

where  $n = (1/2)(n_2 + n_3)$ . This relation can be used to plot the curves of Fig. II-1, which give the ranges of guiding film thickness and aluminum concentration difference allowed for single mode propagation.

A more accurate calculation of the relationship between the film thickness and the aluminum concentration difference has also been performed. In this calculation the Sellmeier equation<sup>1</sup> was used to estimate the refractive indices of  $\text{Ga}_{1-x}\text{Al}_x\text{As}$  for different values of  $x$ :

$$n(x) = A + \frac{B}{\lambda_0^2 - C(x)} - D(x) \lambda_0^2 .$$

The coefficients A, B, C, and D are given in Table II-1. A plot of the refractive index as a function of  $x$  is shown in Fig. II-2; the change in refractive index  $\Delta n = n_2 - n_3$  is shown in Fig. II-3. The ratio of thickness to wavelength for the first two modes of the waveguide structure is plotted in Fig. II-4 as a function of concentration difference  $\Delta x$  between the guide and the substrate for guiding epilayer concentrations of  $x = 0$  and  $x = 0.20$ . It is seen that although the guide thickness is dependent primarily on aluminum concentration difference  $\Delta x$ , some dependence on the absolute aluminum concentration is exhibited.

#### B. Absolute Aluminum Concentration Requirements

The absolute level of aluminum concentration in the guiding layer was estimated by considering the spectral location and shape of the  $\text{Ga}_{1-x}\text{Al}_x\text{As}$  absorption edge as a function of aluminum concentration and assuming a value for maximum allowable absorption

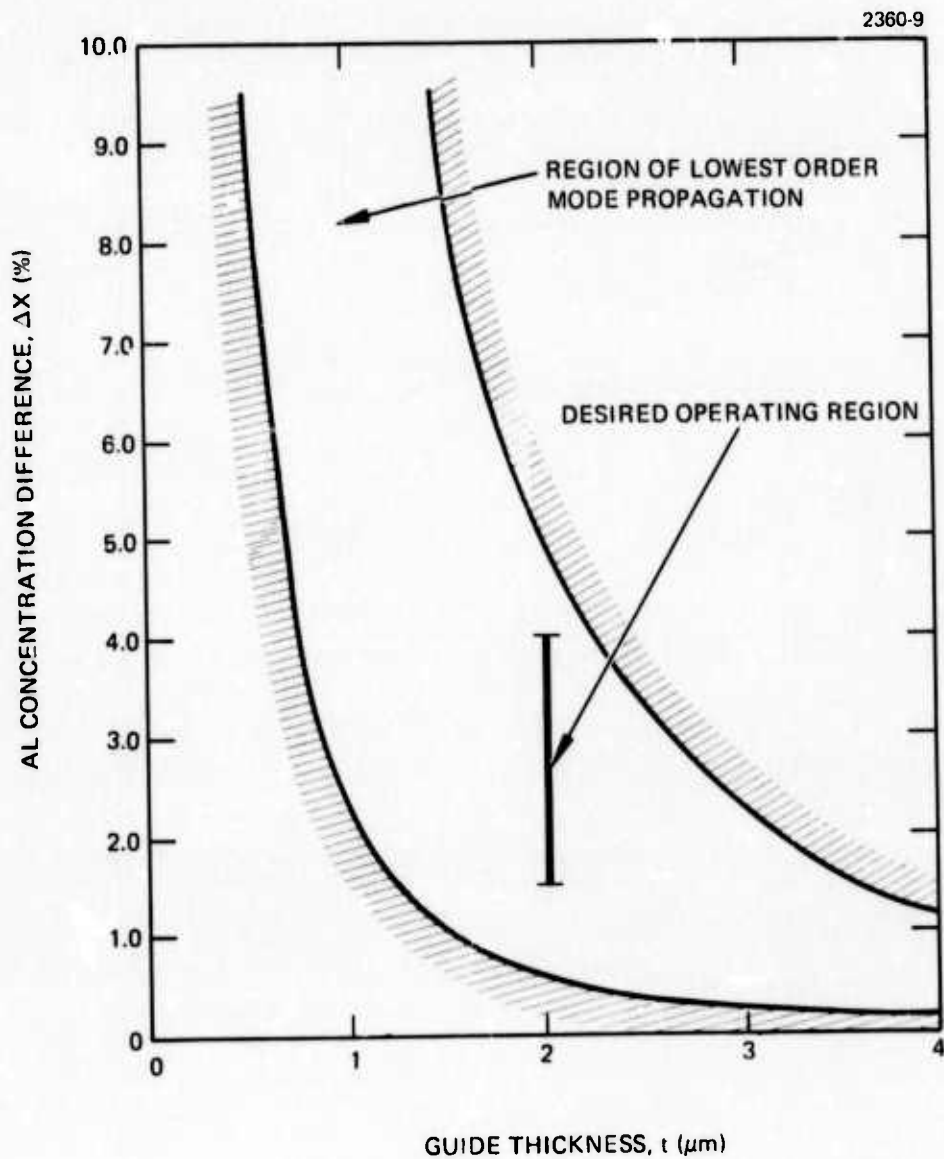


Fig. II-1. Al concentration difference for single-mode propagation ( $\lambda = 1 \mu\text{m}$ ).

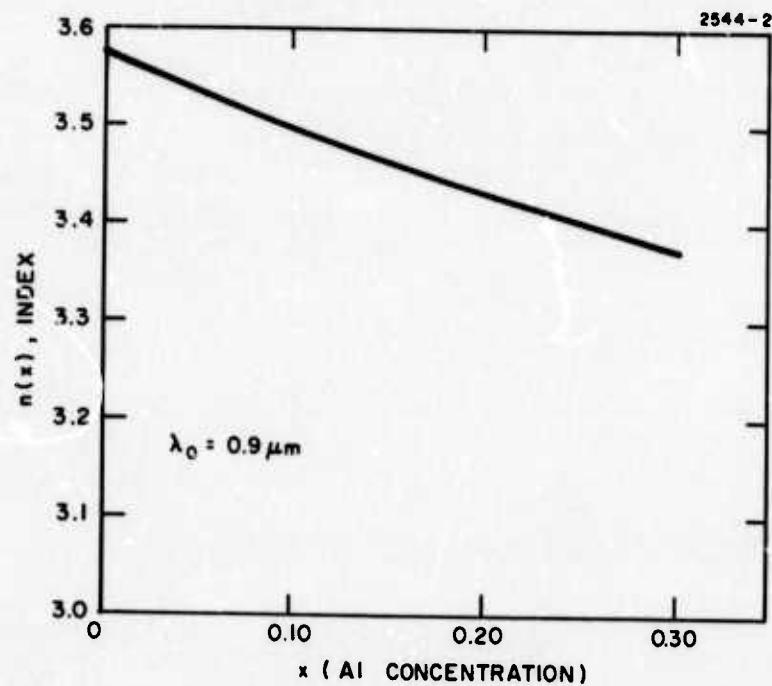


Fig. II-2. Index of Refraction of  $\text{Ga}_{1-x}\text{Al}_x\text{As}$  as a function of Al concentration.

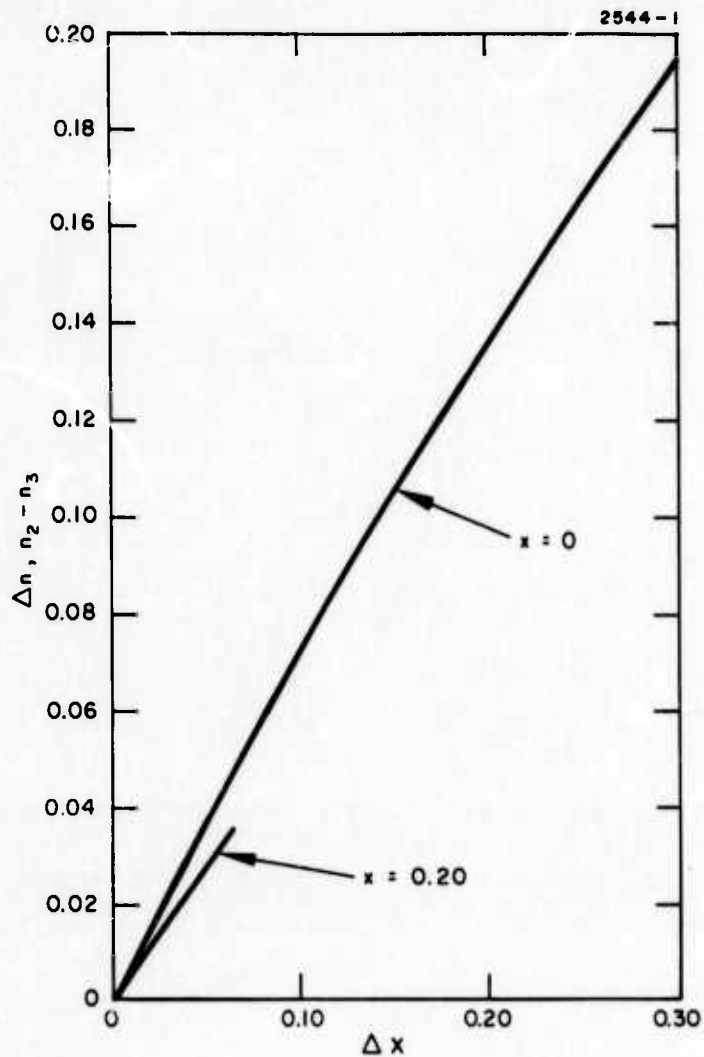


Fig. II-3.  
Refractive index difference as a function of Al concentration difference between two layers of  $\text{Ga}_{1-x}\text{Al}_x\text{As}$  for two values of absolute Al concentration.

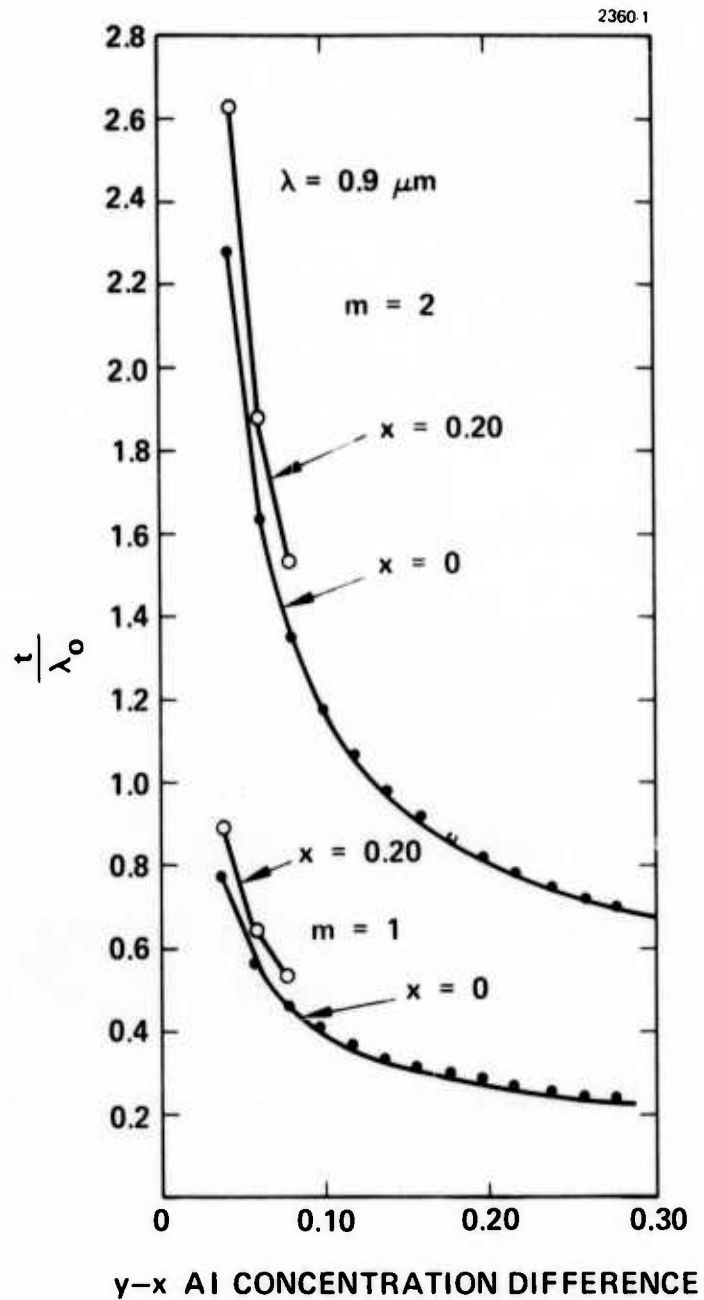


Fig. II-4.  
Guide thickness to wavelength ratio  
as a function of Al concentration  
between layer and substrate.

TABLE II-1  
Refractive Index of  $\text{Ga}_{1-x}\text{Al}_x\text{As}$

$$n^2 = A + \frac{B}{\lambda^2 - C} - D\lambda^2$$

Material	A	B	C	D
GaAs	10.906	0.97501	0.27969	0.002467
$\text{Ga}_{1-x}\text{Al}_x\text{As}$	$10.906 - 2.92x$	0.97501	$(0.52886 - 0.735x)^2$ $x \leq 0.36$  $(0.30386 - 0.105x)^2$ $x \geq 0.36$	$0.002467$ $(1.41x + 1)$

T980

coefficient due to interband transitions. Curves of Fig. II-5 were plotted using available data for GaAs. The absorption edges shown for increasing aluminum concentrations were obtained by calculating the bandgap using the expression<sup>2</sup>  $E_g(x) = 1.439 + 1.042x + 0.468x^2$  and then shifting the band edge of GaAs to correspond to the computed value  $E_g(x)$ . The required aluminum concentration was determined from these curves using two typical allowable values of absorption coefficients and various possible source wavelengths which might potentially be used in integrated optical circuits. The results are shown in Table II-2. The particular value chosen for allowable absorption coefficient would, of course, depend on the application. However a loss of 3 dB/cm ( $\alpha = 0.7 \text{ cm}^{-1}$ ) is certainly acceptable for many applications employing a wafer size  $\sim 1$  or 2 cm. Detailed data on the absorption in the long wavelength tail of the band edge of GaAs has been obtained from the literature,<sup>3</sup> as shown in Fig. II-6. However, as can be seen, the absorption at levels below about  $2 \text{ cm}^{-1}$  varies substantially from

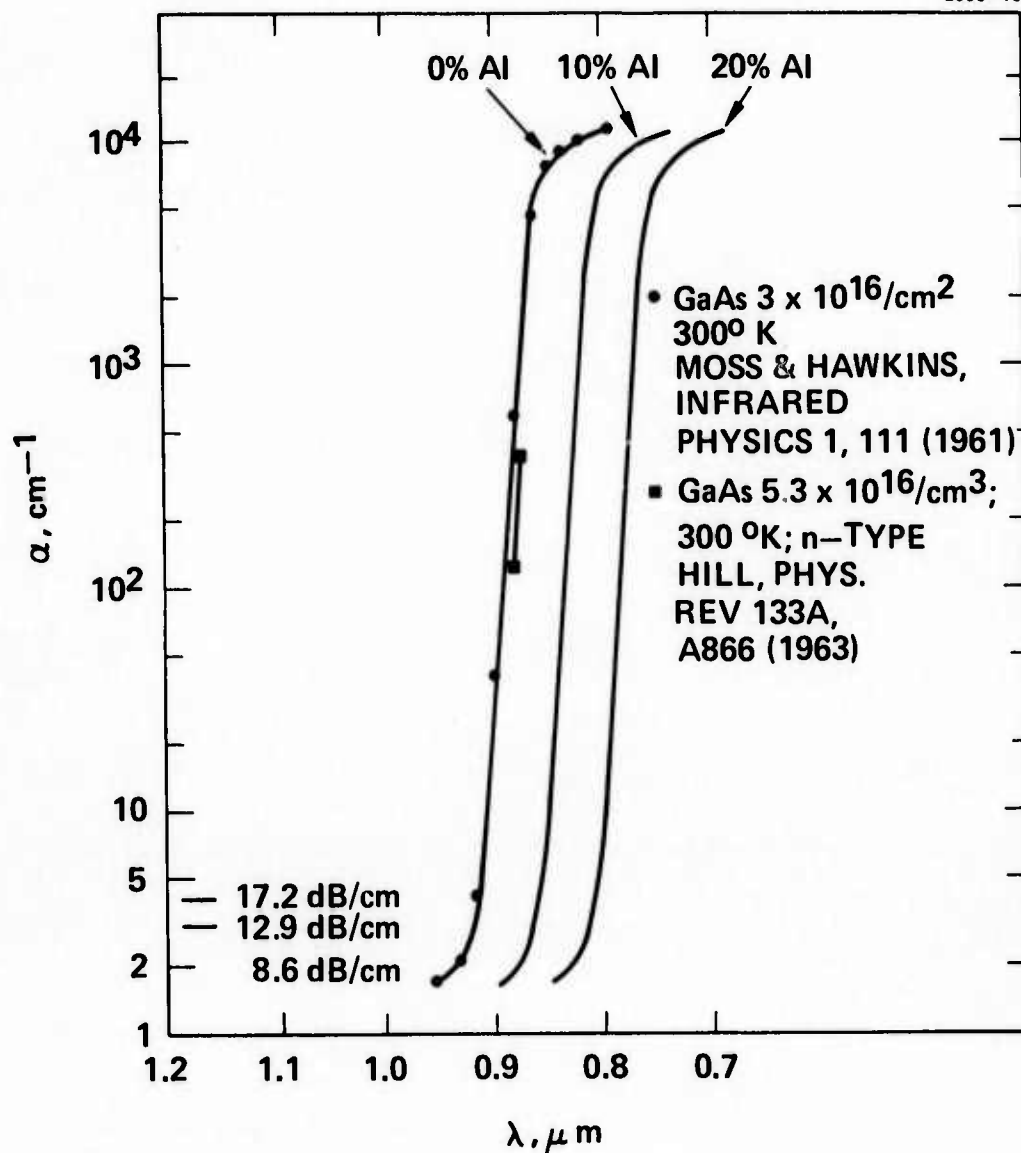


Fig. II-5. Interband absorption as a function of wavelength and Al concentration.

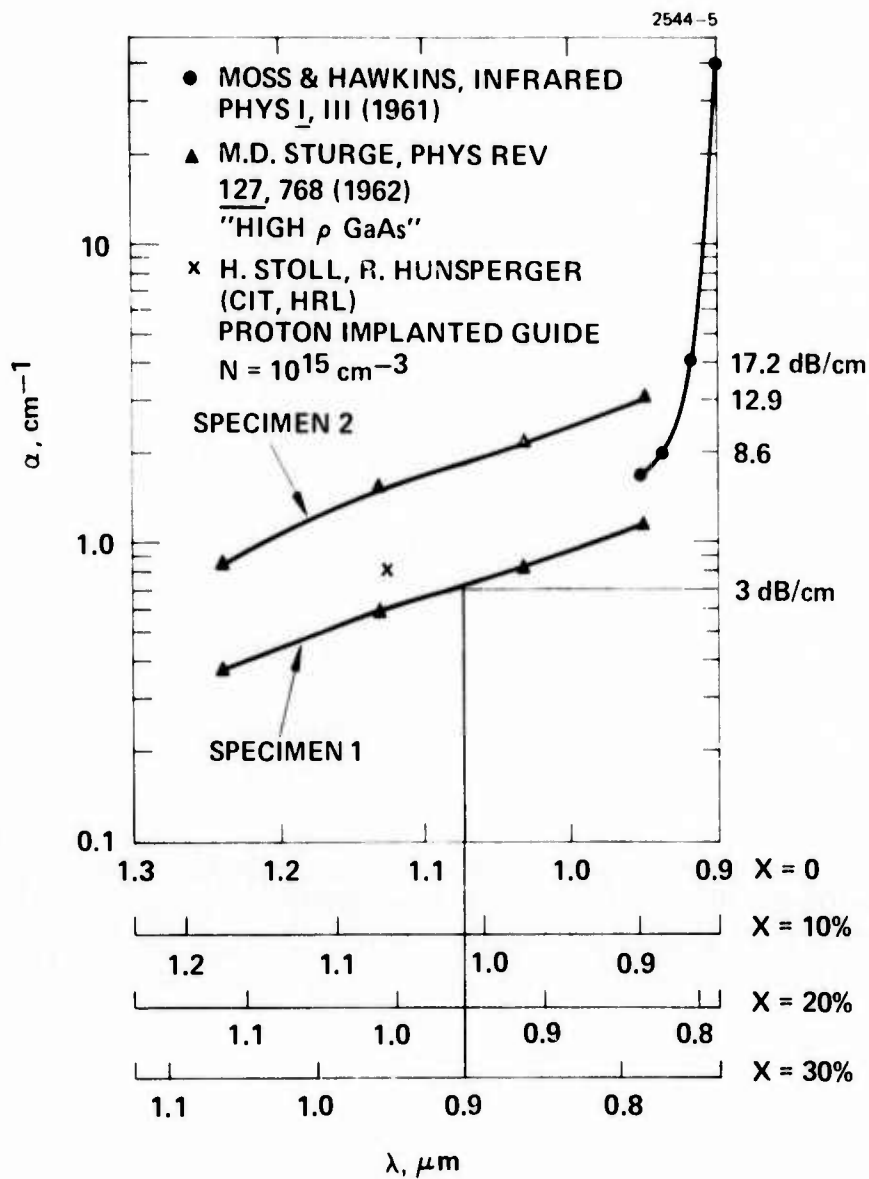


Fig. II-6. Absorption in the long wavelength tail of the GaAs band edge.

specimen to specimen which is presumably a result of impurities. The projected absorption for  $\text{Ga}_{(1-x)}\text{Al}_x\text{As}$  with various  $x$  values has been indicated by shifting the wavelength scale on the abscissa by the amount appropriate to the particular  $\text{Ga}_{(1-x)}\text{Al}_x\text{As}$  bandgap. It is clear from these data that adequately low absorption coefficients are expected in good samples of (GaAl)As. In fact, measurements on samples grown under this program which are described in section VI have demonstrated that losses significantly less than 3 dB/cm are obtainable.

TABLE II-2

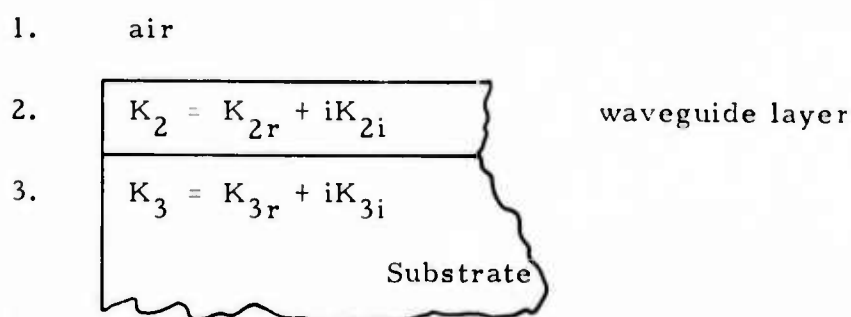
Absolute Aluminum Concentration Requirements

Source Wavelength	Required Aluminum Concentration In The Guide	
	$\alpha = 2 \text{ cm}^{-1}$ (8.6 dB/cm)	$\alpha = 0.7 \text{ cm}^{-1}$ (3 dB/cm)
0.85 $\mu\text{m}$ GaAlAs	17%	40%
0.9 $\mu\text{m}$ GaAs	7%	32%
0.95 to 1.0 $\mu\text{m}$ Si: GaAs	0%	20%
Substrate concentration 4% higher Material becomes indirect at 40% Al		

C. Limits on GaAs Epilayer Impurity Concentrations

The most important sources of loss in a (GaAl)As waveguide are (1) band-to-band transitions and (2) free carrier absorption. Loss caused by the first mechanism can be minimized by a proper choice of the energy gap relative to the operating wavelength as discussed in Section II-B. Free carrier loss will be present, however, since the impurity concentration, although kept to a minimum, is always finite.

In an effort to determine the allowable impurity concentrations we need to solve for the optical losses of the propagating modes as a function of the carrier concentrations in the substrate and the guiding layer. Consider a thin film waveguide such as illustrated below.



$K_1$ ,  $K_2$ , and  $K_3$  are the relative dielectric constants (i.e.,  $K = n^2$  with  $n$  being the complex index of refraction). The fact that the media are, in general, lossy is accounted for by taking the  $K$ 's as complex numbers as shown in the figure. Near cutoff most of the wave energy is in medium 3 and the mode attenuation approaches the bulk loss of medium 3 which is

$$\alpha_3 = \frac{k_o K_{3i}}{\sqrt{K_{3r}}} \quad (1)$$

where  $k_o = 2\pi/\lambda_o$ . Far above cutoff the mode energy is concentrated in medium 2 and the mode loss approaches.

$$\alpha_2 = \frac{k_o K_{2i}}{\sqrt{K_{2r}}} \quad (2)$$

We can obtain a general expression for the mode attenuation constant as a function of  $K_{2i}$ ,  $K_{3i}$ , the guide dimensions, and the frequencies. Such an expression has, indeed, been derived. As expected, the mode loss constant lies between  $\alpha_2$  and  $\alpha_3$ . For the

purpose of design criteria we assume, conservatively, that the loss constant is equal to the larger of  $\alpha_2$  and  $\alpha_3$ , i. e.,

$$\alpha_{\text{mode}} = \frac{k_0 \text{Im}K}{\sqrt{\text{Re}K}}$$

where the imaginary part of K (ImK) is taken as the larger of ImK<sub>2</sub> and ImK<sub>3</sub>.

An expression for ImK can be derived from a simple treatment of the carrier polarization in the presence of collisions of lifetime  $\tau$ . This gives (see Appendix A)

$$\text{Im}K = - \frac{Ne^2 / (m^* \epsilon_0 \omega \tau)}{\omega^2 + 1/\tau^2} \quad (3)$$

where  $m^*$  = effective mass,  $\epsilon$  = dielectric constant of vacuum in MKS units and  $N$  = carrier density.

In GaAs using a mobility  $\mu = 4 \times 10^3 \text{ cm}^2/\text{V-s}$  (which corresponds to an electron concentration of  $1 \times 10^{17}/\text{cm}^3$ ) we have at  $\lambda_0 = 1 \mu\text{m}$

$$m^* = 0.07 m_e = 6.4 \times 10^{-32} \text{ kg}$$

$$\tau = \frac{m^* \mu}{e} = 1.6 \times 10^{-13} \text{ s}$$

$$\omega = 2\pi f \cong 1.88 \times 10^{15} \text{ s}^{-1}$$

$$\omega\tau = 3.0 \times 10^2$$

$$n = 3.51$$

From eqs. (2) and (3) we obtain in the limit  $\omega \gg 1/\tau$

$$\alpha_{\text{mode}} = \sqrt{\frac{\mu_0}{\epsilon}} \frac{Ne^2}{m^* \omega^2 \tau} \quad (4)$$

where

$\mu_0$  = permeability of free space

$\epsilon$  = dielectric constant of the material

With the above data for GaAs we obtain

$$\alpha = 7.7 \times 10^{-19} N(\text{cm}^{-1}) \quad (5)$$

where  $N$  is in  $\text{cm}^{-3}$ .

The theoretical expression (5) for  $\alpha$  indicates values that are somewhat lower than those which are observed experimentally.<sup>4</sup> An empirical expression derived from the data of Spitzer and Whelan<sup>4</sup> is

$$\alpha = 5 \times 10^{-18} N(\text{cm}^{-1}) \quad (6)$$

Using this latter equation to obtain a conservative estimate of maximum allowable carrier concentration we adopt the value

$$N \leq 10^{17} \text{ cm}^{-3},$$

which would be expected to produce  $\alpha \leq 0.5 \text{ cm}^{-1}$ . This corresponds to a loss of 2.1 dB/cm (from free carrier absorption), which is acceptable in integrated optical circuits with typical dimensions up to a centimeter, as long as losses from other sources are of the same order of magnitude. Since we can routinely produce waveguiding layers with carrier concentration  $\leq 10^{16}/\text{cm}^3$  the above requirement can be easily met.

The material requirements established in the preceding paragraphs are summarized in Table II-3.

TABLE II-3  
Summary of Requirements

Impurity Concentration

$$N \leq 10^{17} \text{ cm}^{-3}$$

Al Concentration Difference Between Substrate and Guiding Layer

$$\Delta x: 1.5 \text{ to } 3.5\%$$

$$t: 1.25 \text{ to } 2.5 \mu\text{m}$$

Absolute Levels of Al Concentration

$$\text{For } \alpha = 2 \text{ cm}^{-1} (8.6 \text{ dB/cm})$$

Substrate ~4% - 21% minimum

Guiding Layer ~0% - 17% minimum

$$\text{For } \alpha = 0.7 \text{ cm}^{-1} (3 \text{ dB/cm})$$

Substrate ~24% to 44% minimum

Guiding Layer ~20% to 40% minimum

T982

### III. MATERIALS GROWTH PHASE I - DEVELOPMENT OF GROWTH TECHNIQUES

The program in materials growth can best be considered in three phases: (1) prior to August 1973, (2) August 1973 to January 1974, and (3) January 1974 to August 1974.

During the first phase of the program we evaluated three different possible approaches to the growth of epitaxial layers of III-V compounds for waveguide fabrication. These were vapor phase epitaxy, and two solution growth techniques - (1) limited melt graphite slide bar and (2) infinite melt. (The advantages and problems connected with each were treated in our report of August 1973.)

#### A. Vapor Epitaxy

The primary emphasis in this part of the program was to form simple structures of gallium arsenide layers on gallium-aluminum-arsenide, (GaAl)As, that could be used for studies based on our theoretical analysis of waveguide structures. The vapor deposition system already in use on other programs in the laboratory was used for growing these films.

The (GaAl)As substrates were obtained from Laser Diodes, Inc., Metuchen, New Jersey. They were epitaxial layers of (GaAl)As on GaAs substrates with composition  $\text{Ga}_{0.96}\text{Al}_{0.04}\text{As}$  and a film thickness of about 12  $\mu\text{m}$ . The surfaces were given a light chemical polish before being loaded into the growth apparatus. A brief description of our vapor growth system is given below.

Epitaxial layers of gallium arsenide are grown in an all-glass system using 99.999% arsenic trichloride and 99.999% gallium with a flowing atmosphere of pure hydrogen supplied by a palladium diffusion purifier. The hydrogen is bubbled through arsenic trichloride, passed over gallium kept at about 850°C and subsequently over a gallium

arsenide seed located downstream at about  $780^{\circ}\text{C}$ . The growth system has been used routinely in our laboratory to produce epitaxial layers with thickness larger than  $5\text{ }\mu\text{m}$  and carrier concentrations in the range of  $5 \times 10^{16}\text{ cm}^{-3}$ .

In a series of experiments we used the system for growing gallium arsenide films on gallium aluminum arsenide. The system and control, however, were not quite adequate to grow films thinner than  $4\text{ }\mu\text{m}$  reproducibly. When the films are thin, the thickness uniformity over the entire surface becomes a critical consideration, especially for use in waveguides. The film thickness is strongly dependent on the uniformity of the temperature across the whole cross section of the growth chamber where the seed is located. Besides uniformity in temperature, uniformity in the concentration of the gas phase at the growth front is also critical in producing a good junction at the growth interface. With these considerations in mind we designed a new system on a company-funded program incorporating more sophisticated controls. This was used in our later experiments to provide thin films with a high degree of homogeneity and good surface finish.

Several films of gallium arsenide were grown to familiarize ourselves with the problems involved. A cross section of one such film is shown in Fig. III-1. Also shown in Figs. III-2 and III-3 are the surface of the gallium aluminum arsenide as received and the gallium arsenide film after growth. It can be seen from the figures that the polishing of the (GaAl)As substrate and the procedures used in the growth system are capable of giving a very good layer of GaAs with good perfection and junction delineation. The vapor growth method would thus seem to be capable of growing a layer of GaAs on (GaAl)As.

Using the more sophisticated equipment, additional layers of GaAs were grown on  $\text{Ga}_{1-x}\text{Al}_x\text{As}$  substrates with  $\sim 4\%$  Al. To prepare the waveguide structures, small rectangular pieces with cleaved edges were prepared. To obtain these with smooth bounding faces, the wafers had to be thinned down to below 4 mil total thickness. The samples were used in waveguiding experiments and shown to guide.

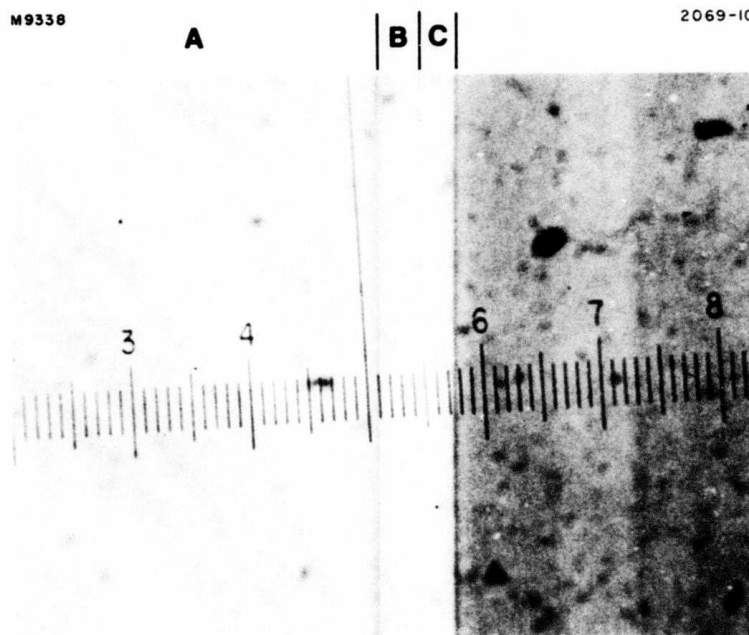


Fig. III-1. Cross-sectional view of wafer.  
Region A — GaAs substrate. Region B —  
GaAlAs epilayer ( $\sim 8.5 \mu\text{m}$ ).  
Region C — GaAs layer grown by vapor  
epitaxy ( $\sim 5.5 \mu\text{m}$ ).

M9335

2069-8

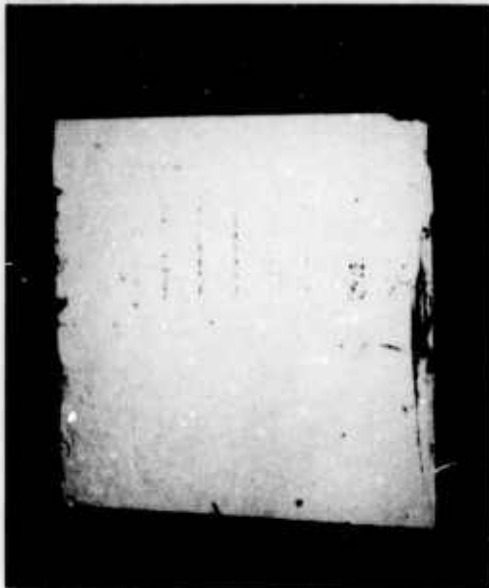


Fig. III-2.  
GaAl As epilayer as  
received.

Fig. III-3.  
GaAs vapor epilayer  
grown on GaAlAs.

M9336

2069-9



In summary, we were able to grow GaAs layers on (GaAl)As substrates and show these would waveguide. However, the source of (GaAl)As substrates is not very reliable and the growth of GaAs layers on (GaAl)As, while feasible, has problems. First, the interface between (GaAl)As and GaAs is not as good as that between the homo-epitaxial layers. The reactivity of aluminum makes it comparatively rough and strained. Second, only GaAs epitaxy is possible, thus limiting the waveguides to use for wavelengths longer than  $\approx 9000 \text{ \AA}$ , the GaAs absorption edge. Because of these limitations, we decided to concentrate on the two liquid epitaxial techniques. Since the ternary layers can be grown by these methods with variable aluminum concentrations, they can lead to a controlled variation in the bandgap and the refractive index necessary for optical waveguiding with low loss.

Liquid epitaxial growth is ideally suited for GaAlAs film growth because the condensed phase eliminates many of the disadvantages that the vapor phase has. We also found that aluminum addition to gallium tends to lower the gallium surface tension causing good wetting of the substrate surface, enabling very good growth of (GaAl)As on GaAs. A further advantage was to be gained by using the liquid epitaxial method because aluminum has a high segregation coefficient during growth that enables the utilization of very dilute solutions of aluminum; for example, a 0.05% solution of aluminum in gallium arsenide under appropriate conditions will give a (GaAl)As layer with 2% aluminum in the epilayer. This low concentration of the solution minimizes the problems caused by the high reactivity of aluminum, especially in the presence of traces of oxygen and water vapor.

In the sections below we give a detailed account of our work in the liquid epitaxial growth effort during the early phase of the program.

#### B. Limited Melt Liquid Epitaxy

A horizontal, open tube growth system was designed, constructed, and utilized to produce epitaxial films of GaAs and (GaAl)As. The following sections describe the growth concepts, system design, and properties of films.

## 1. Growth Method

The method of crystal growth in which a solid crystallizes in equilibrium with a dilute solution at a temperature below the melting point of the solid is referred to as solution regrowth. When the technique is applied to the growth of thin single crystal films on seed crystals it is often called liquid phase epitaxy. This is one of our approaches to the problem of fabricating optical guiding structures which will respond to the application of external fields and will transmit light with low losses at a wavelength of  $8500 \text{ \AA}$ . The solvent material is high purity gallium which is liquid at temperatures over  $50^\circ\text{C}$ .

The first films grown in this program by this method were GaAs homojunctions. The growth of GaAs films involves an initial saturation of gallium solvent with GaAs at the starting temperature and a subsequent cooling which results in supersaturation and precipitation of GaAs on the substrate as an epitaxial layer.

The solubility limit of arsenic in gallium versus temperature has been determined experimentally by R. N. Hall<sup>5</sup> and is depicted graphically in Fig. III-4. Also shown in this figure are points corresponding to an analytical expression we have fitted to the experimental curve:

$$x_{\text{GaAs}}^l = (6 \times 10^{-2}) \times 10^3 \{ 3.71 \times 10^{-3} (T-900) - 6.0 \times 10^{-6} (T-900)^2 \} \quad (7)$$

where  $x^l$  = atom fraction of GaAs in liquid gallium and  $T$  is the temperature of the melt in  $^\circ\text{C}$ . Notice that over the temperature range 500 to  $1100^\circ\text{C}$  the analytical expression corresponds well to the experimental data. From the equation we can establish the relevance of several parameters to controlled thin film growth; thus evaluating  $dx/dT$  near  $900^\circ\text{C}$  yields

$$\left[ \frac{dx_{\text{GaAs}}^l}{dT} \right]_{900^\circ\text{C}} \approx 5.13 \times 10^{-4}/^\circ\text{C} \quad (8)$$

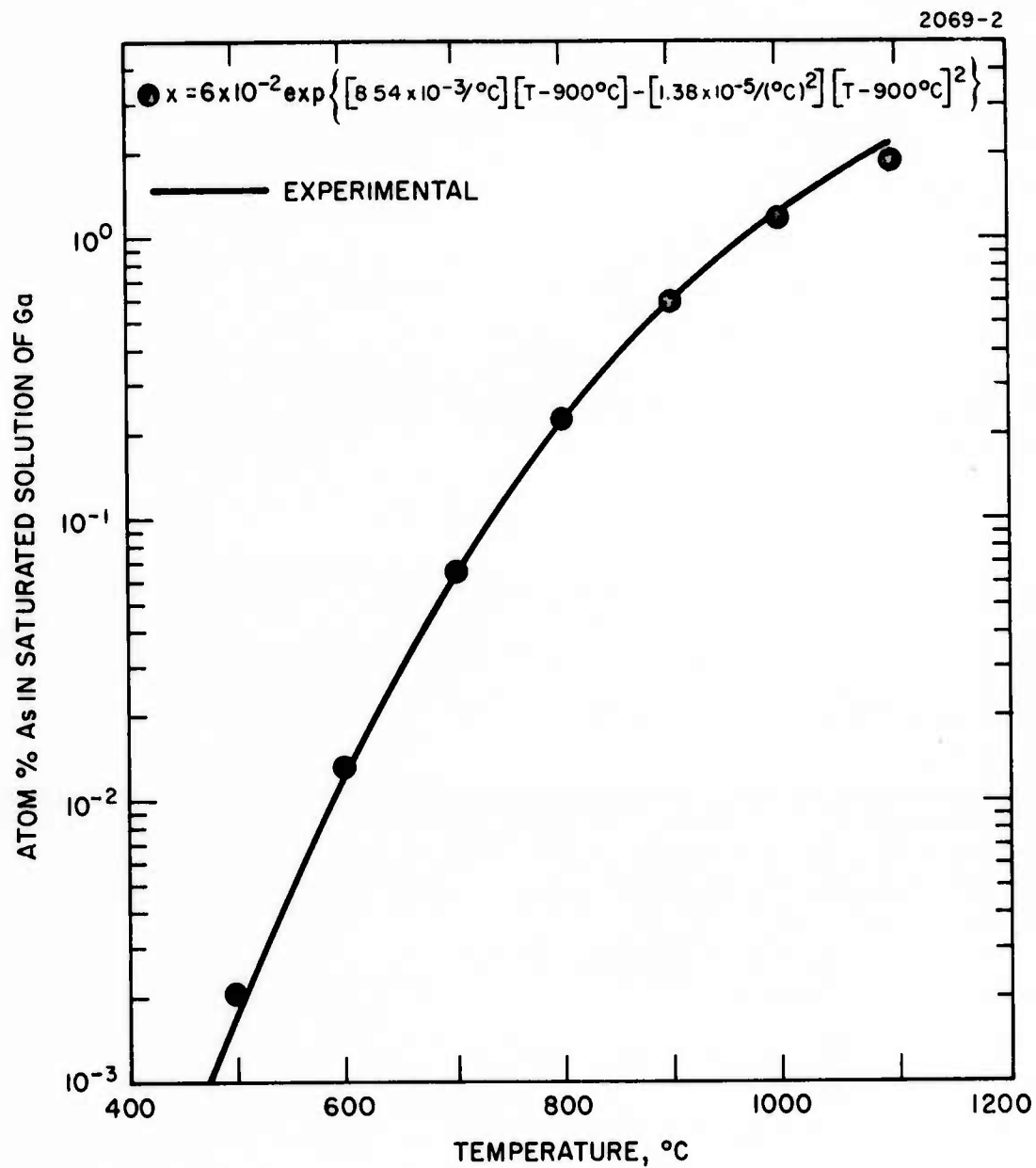


Fig. III-4. Solubility limit of arsenic in gallium versus temperature.

From eq. (8), for a system for which the kinetics are not diffusion limited, we can determine the film thickness produced by an incremental reduction in temperature near 900°C under the assumptions that nucleation occurs only at the substrate in a uniform layer and no super cooling takes place. The change in film thickness ( $\lambda$ ) with temperature is

$$\frac{d\lambda}{dT} = \frac{dx_{\text{GaAs}}^{\ell}}{dT} \frac{M_{\text{GaAs}}}{M_{\text{Ga}}} \frac{W_{\text{melt}}}{\rho_{\text{GaAs}} A} = -2 \left( \frac{W_{\text{melt}}}{A} \right) \mu\text{m}/^{\circ}\text{C} \quad (9)$$

where

$M_{\text{GaAs}}$  = molecular weight of GaAs

$M_{\text{Ga}}$  = atomic weight of Ga

$\rho_{\text{GaAs}}$  = density of GaAs in g/cm<sup>3</sup>

$W_{\text{melt}}$  = weight of the melt in g

$A$  = area of the substrate in cm<sup>2</sup>

In our early experiments a typical ratio of melt weight to substrate area is about 1 g/cm<sup>2</sup>. This implies a growth rate of 2  $\mu\text{m}/^{\circ}\text{C}$ . It is clear from this that reproducibility in thickness requires fine temperature control.

The second part of the growth program involves the growth of  $\text{Ga}_{1-x}\text{Al}_x\text{As}$  on GaAs. While the solubility of GaAs in the gallium melt may not be significantly affected by the addition of a small amount of aluminum to the melt, a new consideration arises regarding the uniformity of the aluminum concentration throughout the grown layer. Consider the mixed GaAs-AlAs system, AB, where A designates cations on an f. c. c. lattice and B designates anions on the other sublattice comprising the zinc blende structure. Near 900°C the "A" site fraction of aluminum in solid AB at equilibrium with a gallium rich melt is about 58 (Ref. 6) times the atom fraction of aluminum in the

melt. Consequently, as the film grows it quickly depletes the melt of aluminum. Again assuming uniform nucleation on the substrate and nowhere else, it can be shown that

$$\frac{d \ln x_{Al}^A (\text{interface})}{d\lambda} \approx -58 \left( \frac{M_{Ga}}{M_{GaAs}} \right) \rho_{GaAs} \left( \frac{A}{W_{Melt}} \right) \quad (10)$$

where  $x_{Al}^A (\text{interface})$  = site fraction of aluminum on the "A" lattice at the growth interface. The solution to this equation is, of course

$$x_{Al}^A (\text{interface}) \approx x_{Al}^{A,0} \exp \left[ -58 \left( \frac{M_{Ga}}{M_{GaAs}} \right) \rho_{GaAs} \left( \frac{A}{W_{melt}} \right) \right] \quad (11)$$

where  $x_{Al}^{A,0}$  = Al site fraction on the "A" lattice at the initiation of growth.

Figure III-5 shows the percentage deviation of the aluminum site fraction on the "A" lattice at the surface of the film to its value at the substrate-epijunction as a function of film thickness for various values of the parameter ( $W_{melt}/A$ ). Clearly large ratios of ( $W_{melt}/A$ ) correspond to more uniform film composition.

It would seem from the above argument that ( $W_{melt}/A$ ) should be kept large. Doing this produces another problem. When thin films are desired, however, eq. (9) indicates that the film thickness produced through a given cooling increment is directly proportional to ( $W_{melt}/A$ ). Conversely, the total cooling increment,  $\Delta T$ , required to grow a film of a given thickness is inversely proportional to ( $W_{melt}/A$ ). Since there are limits to how well the temperature can be controlled, large ratios of ( $W_{melt}/A$ ) reduce control over final film thickness. Problems associated with super cooling further complicated the situation. The discussion above leads to the conclusion that for best results a judicious compromise has to be used in choosing values of  $W_{melt}/A$ , depending on the thickness of the film desired and the aluminum

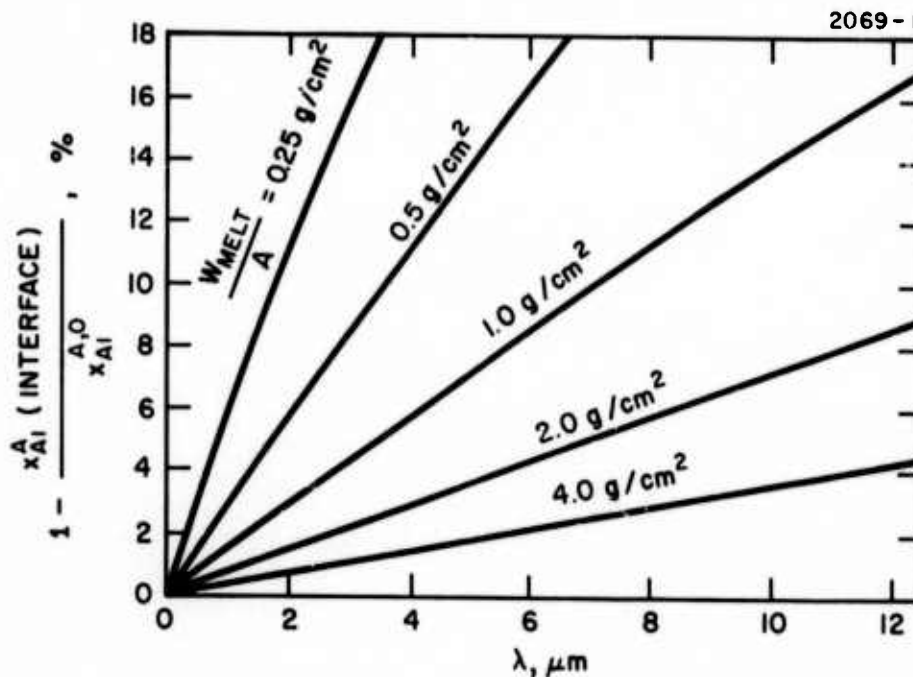


Fig. III-5. Variation of Al Concentration through the Epilayer Film Versus Film Thickness for Particular Values of the Parameter  $W_{\text{melt}}/A$ .

concentration gradient that can be tolerated in the film. It also emphasizes the high degree of sophistication necessary in the control of temperature both at the start of growth and during the cooling cycle. These considerations are seen in better perspective in the treatment below.

Figure III-6 illustrates the dependence of growth rate and the derivative of the logarithm of aluminum concentration with respect to film thickness (eq. (10) on  $(W_{\text{melt}}/A)$ ). Film specifications restrict growth to particular regions of the figure. For instance, suppose a  $10\text{ }\mu\text{m}$  thick film is required with a maximum allowable error in thickness of  $\pm 2\%$ . If the uncertainty in the growth temperature is  $\pm 0.1\%$  the growth rate must be less than  $2\text{ }\mu\text{m}/^{\circ}\text{C}$  to satisfy the requirement on film thickness. This limits the choice of  $(W_{\text{melt}}/A)$  to values less than  $1\text{ g}/\text{cm}^2$ . Figure III-6 shows that under these conditions the variation in aluminum site fraction from substrate to surface of film will be  $15\%$ . To improve control over uniformity, one must pay a price in control of thickness and vice versa.

It should be emphasized that the description of the growth process given above is based on an oversimplified model. The assumptions of chemical uniformity throughout the melt, lack of super saturation and heterogeneous nucleation occurring only on the substrate are all idealized concepts, but the simple model helps clarify general principles underlying the growth process. Equations (9) and (10) should be regarded only as guides illustrating the general dependence of the growth conditions on the various important parameters. Fortunately, the model is especially applicable to our epitaxial growth system where the melt is of limited volume and has a small thickness above the substrate. This allows near equilibrium conditions to be established at the growth interface and minimizes effects of diffusion of various species. The growth rate predicted in eq. (9), for instance, is only about three times higher than that obtained in the horizontal system using  $1\text{ g}$  of melt with  $1\text{ cm}^2$  substrate area.

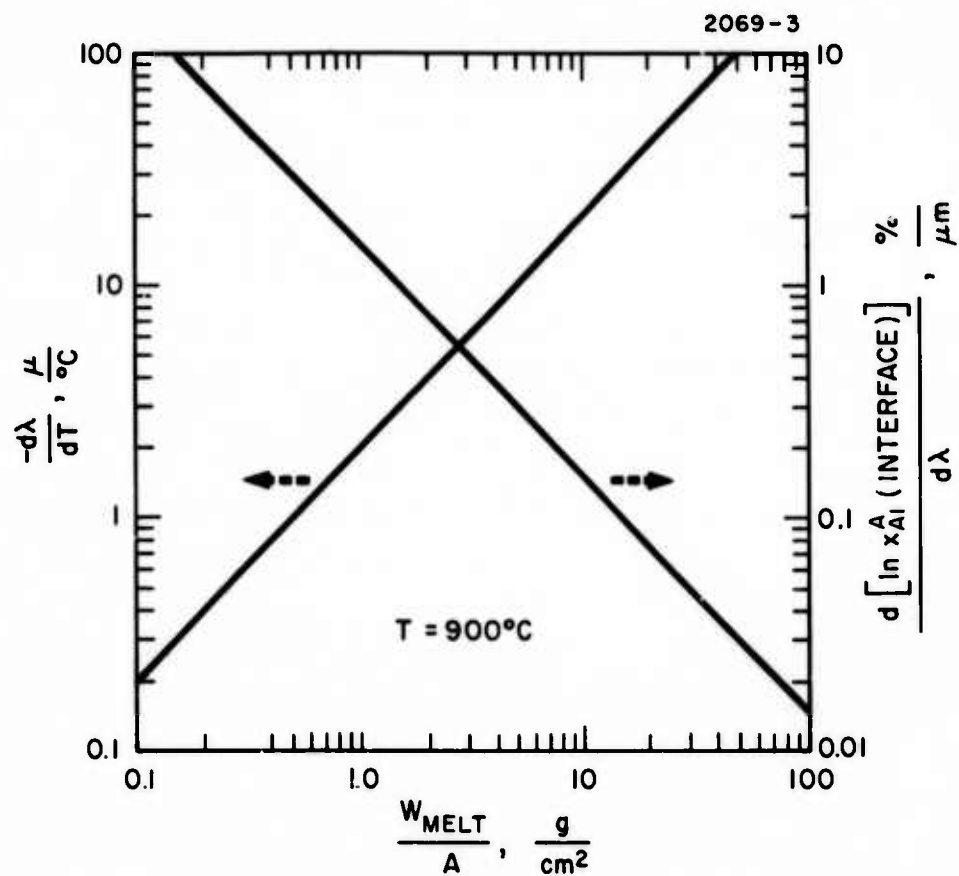


Fig. III-6. Growth Rate,  $d\lambda/dT$  and Percentage Change of Al Concentration for an Incremental Change in Film Thickness Versus  $W_{\text{melt}}/A$ .

## 2. Epitaxial Growth Apparatus

The design of the furnace and gas handling equipment is shown schematically in Fig. III-7. Figure III-8 is a photograph of this apparatus. The system is constructed primarily of quartz, pyrex, and stainless steel, with short sections of kovar tubing used to make the transition from pyrex to stainless and a limited number of compression fittings. The only compression fittings used on the gas input side of the furnace tube are at the stainless steel nitrogen regulator and at the Ag-Pd diffuser output.

The gaseous nitrogen source is the vapor over liquid nitrogen which ensures high purity without the necessity of a cold trap. At the beginning of each run the system is evacuated using a Balzer mechanical vacuum pump which employs a bakeable molecular sieve trap to prevent back streaming of pump vapors. Stainless steel vacuum bellows valves isolate the gas sources from the vacuum pump during evacuation and serve as on-off valves to control the gas flows. The pressure reached during pumpdown measured between the molecular sieve trap and the vacuum pump is less than  $10^{-3}$  Torr. This pressure is continuously monitored with a thermocouple gauge.

After evacuation the system is back filled with either  $H_2$  or  $N_2$ . To monitor the manifold pressure during back filling a Wallace-Tiernan absolute pressure gauge is used. The chamber exhaust goes through a three pound check valve and a bath of silicone oil to prevent oxygen backstreaming.

The furnace itself is a Thermco "Spartans" diffusion furnace having three temperature zones which are controlled by a master-slave, four thermocouple control loop. This type of control system is ideal for maintaining a long, flat temperature profile even during cooling. The maximum furnace cooling rate measured in the thermocouple well is about  $9^{\circ}C/min$  with low gas flow.

The temperature during growth is monitored in a thermocouple-well adjacent to the boat. The thermocouple E.M.F. is applied to a Leeds and Northrup millivolt recorder in series with a temperature

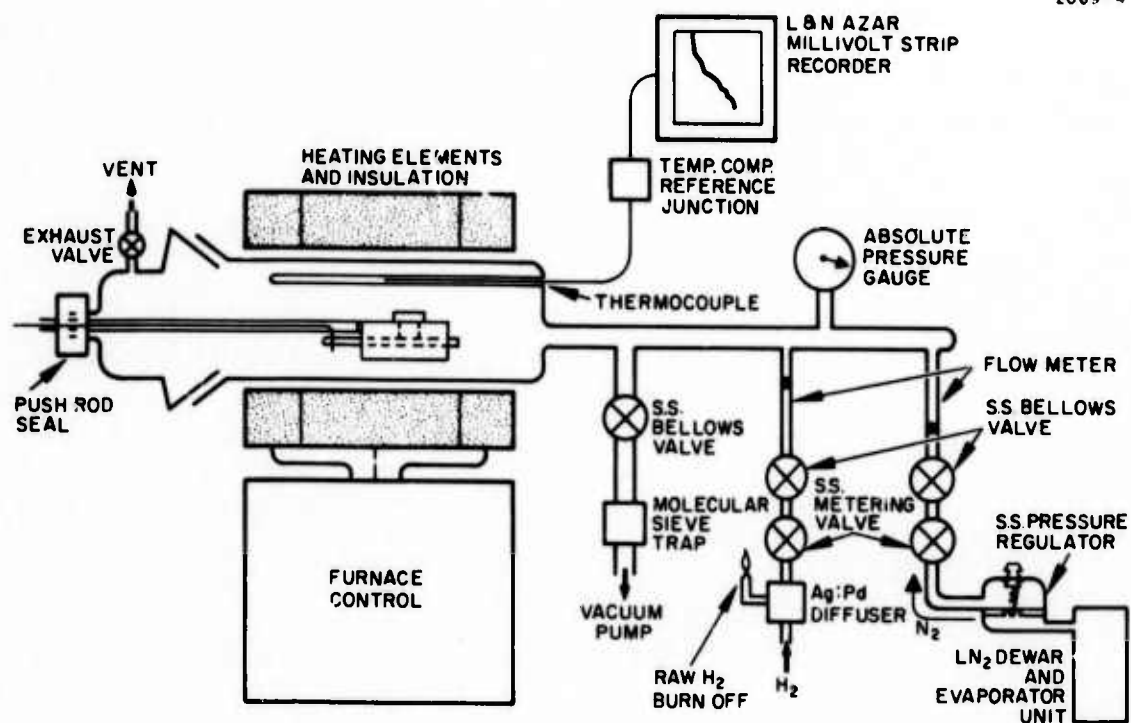


Fig. III-7. Schematic diagram of horizontal liquid epilayer system growth.

M9263

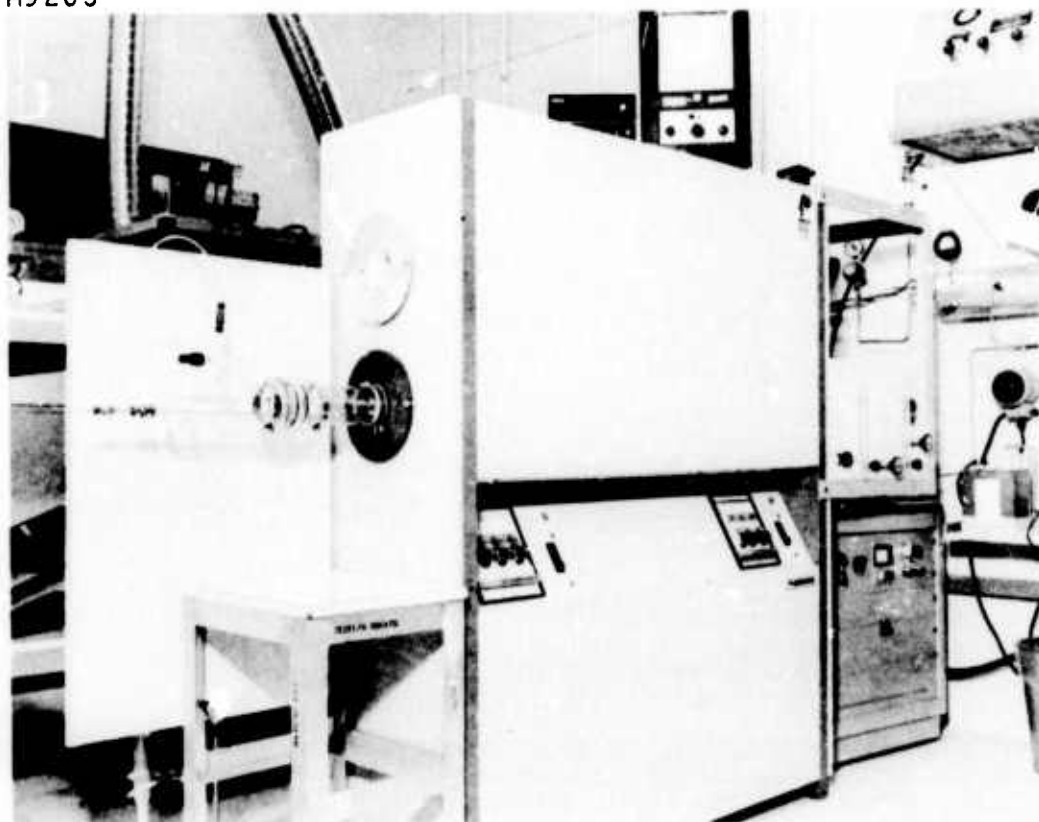


Fig. III-8. Horizontal liquid epilayer growth system.

compensated reference (cold) junction. This recorder is capable of displaying a 2 mV full scale span atop a calibrated dc level of up to 40 mV. Finer temperature sensitivity is possible using a five-digit digital voltmeter with 1  $\mu$ V resolution. This permits measurements of temperature change as small as 0.1°C using a Pt-Pt: Rh(13%) thermocouple. We found it possible to maintain a temperature which is constant to  $\pm 0.1^\circ\text{C}$  in the growth zone of our system.

The early slide bar assemblies containing the substrate and the melt were made of high purity graphite purchased from Ultra Carbon Corporation. They consist of two pieces: the main body of the slide containing the melt which is covered with a graphite cap and a plate which slides through the center of the main body directly under and in contact with the melt. The sliding plate has two machined depressions which accept a GaAs source piece and the substrate. During growth the source piece is placed in contact with the melt by moving the sliding plate with respect to the boat body. This saturates the melt at the starting temperature. The substrate is shifted into contact with the melt just before cooling begins. Figure III-9 is a photograph of the slide bar.

The two-section slide bar is controlled by a double push rod having a concentric design. The outer rod is quartz and holds the main body of the melt in position. The inner rod is tungsten and attaches to the sliding plate.

### 3. Results of Film Growth and Evaluation

After the epitaxial system was completed it was checked out by growing films of GaAs on silicon doped GaAs substrates ( $10^{18}$  electrons/cm<sup>3</sup>). These films are n-type as grown, which is expected since the gallium melt was saturated using silicon-doped GaAs. The growth orientation was  $\langle 100 \rangle$ .

These initial runs were helpful in pointing out problems inherent to the system. One difficulty is the complete removal of the melt from the film after growth. Careful attention to the spacing between the graphite wiping edge and the film surface and the incorporation of a

M9262

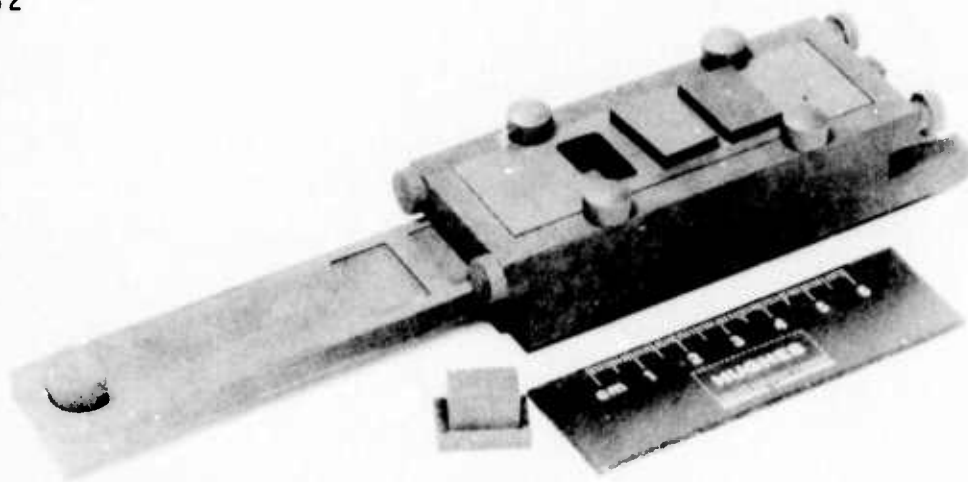


Fig. III-9. Photograph of the graphite slidebar in which  
the epitaxial growth occurs.

second cavity in the graphite boat to provide additional wiping has helped to reduce the problem.

Another problem which was encountered in the growth of the initial GaAs films was that of thermal decomposition of the substrate during melt saturation. Besides pitting the surface to a depth of more than a micron, thermal decomposition converted the surface layer of the substrate to p-type to a depth of several thousand angstroms. This left a troublesome interface layer between the film and the substrate.

This difficulty was successfully eliminated by minimizing the time the substrate is exposed to high temperature and by supplying an equilibrium overpressure of arsenic during the high temperature period. The proper arsenic overpressure can be achieved by placing a wafer of GaAs over the substrate when actual growth is not taking place.

At the end of GaAs growth experiments, growth occurred over the entire surface of a  $1.5 \text{ cm}^2$  substrate even when the weight of the melt covering the substrate was less than 1.5 g. Originally this was not possible since the surface tension of the melt caused it to ball up and wet only that part of the substrate directly beneath the ball. The problem was minimized by using a plunger type of melt cap made of high purity graphite, which presses down on the melt, spreading it across the surface of the substrate. The use of small melt volumes is desirable in the growth of thin films since reproducibility in thickness then becomes consistent with practical temperature control capabilities.

Thus, (GaAl)As films were grown in the system both on GaAs and (GaAl)As substrates. These films were grown with various compositions and thicknesses in order to ascertain our control capability.

Another growth problem was the tendency for pyramidal growth to occur on the surface of the film at specific nucleation sites. These were few enough in number that their presence did not in itself produce problems; however, the graphite wiping edge could scrape them across the surface of the film leaving parallel scratches.

In the early phase, (GaAl)As films were characterized through simple microscopic examination, staining cleaved cross sections, mechanical measurement of surface roughness (Dek-tak), measurement of avalanche breakdown voltage and microprobe examination (x-ray fluorescence).

Figure III-10 is a photomicrograph of a typical thick (GaAl)As epitaxial film surface taken at low magnification (6X). The upper region of the substrate was not placed in contact with the melt and, consequently, has no epitaxial film. The horizontal line is, therefore, the edge of the film.

Several of the anomalies mentioned above are visible in this figure. Notice the vertical scratches originating at growth pyramids on the film. The scratches are in the direction in which the wiping edge was pulled across the surface.

Notice also the exaggerated thickness near the upper edge. This is due to incomplete removal of the melt in regions where the melt remains during the cooldown to room temperature. In these regions growth continues leaving coarse crystalline deposits.

The gentle undulation of the surface is characteristic of thick films grown by the method described above. Figure III-11 illustrates the magnitude of the surface undulation. The measurement was made with a Sloan Dek-tak. Notice that the average deviation from flatness of the surface is about  $\pm 1500 \text{ \AA}$ . This measurement was made on the  $17 \mu\text{m}$  thick film shown in Fig. III-10.

The variation in aluminum concentration across a  $5^\circ$  beveled surface of the film in Fig. III-12 was measured using x-ray fluorescence. The results indicate that  $x$  varies from 4.21% at the substrate-epi-interface to 3.57% at the surface of the film, in qualitative agreement with eq. (11).

The (GaAl)As films were n-type with carrier concentrations on the order of a few times  $10^{17}/\text{cm}^3$  as determined through measurement of available breakdown voltage. Thin layers about  $2 \mu\text{m}$  thick also were grown on (GaAl)As substrates. These layers were reasonably flat, although somewhat scratched.

M9337

2069-7



Fig. III-10.  
Surface of a (GaAl)As  
film.

MAG. 6x

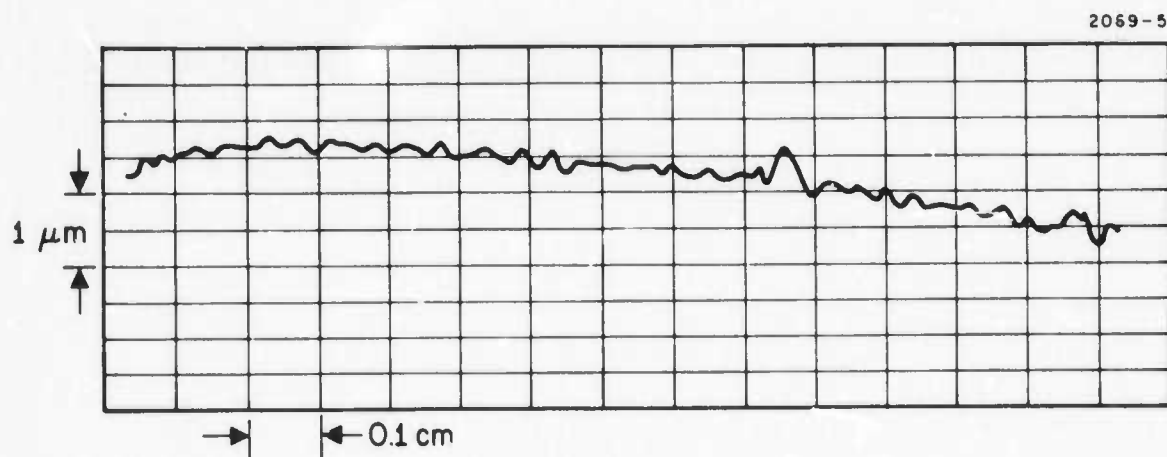


Fig. III-11. Deviation in surface flatness of the film shown  
in Fig. III-10.

M9339

2069-6

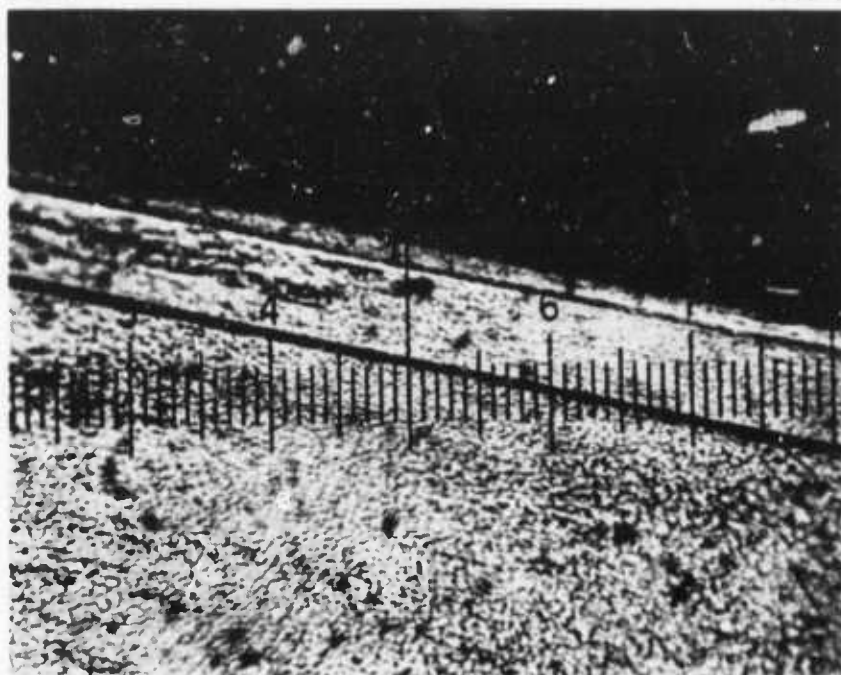
2  $\mu\text{m}$ /DIV

Fig. III-12. Photomicrograph of the cleaved edge of a double layer of (GaAl)As on GaAs. Top layer is  $\text{Ga}_{0.98}\text{Al}_{0.02}\text{As}$  (3  $\mu\text{m}$  thick); lower layer is  $\text{Ga}_{0.96}\text{Al}_{0.04}\text{As}$  (13  $\mu\text{m}$  thick); substrate is GaAs.

Experience from these early experiments led us to make several changes. First, the soft ultracarbon graphite was found to be a problem because of its tendency to abrade easily. We therefore switched to several alternative types of carbon and finally settled on a much denser ultracarbon graphite which has proved to be satisfactory. We also tried pyrolytic coated graphite and when the coating is applied properly, this aided in giving a uniform, trouble-free surface.

The second addition to the system was a temperature programmer that could lower the temperature at various cooling rates. Use of the programmer coupled with the new slide bar enabled us to grow layers with smoother surfaces and greater uniformity in thickness. We attempted the growth of two layers with different aluminum concentrations. After some early problems in wiping were solved, we were able to grow several  $\text{Ga}_{(1-y)}\text{Al}_y\text{As}$  layers over  $\text{Ga}_{(1-x)}\text{Al}_x\text{As}$  so that  $y$  was lower than  $x$ . Experiments in waveguiding showed that the layers could guide but were lossy because of lack of smoothness at the growth interfaces and the surface. While the cleaved edges looked reasonably smooth and the junctions visibly uniform under the microscope, the heterojunctions apparently had many pinpoint defects and irregularities that made them optically lossy.

Our calculations suggested that the guiding performance would be improved by going to higher aluminum concentrations in the layers. The high segregation coefficient of aluminum and its high reactivity, however, militate against the use of higher aluminum concentration in the melt. The large surface-to-volume ratio of the melt in the slide bar method is especially harmful since the melt can be fouled easily by contamination with water vapor or oxygen. To solve these challenges we went to two different alternatives: (1) improve the slide bar system, and (2) try a new alternative, the infinite melt system. Both of these have proved quite successful.

The slide bar system was improved methodically by eliminating all possible sources of leaks. The operating parameters — temperature of growth, the saturation cycle, the cooling or growth cycle and the wiping operation — all were optimized by empirical experimentation

with the theoretical model developed previously as a guide. An example of such an approach with some of the relevant parameters is given in Table III-1.

The series of runs summarized in the table demonstrates the importance of several parameters. It can be seen, for example, that the melt must be saturated at a temperature a few degrees higher than that for starting growth. The etchback that takes place without such a precaution can be seen by cleaving and etching the grown layer and appears as a double junction (see Fig. III-13). Such a regrowth is not always undesirable. In some experiments where crystal perfection is of the essence a controlled etchback and growth is known to improve epitaxial growth. However, it is important to take the possibility of etchback fully into account, to permit the growth of layers as thin as 2  $\mu\text{m}$  reproducibly. In the growth of structures for waveguides the growth of the second layer with the higher refractive index is critically affected by this consideration. Therefore, it is imperative that the time rate of layer growth and the etchback and regrowth cycles, be fully integrated into the operational cycle. Unfortunately, the control of a cycle of this type is highly dependent on the position of the slide-bar assembly in the growth chamber.

Several of the factors mentioned above are illustrated by the series of photographs in Figs. III-13 through III-17. Figures III-13 and III-14, which correspond to samples 0040 and 0042 in Table III-1, show the regrowth area in 0040 and its absence in 0042. The regrowth area can be seen better (Figs. III-15 and III-16) in samples 0055 and 0056 (not listed in Table III-1) in a new graphite assembly. Sample 0056 was prepared using longer time of growth than sample 0055. The results show that increased time of growth only increases the thickness of the grown layer but does not affect the regrowth layer. Figure III-17 shows a typically grown layer with faint scratch lines caused by particles dragging across the face.

The slide-bar assembly method was used successfully to make a multilayer structure with  $\text{Ga}_{0.98}\text{Al}_{0.02}\text{As}$  on top of  $\text{Ga}_{0.96}\text{Al}_{0.04}\text{As}$ .

TABLE III-1  
Epitaxial Films: Limited Melt Growth

Substrate	Melt <sup>a</sup> Composition, Weight in Grams			Temperature, °C		Time, t minutes <sup>e</sup>	Cooling Rate, ΔT/t	d, f μm	Growth Rate, d/t	Saturation Cycle		T <sub>ss</sub> <sup>f</sup> , °C <sup>b</sup>	Remarks
	Ga	GaAs	Al	T <sub>sat</sub> <sup>c</sup>	T <sup>d</sup>					Time in Hours	T, °C		
0039	1.5	0.6	0.082	891	5.5	2.0	0.275	4	0.20	1	894.0	3.0	Etchback at junction, nonuniform layer.
0040	1.5	0.6	0.091	889	3	1.0	0.300	2	0.20	1	894.5	5.5	Etchback reduced; better coverage by grown layer.
0042	1.5	0.6	0.0856	887	3	1.0	0.300	2	0.20	1	894.0	7.0	Etchback not visible. Good uniform layer. Surface scratches.
0043	1.5	0.6	0.113	886.5	6.5	3.0	0.325	7	0.35	1	893.5	7.0	Same as above. Note change in growth rate. Surface scratches.

<sup>a</sup> Besides the crushed GaAs added as specified, the melt was allowed to stay in contact with a thin water of GaAs during the saturation cycle.

<sup>b</sup> T<sub>ss</sub>, °C, super-saturation temperature. After saturation at this temperature, the melt was allowed to cool down to the saturation temperature before the substrate was contacted to the melt.

<sup>c</sup> T<sub>sat</sub> = Saturation temperature.

<sup>d</sup> ΔT = Cooling range of temperature.

<sup>e</sup> t<sub>min</sub> = Cooling time.

<sup>f</sup> d = Thickness.

1983

M9811

2544 - 11

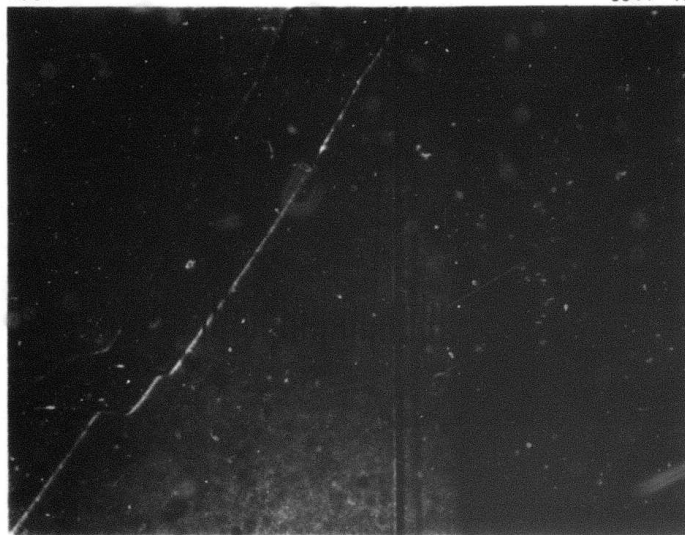
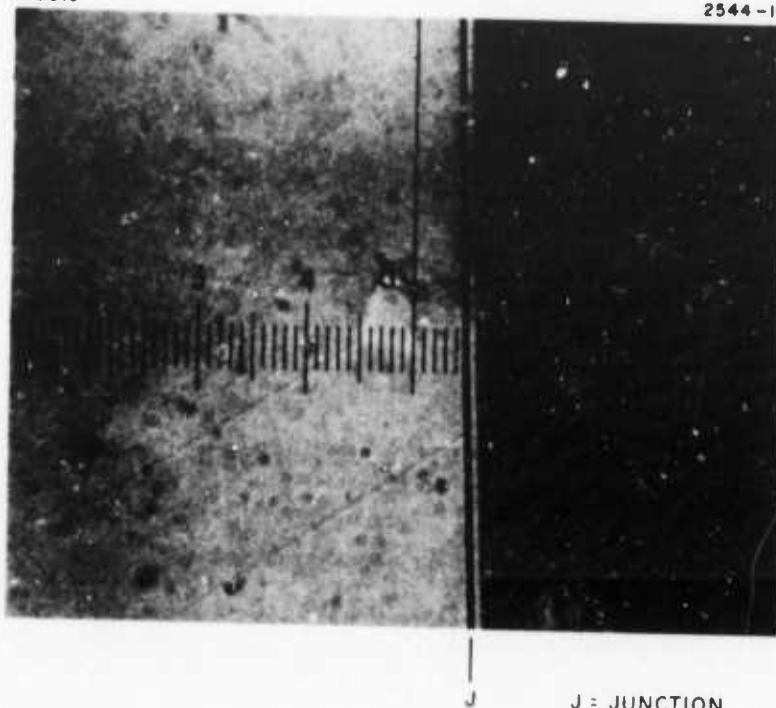
J<sub>1</sub> J<sub>2</sub>J<sub>1</sub> J<sub>2</sub> = REGROWTH REGION

Fig. III-13.  
Sample 0040. GaAs with Ga<sub>0.95</sub>Al<sub>0.05</sub>As epi-  
layer. J<sub>1</sub>J<sub>2</sub> shows the regrowth region close  
to the junction. Scale: 2  $\mu$ m/div.

M9813

2544-10



J = JUNCTION

Fig. III-14.  
Sample 0042. Ga<sub>0.95</sub>Al<sub>0.05</sub>As epilayer on GaAs.  
No regrowth region observed. cf. 0040.  
Scale: 2  $\mu$ m/div.

M9799

2544-9

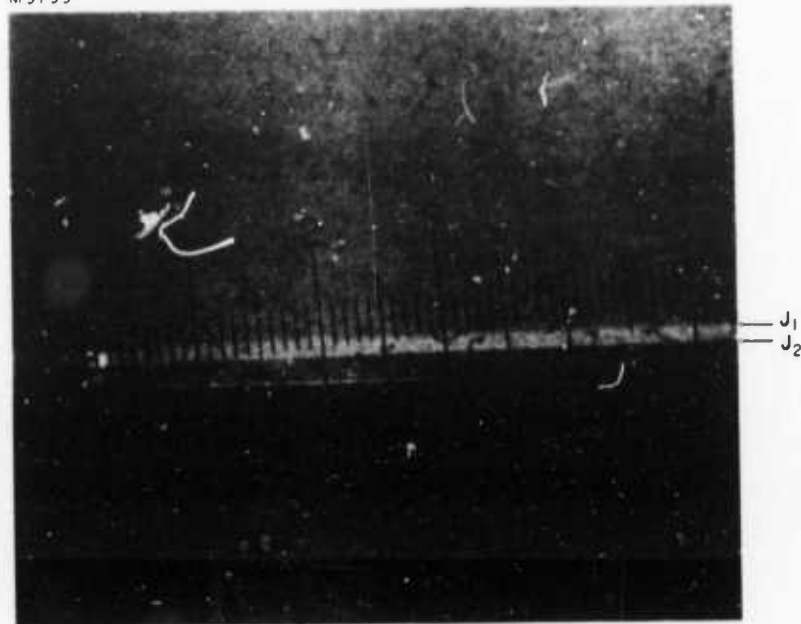


Fig. III-15.  
Ga<sub>0.95</sub>Al<sub>0.05</sub>As layer on GaAs. Note the  
regrowth region J<sub>1</sub>J<sub>2</sub>. Scale: 2.3  $\mu$ m/div.

M9798

2544-8

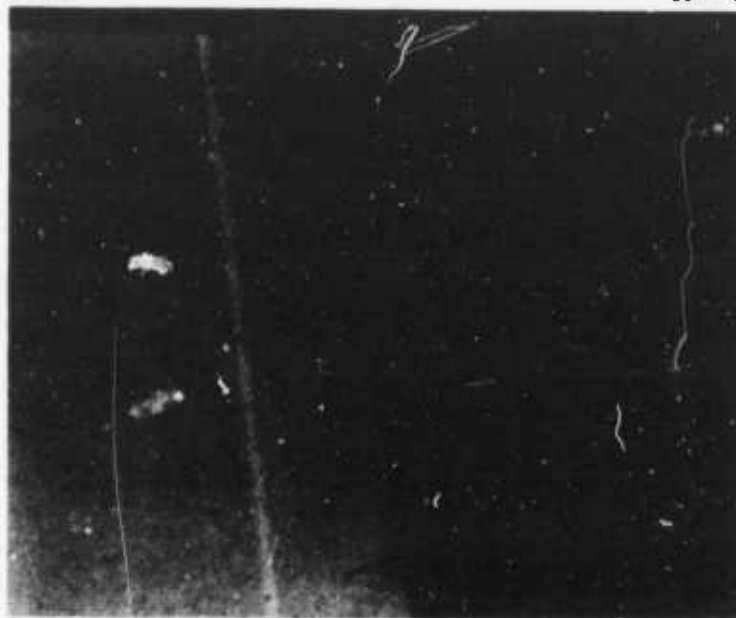


Fig. III-16.  
 $\text{Ga}_{0.95}\text{Al}_{0.05}\text{As}$  layer on GaAs. Note in-  
 creased thickness of epifilm, but same  
 regrowth region  $J_1 J_2$ . Scale 2.3  $\mu\text{m}/\text{div}$ .

M9800

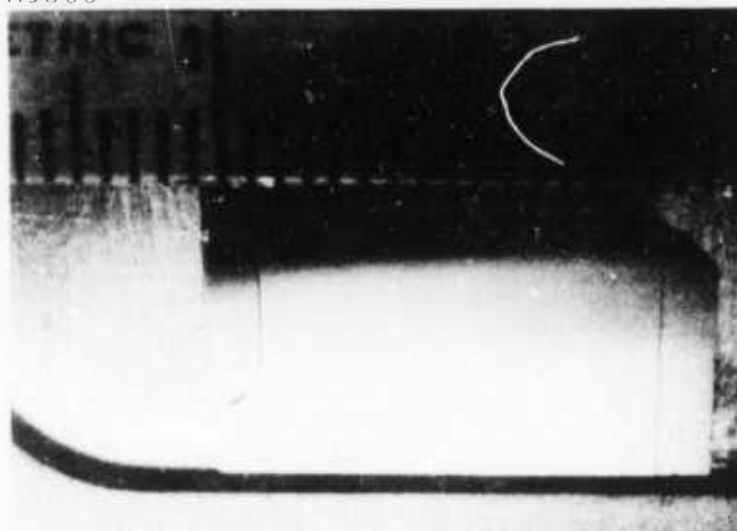


Fig. III-17.  
 $\text{Ga}_{0.95}\text{Al}_{0.05}\text{As}$  layer on GaAs. Sample of  
 a good layer. Note lines running parallel  
 to cleavage lines at right and left end.

The top layer was about 5  $\mu\text{m}$  thick and the bottom layer about 6 to 8  $\mu\text{m}$  thick. The quality of the layers still suffered from the defects mentioned before and the waveguiding was possible only with considerable propagation loss due to surface irregularities and imperfections. One final point needs to be made about the limited melt growth with specific reference to the growth of  $\text{Ga}_{1-x}\text{Al}_x\text{As}$  layers. This concerns the variation of the segregation coefficient of aluminum as a function of temperature. As evident from the literature and calculations given earlier, the segregation coefficient increases as the growth temperature decreases. As a result, there are two factors that influence the aluminum concentration in the grown layer. The segregation coefficient being as high as 30 makes the solution depleted in aluminum, and hence the layer grown lower in aluminum concentration, as the growth progresses. However, this is offset to some extent by the increase in segregation coefficient as the temperature is reduced during the growth period. At any starting temperature, the final aluminum concentration profile in the epitaxial layer will be a reflection of these contradictory factors and the final result is heavily dependent on both the starting temperature and the growth cycle. It can be seen also from the argument that the thickness of the layer to be grown will have an important bearing on the starting temperature and the cycle to be chosen. Because of these considerations the limited melt epi is best used where thin layers are required and the infinite melt method described below has significant advantages when thicker layers of uniform aluminum concentration have to be grown.

### C. Infinite Melt Liquid Epitaxy

The infinite melt technique offers many important advantages to the growth of semiconducting films, in general, and some specific advantages to the growth of  $\text{Ga}_{1-x}\text{Al}_x\text{As}$  films in particular. Since a large melt or saturated solution of GaAs in Ga is the source, the layer growth can be carried out in a stable matrix with very uniform conditions of temperature and concentration, the two prime parameters for

good crystal growth. Again, since aluminum has a very high segregation coefficient, a uniform layer of  $\text{Ga}_{1-x}\text{Al}_x\text{As}$  can be grown easily from a large source so that the growth front concentration of the ambient liquid stays close to invariant during epitaxy.

The major disadvantage to the large melt approach arises from the high reactivity of the aluminum. In the slide-bar approach this difficulty is avoided for two reasons inherent to the technique.

1. A small melt is used only in one experiment and then discarded. Therefore, the melt is exposed to air only once at the beginning of each experiment.
2. The substrate is slid under the melt and hence is not exposed to any reactive films that may be at the surface of the saturated melt. While this is helpful, it is well to remember that in the wiping operation, which is part of this process, any significant amount of surface crystallites or particles can lead to mechanical damage of the grown surfaces.

Thus, under controlled conditions the two points made here make the slide-bar limited-melt approach attractive. Its major advantage, of course, is its ability to make multiple films in one experiment by having more than one melt slide over the substrate in a series fashion. For some very small devices where feasibility and the determination of parameters for research are prime considerations, this is a practical approach for obtaining rapid results. However, where large areas of perfect epitaxy are necessary, as in the case of waveguides, the infinite melt had the ability to provide large-area layers. The advantage of this approach can be appreciated further, when we think ahead to the next generation of device needs, where these waveguides have to be integrated with other structures to form integrated optics components and circuits.

With these goals in mind, we proceeded with the growth of large-area  $\text{Ga}_{1-x}\text{Al}_x\text{As}$  films by the infinite melt technique. In most applications GaAs layers were grown from a melt contained in a quartz crucible heated to about  $850^\circ\text{C}$ . Such layers have been grown in many laboratories. Generally, the layers grown from the undoped melt are p-type with silicon as the major impurity. In our experiments, we have been able to grow layers with p-type carrier concentration less than  $10^{15}/\text{cm}^3$  routinely. However, when we added aluminum to the melt it was soon evident that a quartz crucible was not suitable, since it reacted with the aluminum at a rapid rate (see Table III-2,  $Q_1$  and  $Q_2$ ). We were forced, therefore, to look for alternative materials for crucibles.

One of the simplest of several alternatives is aluminum oxide. High purity aluminum oxide crucibles now are available for semiconductor use. Several of these were purchased and we conducted an extensive series of experiments to evaluate them for the growth of gallium arsenide epitaxial films.

The initial results were very gratifying. Layers of  $\text{Ga}_{1-x}\text{Al}_x\text{As}$  were grown and their electrical properties and chemical composition determined. It was evident from initial experiments that we had to provide for a more sophisticated gas handling and processing system for the crystal growth chambers to eliminate oxidation of the melt due to the addition of the aluminum. A system was modified for  $\text{Ga}_{1-x}\text{Al}_x\text{As}$  crystal growth. A photograph of the system is shown in Fig. III-18. It has a special sample entry chamber which can be independently evacuated and flushed with argon and, subsequently, with high purity hydrogen. Any sample that has to be introduced into the growth chamber must be introduced through this chamber. This eliminates all possibility of contamination of the melt during the long series of runs required to produce a number of samples. As the source melt itself is maintained in a constant flow of ultra-high-purity hydrogen at all times, it remains free of oxide and other contaminants which may be introduced inadvertently during the entry of the substrate into the

**TABLE III-2**  
**Growth of  $\text{Ga}_{1-x}\text{Al}_x\text{As}$  by Infinite Melt Epitaxy**

Melt Number	Composition Weight in Grams	Growth Temperature °C	Epilayer			Mobility, $\text{cm}^2/\text{V-s}$
			Al Concentration Atomic Percent <sup>b</sup>	Layer Thickness, $\mu\text{m}$	Carrier Concentration, $\text{cm}^{-3}$	
Q <sub>1</sub>	Ga = 80 GaAs = 7.5 Al = 0.048	829	0	28	$2 \times 10^{17}$ (p-type)	140
Q <sub>2</sub> <sup>a</sup>	Ga = 80 GaAs = 7.5 Al = 0.048	860	0	29	$4.5 \times 10^{17}$ (p-type)	93
A <sub>1</sub>	Ga = 100 GaAs = 10	840	0	50	$4 \times 10^{16}$ (n-type)	2950
A <sub>2</sub>	Ga = 100 GaAs = 10	860	5	10	$1.5 \times 10^{17}$ (n-type)	1370
A <sub>3</sub>	Ga = 100 GaAs = 10 Al = 0.3	875	14		Data Incomplete	
A <sub>4</sub>	Ga = 100 GaAs = 10 Al = 0.5	876	24	23		

<sup>a</sup> Q<sub>2</sub> is the same melt as Q<sub>1</sub>, but the layer was grown after the melt stayed at temperature for 48 hours longer. Both were grown using quartz crucibles.

<sup>b</sup> Concentration determined by electron microprobe. The values in x units would be twice the atomic percent.

T984

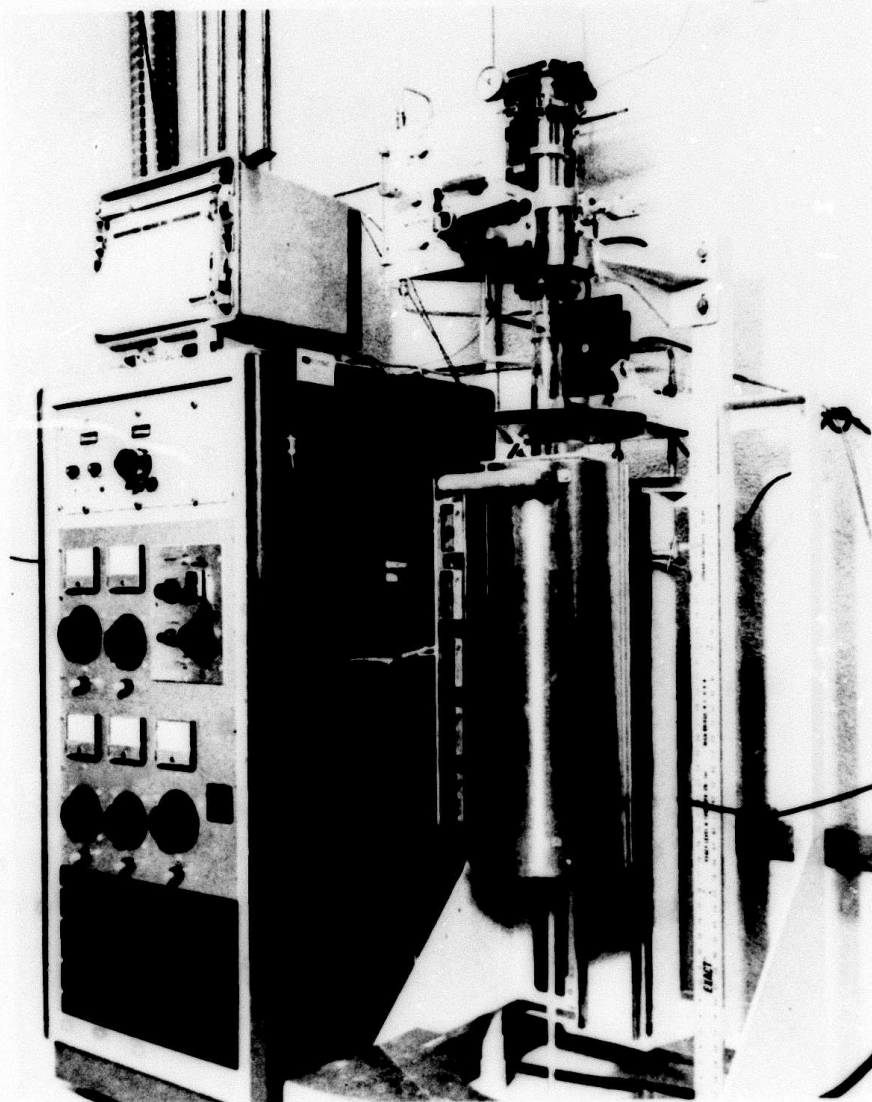


Fig. III-18. Reactor for liquid epitaxy.

chamber. We have observed that over a period of time the melt gets cleaner progressively and then stays extremely clean throughout a long series of experiments.

The growth system was equipped with an Azar recorder-controller backed up by a very sensitive proportional-type controller that allows accurate measurement and control of temperature in a five-zone furnace. We also perfected a programmer that can smoothly vary the rate of temperature change as a function of time. The combination allowed us to study the epitaxial layer growth as a function of the temperature cycle and hence to establish an optimum program for fully reproducible epitaxial layer growth.

Data gathered from the slide-bar assembly experiments were used as a starting point to calculate the concentrations of aluminum and gallium arsenide necessary to obtain layers with different compositions. Table II-2 gives the growth parameters and characterization results for several melts and the properties of crystals grown from them. The first two,  $Q_1$  and  $Q_2$ , refer to layers grown from quartz. It is interesting to note that both these layers show no trace of aluminum in the grown layer. Layer  $A_1$  gave the characteristics of a layer grown from the undoped melt in the aluminum oxide crucible. Since it was a new crucible and an early experiment in a series with aluminum oxide crucibles, the carrier concentration was considerably higher than the method is capable of giving. It is interesting, however, that the layer was well behaved as shown by the mobility. Note that aluminum is absent from the epitaxial layer, even though aluminum oxide crucible was used.

Layers  $A_2$  through  $A_4$  were grown with the addition of aluminum. The values of aluminum concentration obtained by the electron microprobe need to be corrected to take into account absorption caused by gallium arsenide and aluminum. We perfected a computer program which enabled us to do this routinely on our samples. The data given here, however, indicates that the method is dependable and can be used controllably to produce  $Ga_{1-x}Al_xAs$  layers with predictable aluminum concentrations.

The surface of the grown layers is smooth and uniform, and the grown junction is free from imperfections (see Figs. III-19 and III-20).

In summary, by August 1973 we had succeeded in growing a series of layers using the limited melt epitaxy and established the kinetics of growth. Correlation of the parameters of the starting solution, the growth temperature cycle and the layer grown were established. Layers of (GaAl)As with varying concentrations of aluminum were grown using the infinite melt technique. The layers were characterized and shown to be better than those from the limited melt, since they had lower carrier concentration and higher mobility. They were also grown in large-area configurations for possible use as substrates for integrated optics applications.

In parallel with the growth programs we also developed characterization techniques such as Hall measurements and electron microprobe and photoluminescence measurements to determine aluminum concentration profiles; we also developed etching and processing techniques to allow us to study the layers and interfaces by optical examination to determine their crystal characteristics.

Thus, the first phase of the program provided a strong base to the integrated optics materials program.

The second phase covering August 1973 to January 1974 was devoted mainly to accumulating data on epitaxial layers both from the materials characterization and from the waveguide data. In the following sections we give the details of this phase.

M9810

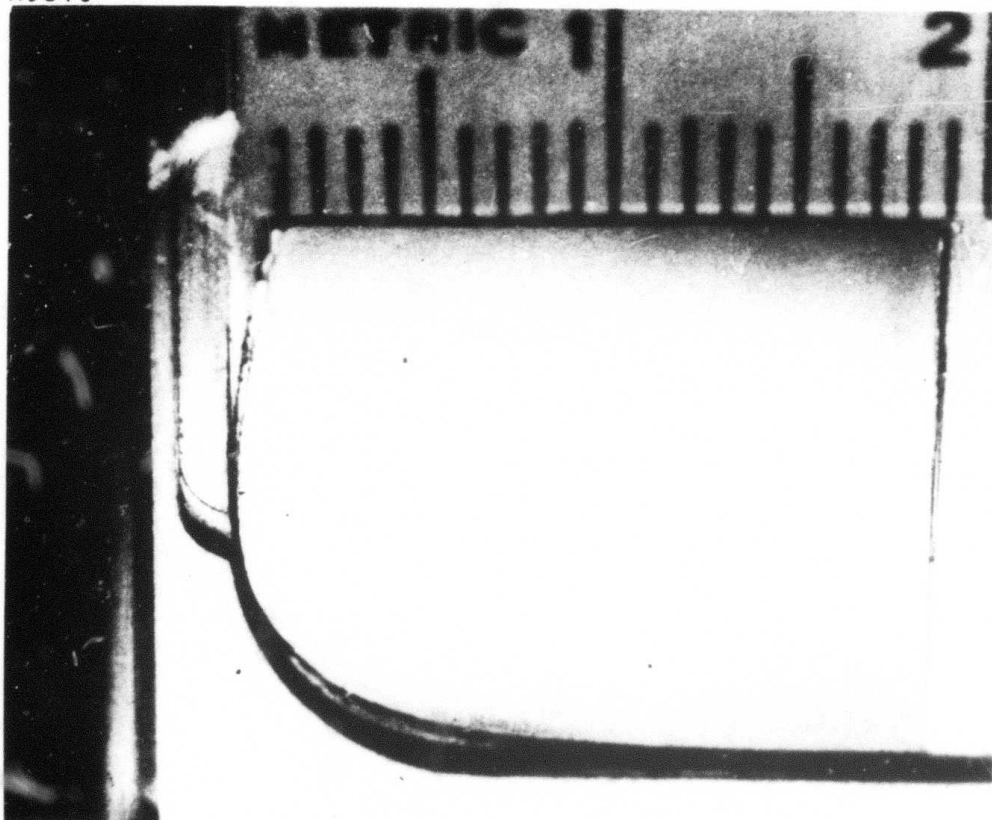
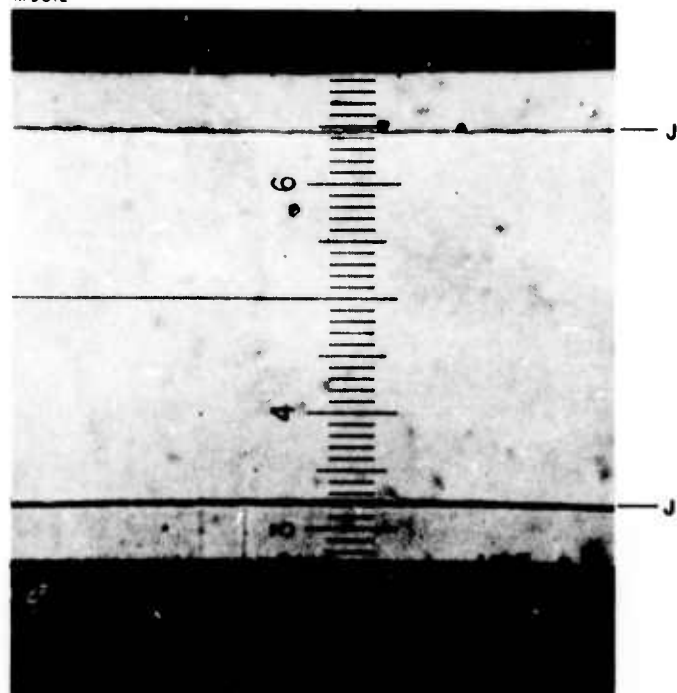


Fig. III-19. Ga<sub>0.95</sub>Al<sub>0.05</sub>As grown by infinite melt melt method. Layer thickness 65  $\mu\text{m}$ . Note the smooth, featureless surface over the entire area.

M9812

2544-12



J - JUNCTION  
A & B SIDES ARE  
BOTH SHOWN

Fig. III-20. Ga<sub>0.95</sub>Al<sub>0.05</sub>As grown by infinite melt method. Thickness 65  $\mu$ m. The two epitaxial layers on the crystals are clearly brought out to show the uniformity of the layers.

#### IV. MATERIALS GROWTH PHASE II - GROWTH AND EVALUATION OF EPITAXIAL LAYERS FOR OPTICAL INTEGRATED CIRCUITS

##### A. Limited Melt Liquid Epitaxy

The system used and the theory behind the technique have been described in the previous section. Several significant improvements were made in our growth system.

1. A transfer chamber was added at the tail end of the growth chamber.
2. The gas flow was altered to minimize contamination.
3. A new graphite assembly made of pyrolytic graphite, incorporating alterations in mechanical design, was used successfully to improve the surface quality of the layers. These steps resulted in improved reproducibility of the layers and also lower impurity levels and smoother surfaces. Details are given below.

The transfer chamber, which is an extension of the quartz growth tube outside the furnace, allows us to move the slide bar assembly into, and out of, the furnace without exposing the graphite to air. The slide bar with the melt, the source and the substrate are placed in the transfer chamber, and the whole tube flushed with hydrogen until all traces of air are removed before the slide bar is pushed into the growth chamber. This has eliminated occasional evidence of oxidation of the melt surface causing bad wiping action and some scratching of the surface of the grown layer. When the slide bar is removed after growth, it is allowed to cool to room temperature in hydrogen before being extracted. This procedure minimized the tailing of gallium over the graphite making it difficult to reuse the slide bar without elaborate cleaning between successive runs. Such cleaning was kept to a minimum in practice, to minimize the risk of contamination. The transfer chamber helped considerably, and the use of pyrolytic graphite has further alleviated the problem.

Another significant improvement in the present system results from optimizing the gas flow pattern in the growth chamber. Provision had been made to introduce both hydrogen and nitrogen into the input side of the tube without interference with each other. The tube is evacuated from the extension transfer chamber so that no gas is ever allowed to flow from the tail end to the front. Provision was also made to supply an independent input of nitrogen to the transfer tube so that it could be filled and evacuated without having to disturb the flow through the main growth chamber.

Apart from using pyrolytic graphite as the slide bar material, the geometry of the melt walls were altered to minimize the travel of the slide bar during the wiping operation. The construction also enabled better registration of the melt cavity with the substrate position, permitting more uniform growth over the whole substrate, and eliminated problems due to uneven growth at the edges of the substrate. The results are shown in the smooth layers shown in Fig. IV-1.

More than a dozen layers were grown using the pyrolytic graphite slide bar assembly. The characteristics of the layer are shown in Table IV-1. The values of thickness of layers obtained is proof of the reproducibility of the process. Thickness control is an essential consideration in the fabrication of single mode waveguides. The quality of the layer can be seen from the carrier concentration, ( $10^{16}/\text{cm}^3$ ), and mobilities in excess of  $4000 \text{ cm}^2/\text{V-s}$  obtained for the epitaxial layers. Since the slide bar method suffers from a large surface-to-volume ratio for the melt in the well, this has to be considered an exceptionally low level of impurity, and the mobility value is a strong indication of the low degree of compensation in the layer. It may be worth mentioning that when graphite containers were used, the first layers obtained show some compensation presumably due to surface impurities. After a series of runs are made with the same graphite piece, the layers stabilized to an "undoped" characteristic as shown in our present series.

2957-10

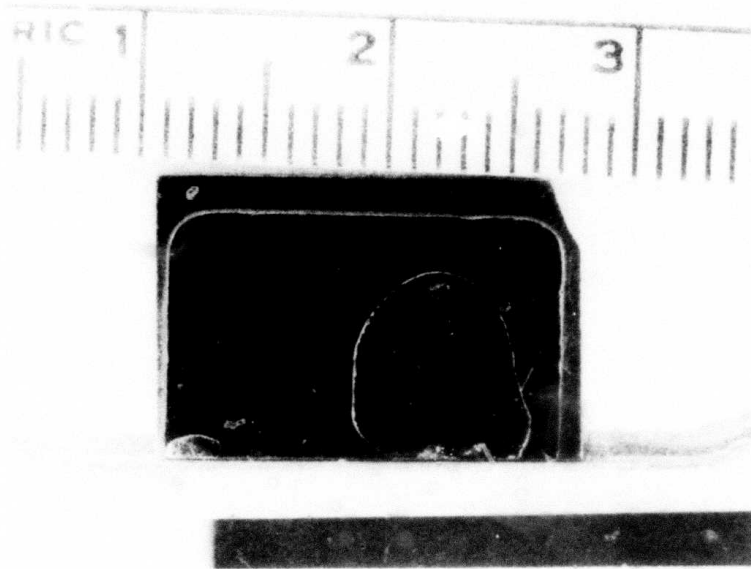


Fig. IV-1. Limited melt liquid epi sample No. 122. Note the smooth surface. The as-grown surface shows a slight amount of residual melt at the right; this problem can be minimized by reducing the gap between the grown layer and the graphite wiping surface.

TABLE IV - 1  
Ga<sub>1-x</sub>Al<sub>x</sub>As Epitaxial Layer (slide bar) Characteristics

Sample No.	Growth Temperature, °C	Thickness, $\mu\text{m}$	Hall Measurement Data		Aluminum Concentration, X
			Carrier Concentration, N/cm <sup>3</sup>	Mobility, cm <sup>2</sup> /V-s	
0112	886	2.9	$1.6 \times 10^{15}$	4600	0.2
0113	886	2.9			
0114	885	2.3	$1.08 \times 10^{16}$	4100	
0120	889	3.5		4200	
0121	888	3.5		4200	
0122	888	4.5	$1.5 \times 10^{16}$	4200	

T1193

Figures IV-2 and IV-3 give a representation of the electron microprobe profile of the layers for aluminum concentration. Figure IV-2 is a profile of the surface and gives an idea of the variation of aluminum concentration inherent to the growth process in our system. This should be compared with the layers made in our early experiment using the old growth system and slide bar assembly. The variation in aluminum concentration has been reduced from  $\pm 15\%$  to  $\pm 6\%$ .

Figure IV-3 is a graphical representation of the aluminum concentration profile in the cross section of the beveled layer. Problems of accurate determination of the profile are complicated by the very thin layers involved. The measurement was made somewhat more convenient by using a beveled layer with  $1^\circ$  angle. The main difficulty is that the shallow angle makes the region, close to the junction, very thin and hence the electron beam penetration, even with low energy, goes beyond the epitaxial layer. Since the volume element seen by the electron beam encompasses an aluminum-free region, corrections have to be made to obtain the true concentration in the epitaxial layer only. The definition of the junction is also somewhat difficult by a simple examination of the x-ray scattering data.

To overcome this problem we decided to start from the surface of the layer at the other end of the bevel and work toward the junction, since the thickness of the layer is independently verifiable. In this procedure, the complication arises due to the processing steps involved. When the bevel is finished it has to be etched chemically to remove the mechanically damaged surface. The etch results in a rounding of the edges of the bevel, making it difficult to pinpoint the top surface of the epitaxial layer during microprobe analysis. We resorted to depositing a thin layer of gold on the top surface before beveling to avoid this problem. It can be seen from the results that for thicknesses in the range of 2 to 3  $\mu\text{m}$ , the slide bar method can produce layers which do not have too severe a gradient in aluminum concentration.

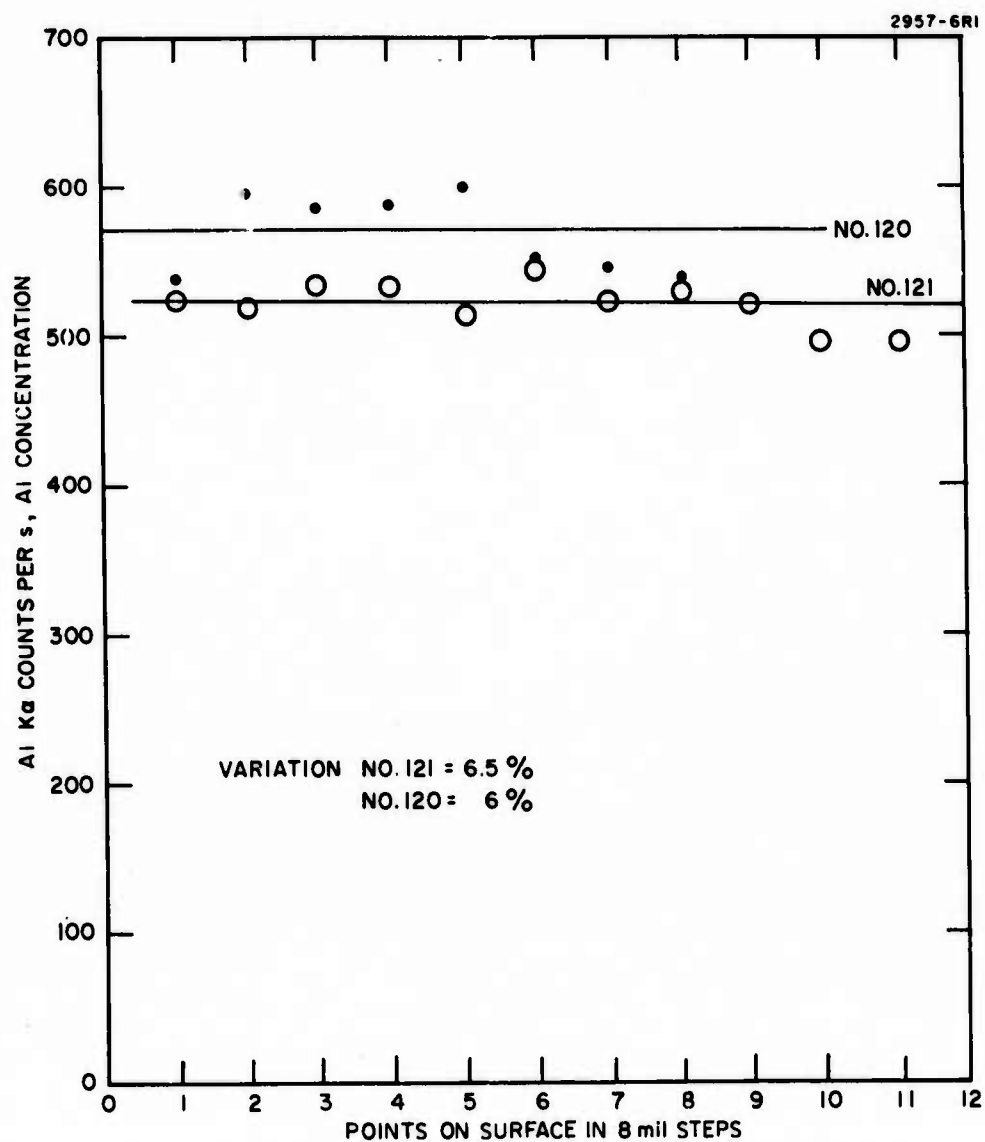


Fig. IV-2. Electron microprobe profile of epitaxial layer surface - limited melt slide bar).

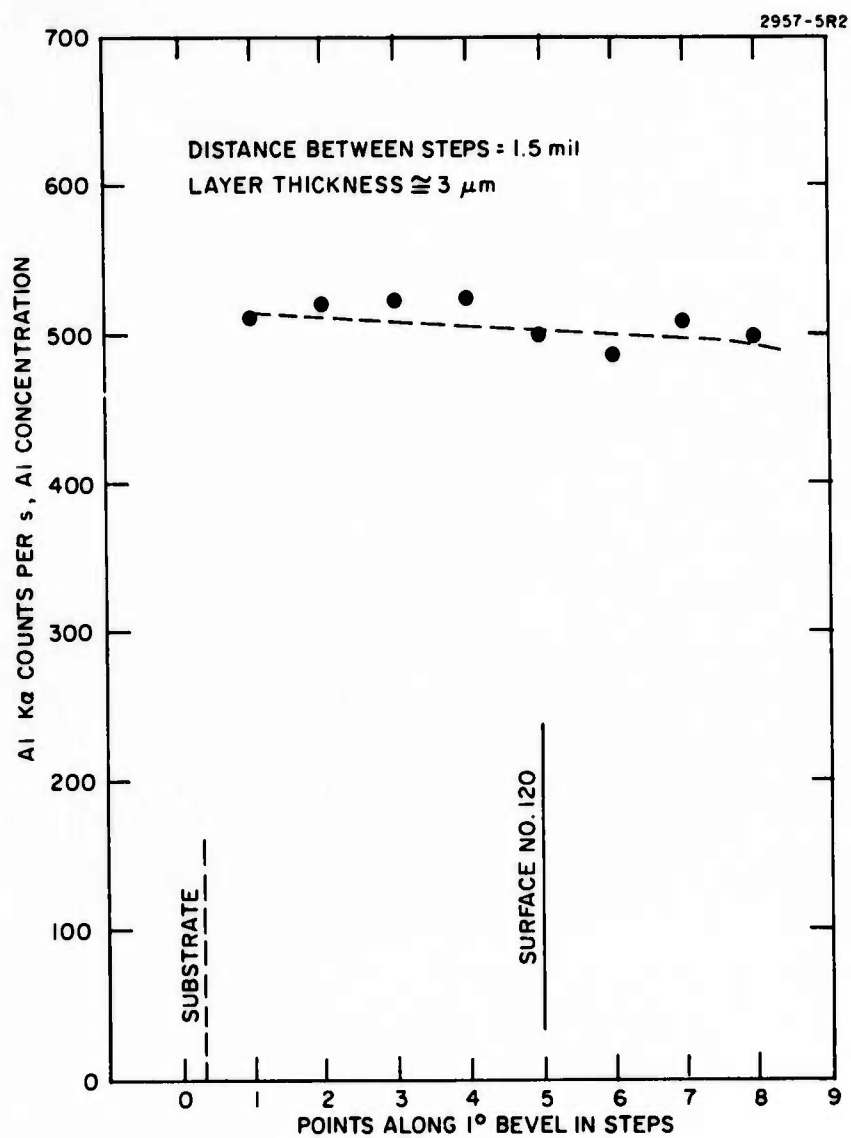


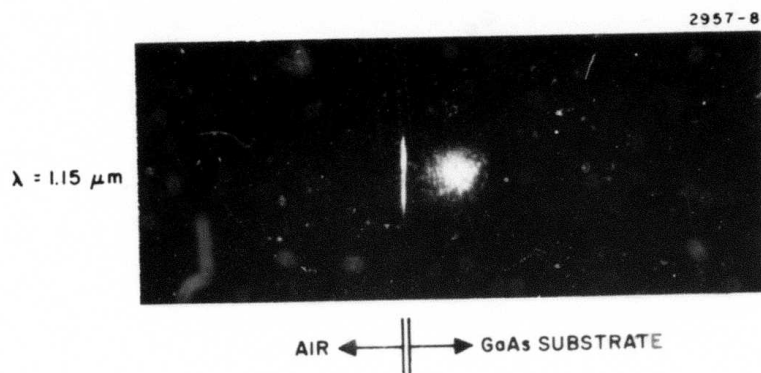
Fig. IV-3. Aluminum concentration profile in limited melt epitaxial layer on a 10° bevel in cross section.

Such measurements are of special significance since we have been able to demonstrate that the epitaxial layer of (GaAl)As grown on GaAs can be used as a waveguide. The result is to be expected if, at the junction, aluminum concentration is highest and then drops off toward the surface; the decreasing aluminum concentration will be reflected in an increasing refractive index in the layer from the junction to the surface. Figure IV-4 shows the transverse intensity distribution of 1.15  $\mu\text{m}$  light being transmitted through such a guide. Since the graded layer is easy to grow, because of the high segregation coefficient of aluminum during growth from solution, we decided to study waveguiding characteristics as a function of the aluminum profile.

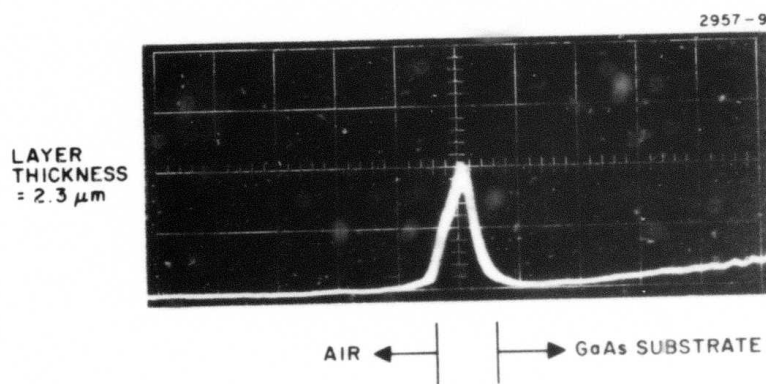
About a dozen layers of (GaAl)As were grown using the new pyrolytic graphite assembly and the improved growth chamber mentioned in the previous paragraphs. These experiments have helped define the growth parameters and processing procedures necessary to optimize layer growth at  $\sim 800^\circ\text{C}$ . Using these as a guide, a few double layers of (GaAl)As also were grown. An example of such a layer is shown in Fig. IV-5. The main improvement over the previous layers is in two aspects. (1) We obtained enough growth data to make "reproducible" layers with well defined aluminum concentration and (2) the use of the pyrolytic graphite assembly made the wiping operation at the end of each growth smooth, resulting in a scratch-free interface and top surface. Both of these are essential for waveguiding applications.

#### B. Infinite Melt Liquid Epitaxy

Using the infinite melt technique, a series of layers of  $(\text{Ga}_{1-x}\text{Al}_x)\text{As}$  were grown with increasing aluminum concentration from a melt maintained in our equipment for a period of over two months. The layers grown varied in aluminum concentration from 4 to 40% in  $x$ , the region of interest to integrated optics. The characteristics of the layers were studied in detail; the results demonstrate



(a) Photograph at cleaved face.



(b) Intensity profile.

Fig. IV-4. Waveguided light in a (GaAl)As layer with graded aluminum concentration.

2957-7

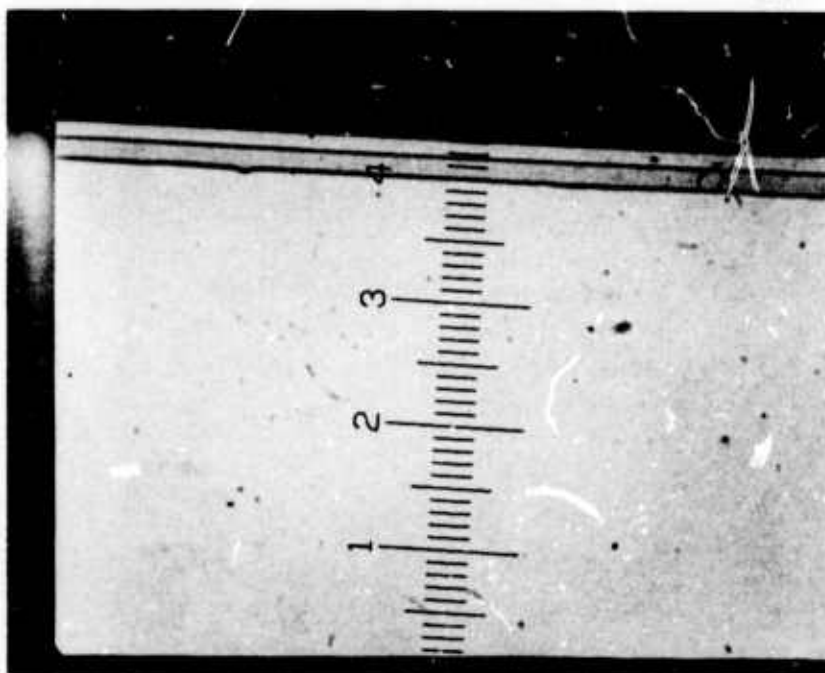


Fig. IV-5. A double layer of  $\text{Ga}_{1-y}\text{Al}_y\text{As}/\text{Ga}_{1-x}\text{Al}_x\text{As}$  grown on GaAs. Scale is  $2\text{ }\mu\text{m}/\text{div}$ . LEPI No. 127.

the versatility and capability of the growth system that we have perfected.

We have given above a detailed description of the use of the infinite melt epitaxial system and the growth of (GaAl)As using  $\text{Al}_2\text{O}_3$  crucibles. The films obtained had a carrier concentration of  $2 \times 10^{16}/\text{cm}^3$  or higher. The layers had a slight orange-peel appearance, especially when viewed under proper lighting. Since the carrier concentration was higher than what we normally obtain for GaAs using quartz crucibles ( $\sim 10^{14}/\text{cm}^3$ ) we decided to improve the growth system to eliminate all possible air leaks. We also proceeded to clean the aluminum oxide crucible more carefully, including a gallium soak to clean the aluminum oxide.

The new growth system proved to be very satisfactory. It has a larger diameter growth chamber that can house an aluminum oxide crucible within a quartz crucible. The drive for rotating the seed has been refined to permit very slow speeds of less than a rotation per minute and the temperature programmer is capable of cooling the melt at the rate of  $0.1^\circ/\text{min}$ . Starting with a melt of approximately 250 g of Ga saturated with GaAs, a series of runs was performed to grow (GaAl)As of increasing aluminum concentration.

The results of the infinite melt growth series are shown in Table IV-2. After a few initial runs to remove the effects of the newly cleaned tube, the layers stabilized in their characteristics to give a carrier concentration below the  $10^{14}/\text{cm}^3$  with good mobility and very smooth surfaces. Tin was added to bring the level of doping to  $10^{15}/\text{cm}^3$ , and it was gratifying to find the measured doping level to match what would be expected from the segregation coefficient of tin in GaAs solution. After the addition of tin, a series of growth runs were made with addition of aluminum every few days to increase the aluminum concentration. The  $\text{Ga}_{1-x}\text{Al}_x\text{As}$  grown covered the aluminum concentration range of  $x = 0.04$  to  $x = 0.4$ , which is of special interest for integrated optics.

TABLE IV - 2  
(Ga<sub>1-x</sub>Al<sub>x</sub>As) Epitaxial Layer Characteristics

Layer No.	Aluminum Concentration, X	Layer Thickness, $\mu\text{m}$	Type	Carrier Concentration, $\text{cm}^{-3}$	Mobility, $\text{cm}^2/\text{V-s}$
19	0.04	47	p	$5.5 \times 10^{13}$	310
20	0.04	56	p	$9.0 \times 10^{13}$	319
28	0.07	38	n (Sn)	$2.0 \times 10^{15}$	4338
32	0.07	56	n (Sn)	$2.5 \times 10^{15}$	4652
41	0.13	51	n (Sn)	$2.0 \times 10^{15}$	2979
47	0.40	13	n (Sn)	$8.0 \times 10^{14}$	1724
49	0.40	21	n (Sn)	$3.5 \times 10^{15}$	1840

T1194

Several facts can be seen easily from the data in the table. The carrier concentration stayed very uniform and reproducible over a period of about 1 month, while aluminum concentration was being progressively increased. The quality of the layers, as given by the Hall measurements, was consistent with what should be expected. The layer quality as evidenced by surface examination and study of the cleaved edges is uniform, smooth, and defect-free. The absorption edge measured for the (GaAl)As agrees with that calculated from the aluminum concentration obtained by the electron microprobe. These results are very significant and provide the capability of the infinite melt technique to produce layers that have the quality necessary for large area substrates for integrated optics applications.

One other noteworthy improvement was achieved using the improved seed rotation capability built into the new system. It had been observed, when the GaAs layers were grown with the seed stationary, that the surface has submicron contour lines at the surface. These appear to be growth features caused by a steady-state pattern in the melt that results in a growth variation at various points on the substrate surface. In the case of (GaAl)As, this is further aggravated by a slight orange-peel effect. We introduced the rotation of the seed as a way to eliminate static conditions in the melt and also to avoid any possible depletion of aluminum at the growth front due to the high segregation coefficient of aluminum. The layers obtained with the seed rotation have smooth surfaces with no contour lines. A study of the cleaved cross section indicates that the variation of thickness in a 1-in. long substrate is also reduced below the 10% that normally is observed on a nonrotated substrate.

With the improvements described in the previous paragraphs, the infinite melt system is capable of producing excellent (GaAl)As layers of over  $6 \text{ cm}^2$  with good control of thickness, carrier concentration and surface finish. The next step is to design a multicrucible system that can grow several layers in succession.

Some electron microprobe measurements have been made on the (GaAl)As layers grown by the infinite melt method. The results are shown in Figs. IV-6 and IV-7.

It can be seen from Fig. IV-6 that the surface variation of aluminum concentration is  $\approx 5$  to 6% for samples 41 and 61. Neglecting one or two extreme points in each case, the variation is even less,  $\approx \pm 2$  to 3%. This is well within the errors of measurement using the microprobe for the type of surface involved. When the slide bar epitaxial layer is thin enough and the central areas of the layer are examined we see that these layers are almost as good as the infinite melt layers. However, the variations are more random and the electrical properties in Tables IV-1 and IV-2 show the difference in quality even in these cases.

Figure IV-6 shows the variation of aluminum concentration on a bevel without the corrections mentioned in the previous section for the junction region. The bevel in this case is a  $3^\circ$  one, however, and this reduces the error, and the profile is more amenable to measurement. It is interesting to note that within the limits of the technique the infinite melt technique can produce 50  $\mu\text{m}$  thick layers with an almost invariant aluminum concentration in the cross section of the layer. If we compare the measurements with our previous ones, the present samples are seen to have a smoother profile. This comes primarily from using a larger melt and also including rotation of the substrate at a controlled rate during growth. The results support our thesis that good substrate layers of (GaAl)As, with compositional uniformity and homogeneity and with smooth surfaces, can be produced by the infinite melt technique. These substrates can be used for monolithic technology in integrated optics, a necessary step if the full benefits of the new field are to be realized. The quality of the layers is further emphasized by the excellent bulk properties shown in Table IV-2 for impurity concentrations and carrier mobilities.

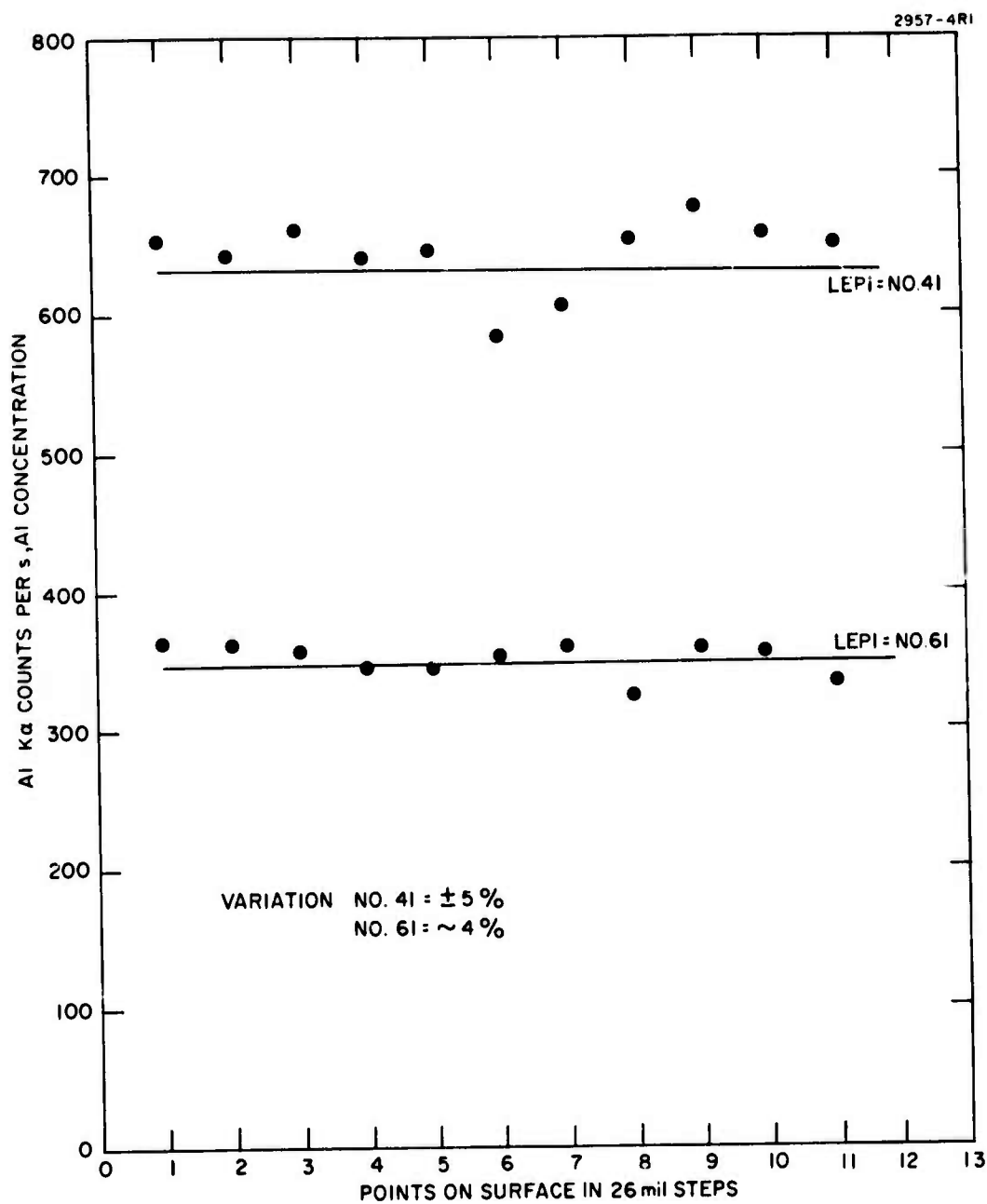


Fig. IV-6. Aluminum concentration profile on  $\infty$  melt LEPI layers (surface of epilayer).

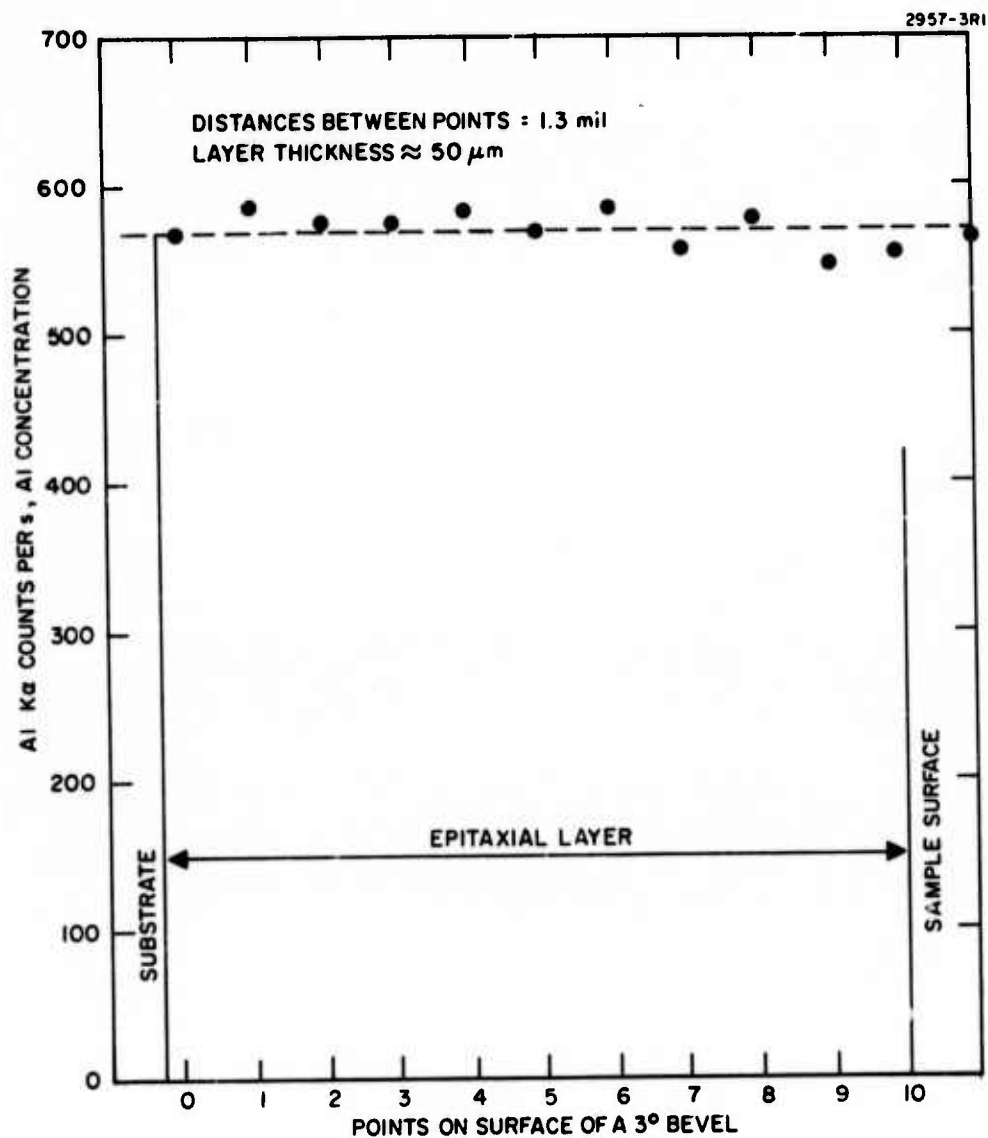


Fig. IV-7. Aluminum concentration profile in  $\infty$  melt liquid epitaxial layers on a 30° bevel in cross section (LEPI No. 41).

In summary, a significant achievement during this period was the progressive improvement of our understanding of the relationship between the layer growth parameters (such as the temperature cycle for growth, the surface preparation prior to epitaxy, and the role of supersaturation of the source melt) and the heterojunction characteristics. By studying the electron microprobe data on Al concentration in the epilayer, we were able to optimize the growth parameters to produce a series of layers with aluminum concentrations ranging from 0 to 20% (atomic) in aluminum. In parallel with achieving this control over composition, we also optimized the processing of the substrates to yield good even heterojunctions and surfaces to permit efficient optical waveguiding. At the end of the second phase we were in a position to produce (GaAl)As epitaxial layers with optical attenuation coefficients of approximately  $1 \text{ cm}^{-1}$  matching the state of the art in the literature.

In the third phase of the program we have succeeded in fine tuning the epitaxial layer growth techniques to improve layer perfection and aluminum profile control to reduce the attenuation to less than  $0.2 \text{ cm}^{-1}$  and produce large area layers that provide waveguides of larger dimensions to permit optical loss measurements to be made more accurately. The details of the program in the various areas of epitaxial growth are given in the next section.

## V. MATERIALS GROWTH PHASE III - OPTIMIZATION

### A. Limited Melt Liquid Epitaxy

The major emphasis during the last seven months has been on improving the limited melt techniques. We have investigated three growth temperatures to grow the (GaAl)As layers -  $880^{\circ}\text{C}$ ,  $840^{\circ}\text{C}$ , and  $800^{\circ}\text{C}$ . Table V-1 gives the growth data. It can be seen from the table that the rate of the growth of the layer increases at the higher temperature and the aluminum concentration in the layer goes down. The aluminum concentration is affected by the segregation coefficient of aluminum from a gallium solution; the coefficient decreases between  $800^{\circ}$  and  $880^{\circ}$ , so that at the higher temperature the layers are ~50% lower in aluminum concentration when the growth solutions have the same concentrations. The lower temperature of growth has some advantages. First, the growth rates are slower and all reactivities, including that of aluminum, are lower; hence problems due to low level ambient impurities in the growth system are reduced. Second, spurious nucleation and dendritic growth in and around the substrates due to high energy nucleation sites is reduced. As a result, the epitaxial growth can be restricted to the substrate. Because of these advantages, we have preferred to do most of our recent work at the low temperature.

The characteristics of the layers grown are further proof of the differences between the two temperatures of growth (see Table V-2). It can be seen from the data that the growth rate increases with increasing temperature in a systematic fashion. The aluminum concentration in the layer, on the other hand, increases as the temperature is lowered. This is to be expected, since the segregation coefficient of aluminum increases with decreasing temperature. Then we see that starting with initial melts of the same aluminum concentration, the aluminum concentration in the grown layer goes up almost 50% (5% to 7.5%) with the temperature of growth dropping from  $880^{\circ}\text{C}$  to  $800^{\circ}\text{C}$ .

TABLE V - 1  
(GaAl)As Growth Rate as a Function of Temperature

Sample No.	Growth Temperature, °C	Time Grown, Min	Cooling Rate, °C/min	Layer Thickness, $\mu\text{m}$	Growth Rate, $\mu\text{m}/\text{m}$
121 <sup>a</sup>	889	10	0.6	3.5	0.35
122 <sup>a</sup>	889	10	1.0	4.5	0.45
132	888	20	1.0	Layer nonuniform	
147	885	10	1.0		
149	884	10	1.0	10.0	1.0
153	842	5	0.85	2.3	0.5
154	842	5	0.85	2.3	0.5
192	840	20	0.6	11.0	0.55
175	806	20	0.5	5.0	0.25
185	807	20	0.6	4.5	0.23
189	806	20	0.6	5.0	0.25
190 <sup>b</sup>	806	20	0.6	4.5	0.23

<sup>a</sup>Solution not supersaturated. Note decrease in growth rate.

<sup>b</sup>Solution saturated for 60 hours as against 4 for other experiments. (See text.)

T1500

TABLE V-2  
Epitaxial Layer Characteristics  
 $\text{Ga}_{(1-x)}\text{Al}_x\text{As}$  as a Function of Growth Temperature

Sample No.	Temperature of Growth, $^{\circ}\text{C}$	Al Concentration $x$	Carriers, $\text{n cm}^{-3}$	Hall Mobility, $\mu\text{-cm}^2/\text{V-s}$
121	889	0.2	$1.4 \times 10^{16}$	4000
122	889		$1.6 \times 10^{16}$	
147	885	0.1		
192	840	0.15	$7 \times 10^{16}$	2000
175	806	0.28		
189	807	0.3	$4.8 \times 10^{16}$	1500

T1501

We have characterized several of the epitaxial layers by Hall measurement. It is significant that the carrier concentration in the grown layers increases slightly as the temperature of growth is reduced. This is somewhat contrary to what would be normally expected, since one would expect the reactivities of all components in the system to be lower at the lower temperature. However, this factor is outweighed by a separate consideration; the slide bar method has a large surface-to-volume ratio for the reactive melt. Under operating conditions, apparently, there are enough n-type impurities normally present in the system and the melt tends to produce n-type layers. With long hold times at somewhat elevated temperatures, these impurities can be driven out and the impurity concentration reduced. We have confirmed such a possibility using our infinite melt system. It is the presence of these residual impurities in the system that cause the n-type characteristics of the epitaxial layer. It is obvious from this point of view that at elevated temperature the n-type impurities will be reduced and a lower carrier concentration will result.

Early in this optimization phase of our program we observed waveguiding in single layers of (GaAl)As grown on GaAs. Since they were grown on GaAs which has a higher refractive index, we had to assume that the confinement of the wave was due to high aluminum concentration at the heterojunction. We therefore instituted a detailed investigation of the aluminum concentration in the cross section of the grown layer using the electron microprobe, paying particular attention to the concentration in the region of the GaAs-(GaAl)As interface. To observe the profile in detail, the layer was beveled at a  $1^\circ$  angle. The bevel was examined using an electron beam such that each step was effectively  $0.2 \mu\text{m}$  in layer cross section. A typical profile of aluminum concentration obtained in this fashion for one sample (0147) is given in Fig. V-1. The aluminum peak in concentration at the heterojunction is clearly visible. The peak is not clearly visible in some of the other profiles measured, such as that for sample (0175) in Fig. V-2, because (1) the measurements must be done very carefully on samples

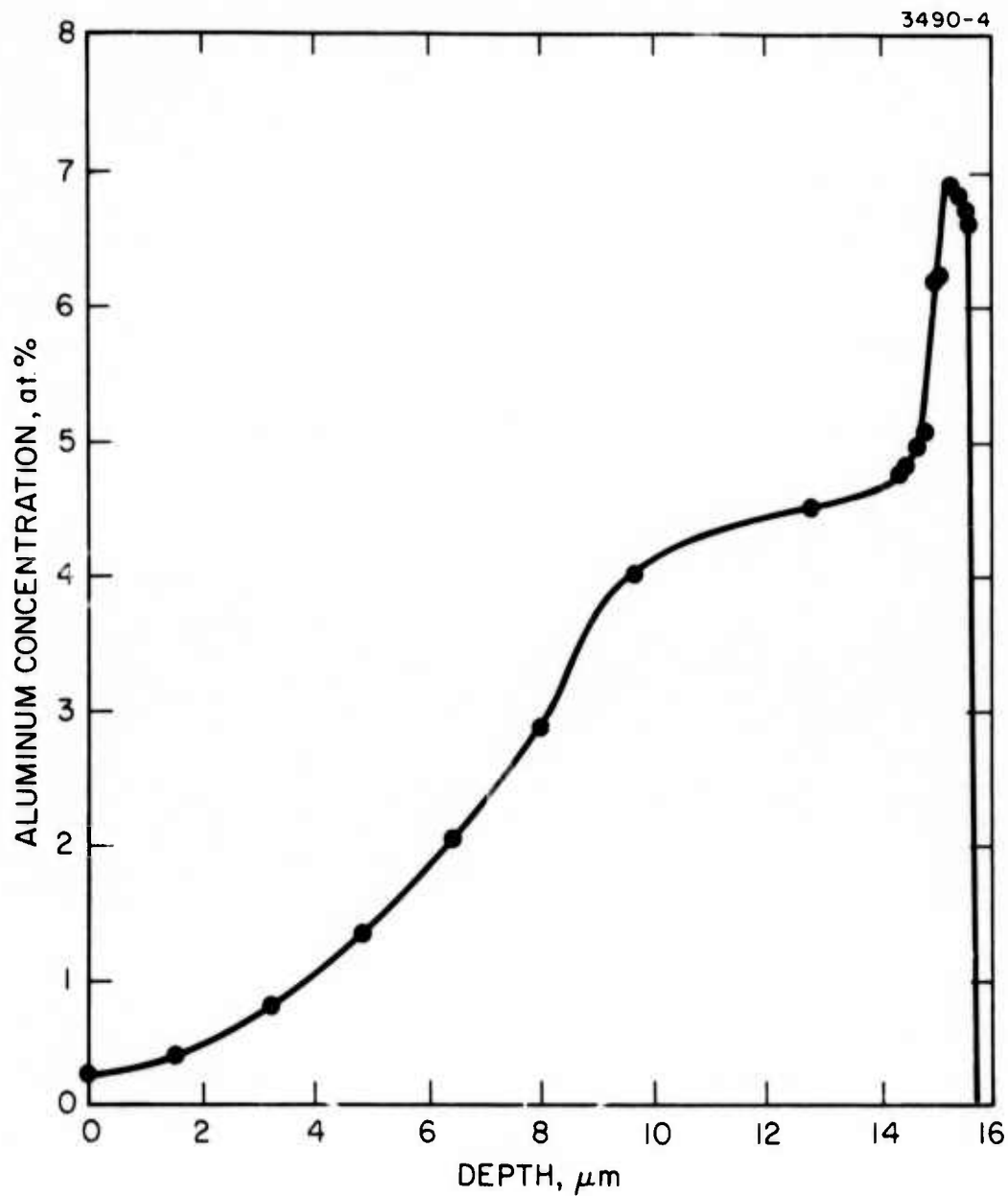


Fig. V-1. Al concentration profile of graded (GaAl)As waveguide sample (0147).

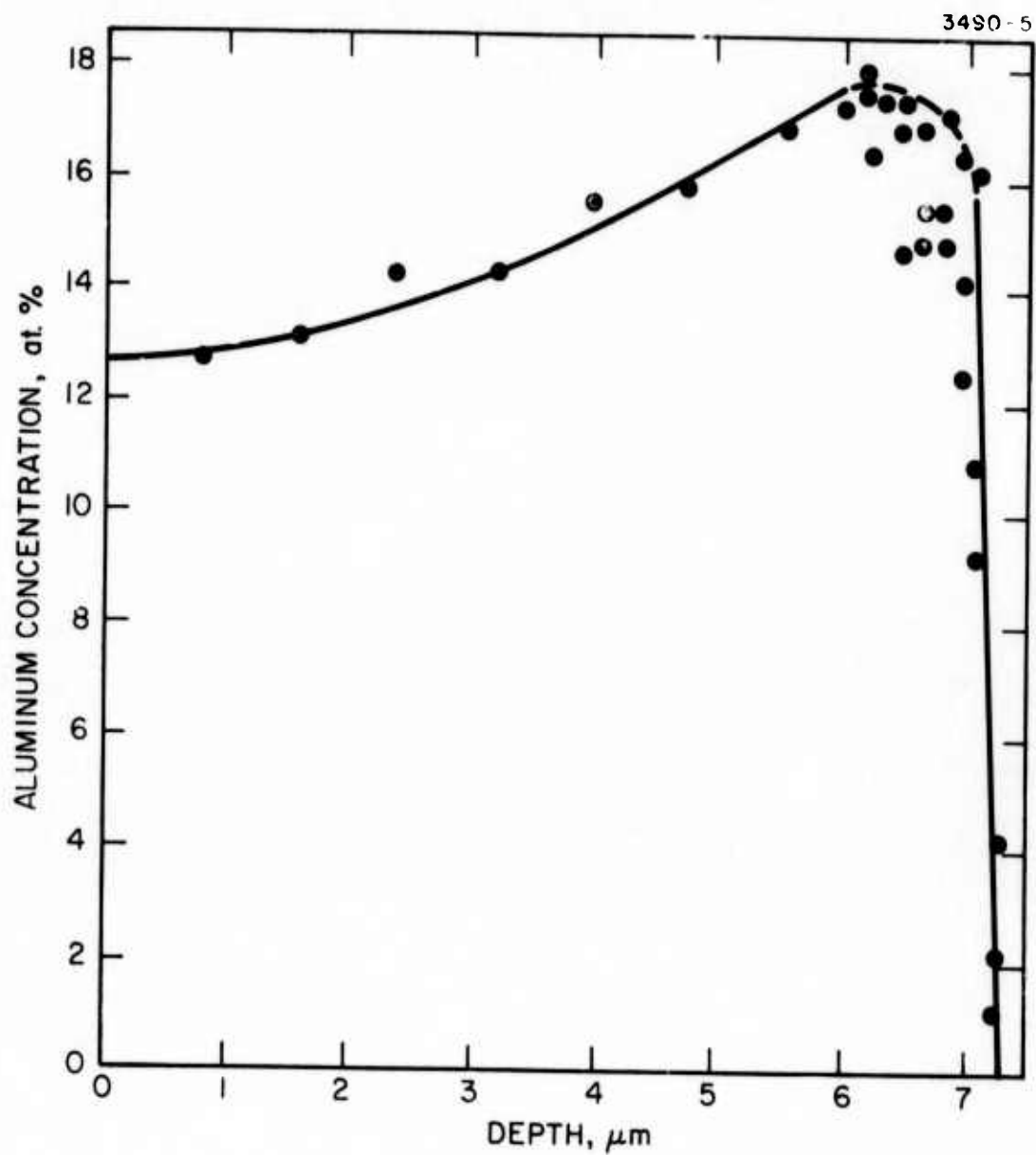


Fig. V-2. Al concentration profile of graded (GaAl)As waveguide sample (0175).

that are properly cleaned and etched to prevent a smearing of the junction when beveling is done, and (2) since the electron beam penetrates about  $4500 \text{ \AA}$  at 7.5 kW primary electron energy (the radiation used in our experiments), the beam sees not only the epilayer, but also a part of the GaAs substrate in the region at the heterojunction. The aluminum concentration then has to be corrected to take into account this factor. When this is done, the peak should be visible in the samples where waveguiding occurs.

The electron microprobe data for the low temperature ( $804^{\circ}\text{C}$ ) layers show a somewhat greater gradation than the early higher temperature ones. Since the waveguiding is not adversely affected by the graded nature, we have not attempted to smooth out the profile.

#### B. Double Layers of (GaAl)As

Since a single layer of (GaAl)As was sufficient to permit waveguiding, most of the optical experiments described in this report were conducted using single layers. However, we felt it would be desirable to grow some double layers with the second layer having higher aluminum concentration than the first. Such a procedure should permit the confinement of the wave between the high aluminum concentration region at the GaAs-(GaAl)As interface described before and the lower refractive index-high aluminum concentration top layer. We have determined that, when properly made, the top GaAs-(GaAl)As interface provides a better confining surface than a (GaAl)As-air interface. An example of the properties of layers grown in this fashion is given in Table V-3, and the electron microprobe data for a typical sample (0171) are shown in Fig. V-3.

#### C. Infinite Melt Liquid Epitaxy

In previous reports we have described our infinite melt epitaxial system in detail. Large area (GaAl)As layers of  $>4 \text{ cm}^2$  have been grown by the technique with aluminum concentrations up to

M10498

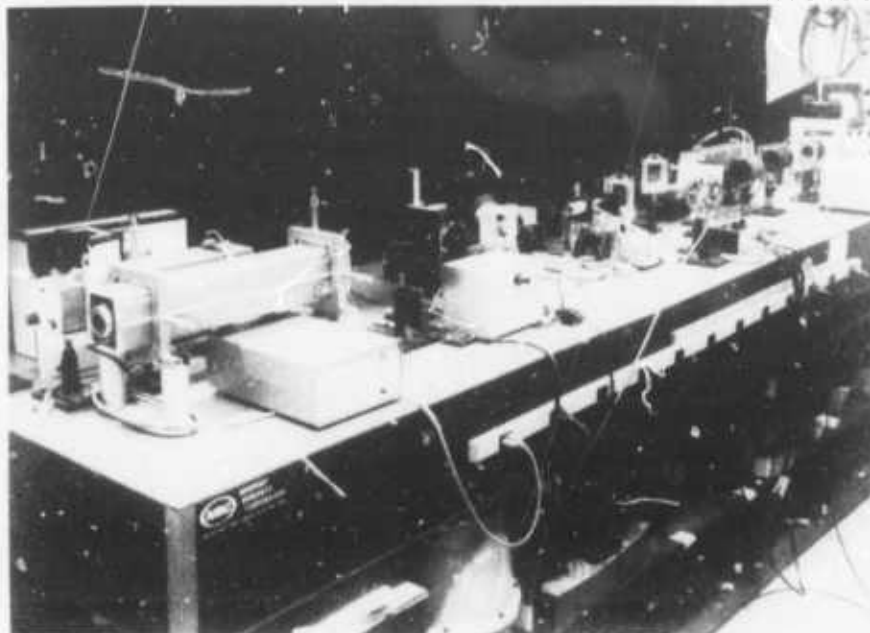


Fig. VI-2. Experimental setup for laser/waveguide alignment and optical measurements.

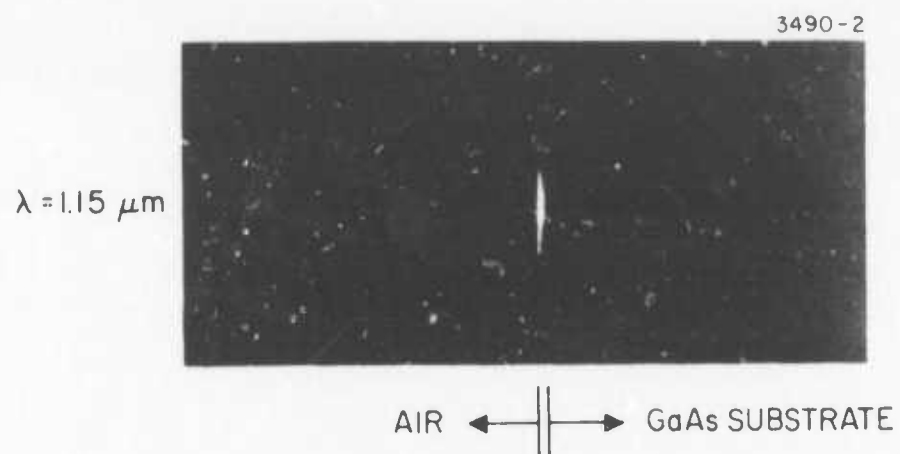
rotating mirror to produce a real time display of optical power density versus distance (y) transverse to the waveguide. Figure VI-3 is such a display for a single layer (GaAl)As waveguide with a thickness of 6  $\mu\text{m}$ . In this case only a single TE mode was propagating in the waveguide. The complete experimental setup is more elaborate than the basic system shown in Fig. VI-1 and includes two 6328  $\text{\AA}$  He-Ne lasers for alignment, a lens and Polaroid camera for photographing the image converter output, and an optical microscope for viewing the sample. Alignment of the waveguide and the focusing lens is accomplished by means of three micropositioner mounts shown in Fig. VI-4. The micropositioners are capable of x-y-z linear motion, rotation and tilt.

A Tropel piezoelectric micrometer head allows extremely accurate control of linear motion (a mechanically adjustable range of 2.5 cm with an electrical fine adjustment of 4  $\mu\text{m}$  at a rate of 0.004  $\mu\text{m}/\text{V}$ ).

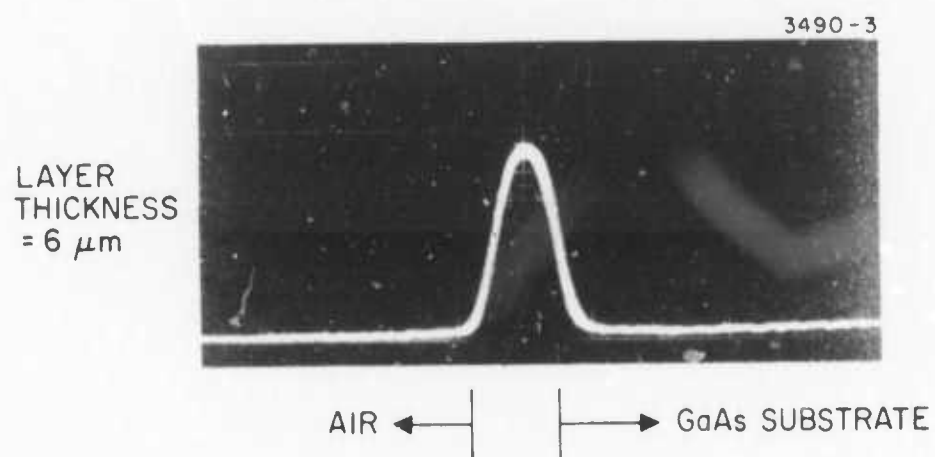
Attenuation in a waveguide can be determined by coupling to waveguides of different length and measuring the optical output from the waveguides. This procedure yields a curve of relative transmission versus waveguide length such as that shown in Fig. VI-5, which was measured for waveguides cleaved from sample 0175. The attenuation coefficient  $\alpha$  is calculated from the slope of the curve according to the relation

$$\alpha = \frac{\ln \left( \frac{P_1}{P_2} \right)}{X_2 - X_1}$$

where  $P_1$  and  $P_2$  are the relative emitted optical powers from waveguides of length  $X_1$  and  $X_2$  ( $X_2 > X_1$ ). The fact that the points lie on a straight line as in Fig. VI-5 indicates that the coupling coefficient remained constant from waveguide to waveguide. (The departure from linearity at lengths greater than 5 mm for the data shown was caused by aperturing and is not related to waveguide loss.)



(a) PHOTOGRAPH AT CLEAVED FACE



(b) INTENSITY PROFILE

Fig. VI-3. Waveguided light in a graded (GaAl)As layer.

M10499

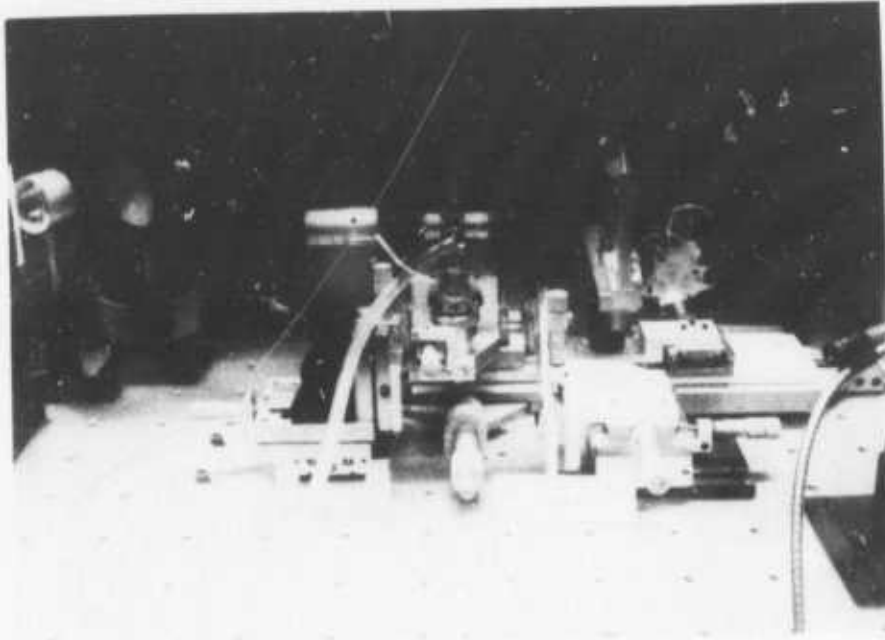


Fig. VI-4. Micrometer adjusted alignment fixtures.

TABLE V-3

Double Layers of  $\text{Ga}_{1-x}\text{Al}_x\text{As}$ 

Sample No.	Growth Temperature $^{\circ}\text{C}$	Time, Min	Cooling Rate, $^{\circ}\text{C}/\text{min}$	Growth Rate, $\mu\text{m}/\text{min}$	Al Concentration $x$
171 Layer 1	806	10	1	0.5	0.16
Layer 2	796	10	1	0.4	0.30
157 Layer 1	845	5	1	0.92	0.48
Layer 2	840	6	1	0.87	0.24
Layer 171 grown with the first melt having 1/2 the Al of the second.					
Layer 157 grown with the second melt having 1/2 the Al of the first.					

T1502

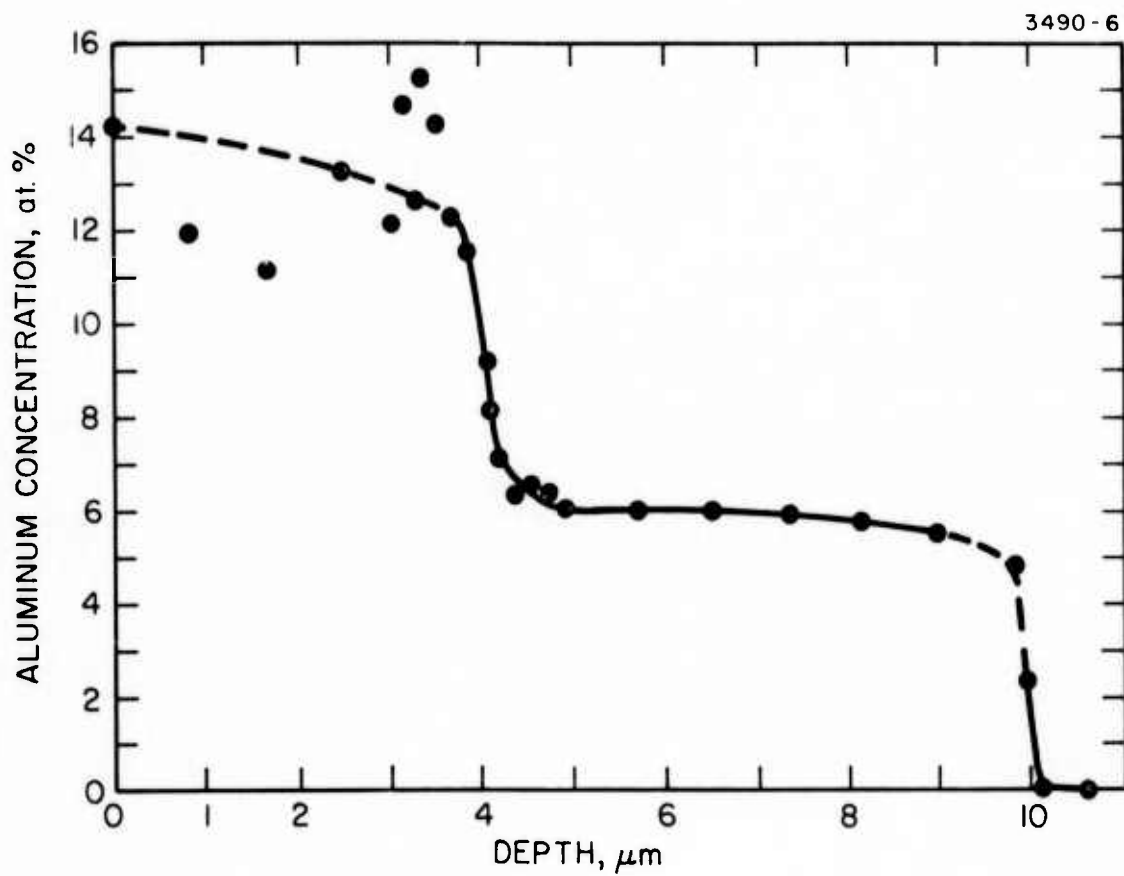


Fig. V-3. Al concentration profile in double layer waveguide sample (0171).

$x \leq 0.5$  for integrated optics applications. The original idea was to use these for substrates for monolithic integrated circuits. The quality and characteristics of the layers have been found to be eminently suitable for this application. Since the single layers grown by limited melt slide bar technique were found to be suitable for waveguiding, we felt it would be desirable to try similar experiments with our infinite melt layers. Cleaved pieces of the layers were accordingly fabricated. The samples used and their characteristics are described in Table V-3. It has been shown that they are capable of guiding. This suggests new approaches which may simplify the technology for producing integrated optics devices in some cases. It may be unnecessary to grow a second layer of  $\text{Ga}_{(1-y)}\text{Al}_y\text{As}$  on a layer of a different aluminum concentration  $\text{Ga}_{(1-x)}\text{Al}_x\text{As}$  for several simple device assemblies. Instead by using alternative techniques of etching, masking, diffusion and ion implantation presently available, simple circuit assemblies can be fabricated on single layers of  $(\text{GaAl})\text{As}$  that are easily grown by our infinite melt technique on  $\text{GaAs}$  substrates. We intend to pursue this approach in our future plans.

In summary we have grown  $(\text{GaAl})\text{As}$  layers of  $\text{GaAs}$  by both limited melt and infinite melt epitaxy and demonstrated that both methods are capable of producing layers of adequate quality for integrated optics application. Single layers of  $(\text{GaAl})\text{As}$  grown on  $\text{GaAs}$  are shown to provide good confinement and hence act as waveguides with acceptable characteristics for use in device fabrication, and a model has been postulated to explain the confinement in a single layer of  $(\text{GaAl})\text{As}$  grown on  $\text{GaAs}$ .

#### D. The Two-Liquid Epitaxial Techniques: A Critique

A critique of the two methods — limited melt and infinite melt — would be instructive in the light of our experience and results.

The limited melt technique has advantages for feasibility studies since it uses small melts that can be discarded after each growth, and experiments can be conducted in a short time to prove

research feasibility for various devices. However, its use is severely limited by the large surface to-volume ratio of the growth matrix that minimize purity of the layer that can be grown. We see that the  $10^{16}/\text{cm}^3$  is a realistic level of background impurities that can easily be obtained, although by careful handling and long-heating cycles the level could be reduced to  $\sim 5 \times 10^{15}/\text{cm}^3$ . Problems of purity are especially severe when corrosive elements such as aluminum have to be used.

In applications where the impurity levels of this magnitude are satisfactory, the method still has other disadvantages. Since there is no easy way to stir the melt to cause homogeneity, the melt never really reaches a totally homogeneous condition. Rather, it establishes a certain concentration profile in the melt volume over the source wafer that is conditioned by the temperature and the time for which the melt is allowed to homogenize largely by diffusion. The geometry of the well and its location in the slide bar as well as the temperature cycle all influence the rate at which the homogenization occurs. Since GaAs and aluminum have different mixing characteristics with gallium, the exact nature of the melt with all three components is even less fully predictable. By using ingenious techniques, such as placing source materials on top and bottom of the melt and cycling temperatures, improved mixing can be promoted. Ultimately, however, the optimum procedure has to be purely empirically established for a specific goal and "reproducibility" of the system is purely operational and not theoretically predictable on a simple model. Thus we see in our own experiments we use a source saturation of the melt for a certain number of hours, a fixed cycle for growth and we end up with layers which are comparable in properties.

Even if we were to fully homogenize the melt, problems arise when we move it over to the substrate to start growth. At this point aluminum, for example, tends to segregate into the grown layer depleting the melt immediately above it. This results in a lower concentration in the layer grown subsequently. The aluminum now has to

be supplied to the melt from regions farther away and the profile in the epitaxial layer would be determined by the segregation coefficient and the ability of the melt to replenish the aluminum as growth progresses. Needless to say, combination of the considerations above limits layer growth with controlled properties within certain ranges to be established for each system as a function of the components involved and the geometry of the slide bar.

The arguments above can be clearly seen by looking at some typical examples. In Table V-1, sample 190 was grown from a melt saturated with GaAs for 60 hours at growth temperature. It used up almost all the source (~0.3 g). In the other experiments at the same temperature, samples 175 to 189, the saturation times were only 4 hours, the source was used up only ~50% and yet the growth parameters and layer properties are almost identical. The amount of GaAs necessary to saturate the 5 g gallium used is about 0.35 g as ascertained from the values in the literature as well as from our own experiments in the infinite melt system.

The infinite melt system overcomes most of those problems, since the growth matrix can be maintained uniform with predictable properties. Large area layers with controlled characteristics can be grown with a minimum of effort. The main disadvantage is the lack of flexibility in the parameters of the system. When a large melt is made up to a specification, prior experiments must already have provided a good indication of the composition to start, since otherwise it may be difficult to change the melt easily. However, if the melt is made up for a specific application, it will yield reproducible layers with a minimum of time and effort and with very good homogeneity and crystal perfection.

The best combination would then seem to be the ability to use the two techniques in a complementary fashion. The limited melt epitaxy should be used for preliminary experimentation to establish optimum composition, impurity levels and temperatures of operation. These should be later refined and put on a sound basis to grow

reproducible layers with controlled properties from the infinite melt system. We have demonstrated in the case of the integrated optics field such a procedure is fully consistent with practical demands of waveguide fabrication.

## VI. OPTICAL WAVEGUIDE EVALUATION

Measurements of the chemical and electrical properties of (GaAl)As layers grown under this program, which have been described in the previous sections, have demonstrated that the layers have Al concentration profiles and low carrier concentrations as desired for optical waveguides. However the final test of their suitability lies in actually using them as waveguides for light of the desired wavelength. Therefore, the optical waveguiding properties of (GaAl)As layers grown under this program have been measured and evaluated with respect to mode shape and attenuation. To facilitate measurements a He-Ne laser source ( $\lambda = 1.15 \mu\text{m}$ ) was used. This collimated source can be easily coupled to the waveguide under test by directly focusing the beam onto a cleaved end face of the sample. (The focused spot size was approximately  $5 \mu\text{m}$ .) Although all of our measurements were made with  $1.15 \mu\text{m}$  light the results can be easily extrapolated to the  $0.85 \mu\text{m}$  wavelength emitted by a (GaAl)As diode such as would be used in an optical integrated circuit. The Al concentration in all of the samples tested was sufficient ( $x > 10\%$ ) to displace the absorption edge to shorter wavelength so that there is little difference between absorption at  $1.15 \mu\text{m}$  and that expected at  $0.85 \mu\text{m}$ .

The basic experimental setup used to determine waveguided optical mode shape or power density distribution and optical attenuation is diagrammed in Fig. VI-1 and shown in the photograph of Fig. VI-2. The He-Ne laser source ( $\lambda = 1.15 \mu\text{m}$ ) is coupled to the waveguide undergoing evaluation by focusing the beam onto a cleaved face of the sample with a microscope objective lens. A second lens of this type is used to image the output face of the sample alternatively onto either an image converter tube for visual observation of the guided mode or onto a rotating plane mirror for quantitative measurements. This rotating mirror scans the image of the optical mode across a slit-masked Ge detector. The signal from the detector is amplified and monitored on an oscilloscope with its sweep synchronized with the

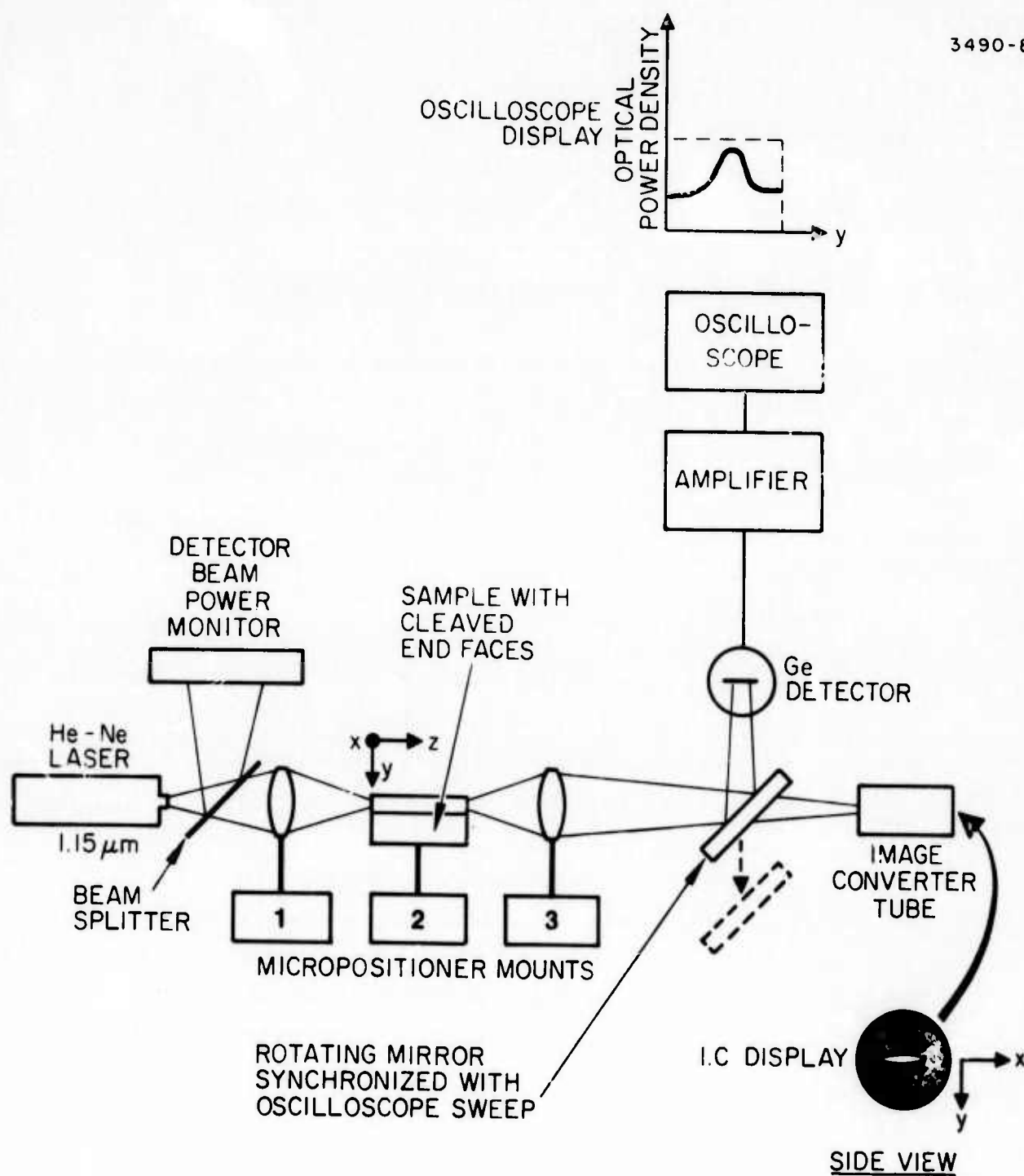


Fig. VI-1. Experimental setup for waveguide alignment and optical measurements.

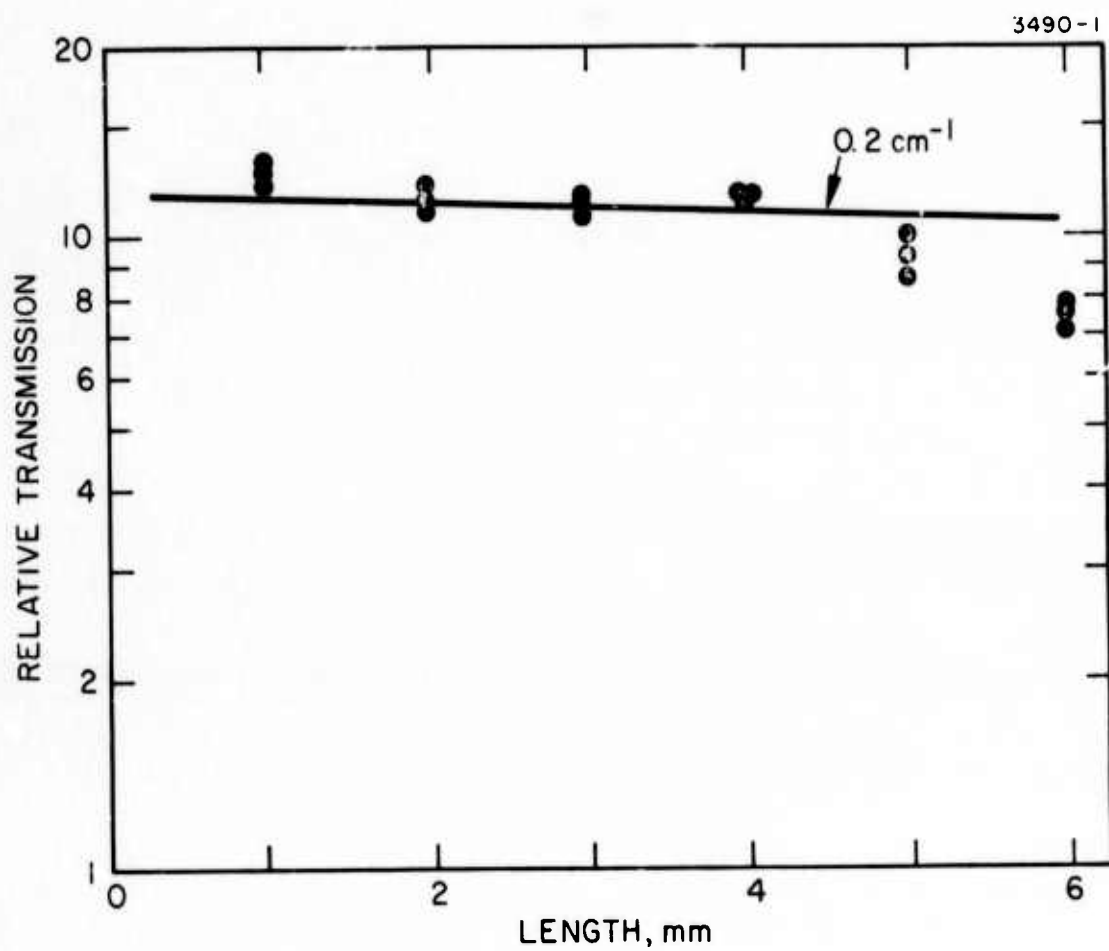


Fig. VI-5. Optical transmission of (GaAl)As waveguides from sample (0175).

Optical mode shape and attenuation has been measured and evaluated for a number of the waveguiding layers produced under this program. Consider first the case of single layer (GaAl)As waveguides on GaAs substrates.

A single layer of  $\text{Ga}_{(1-x)}\text{Al}_x\text{As}$  on top of a GaAs substrate would not support a guided mode under the usual conditions. That is, if the index of refraction in the guiding layer were a constant, guided modes would not exist because of the higher index of the substrate. However, by exploiting a gradient and peak in Al concentration, and the resulting gradient and dip in the index, optical waveguiding can be obtained. We have observed optical waveguiding in such graded  $\text{Ga}_{(1-x)}\text{Al}_x\text{As}$  waveguides that were grown both by the limited melt slidebar method, and by the infinite melt method. The details of the growth process have been described in previous sections of this report. Because of the high segregation coefficient of Al  $\sim 50$  and the nature of the limited melt growth technique a peak of very high Al concentration is created at the interface with the GaAs substrate. In addition to this, because of the high segregation coefficient the Al grows more rapidly than Ga thus depleting the melt and causing a gradient in Al concentration decreasing as one moves toward the surface. (Al concentration profiles for two typical samples 0147 and 0175 were shown in Figs. V-1 and V-2.) The peak in Al concentration was observed in one sample, No. 0147, although microprobe analysis has not observed similar peaks in other samples, implying that the thickness is somewhat below our resolution of  $\sim 2500 \text{ \AA}$ , as explained in Section V. The  $1/e$  depth of the electric field for the first order mode in a region of very high AlAs concentration  $\sim 100\%$ , is  $\sim 1000 \text{ \AA}$ . Thus a high Al concentration peak of  $2000 \text{ \AA}$  thickness could be sufficient for good optical confinement of low order modes. The theoretically expected index of refraction profiles for these two samples are shown in Figs. VI-6 and VI-7. The index profiles were calculated using the Sellmeier equation (see Section I.) based on the Al concentration profile data of Figs. V-1 and V-2. Because of the graded index profiles one would

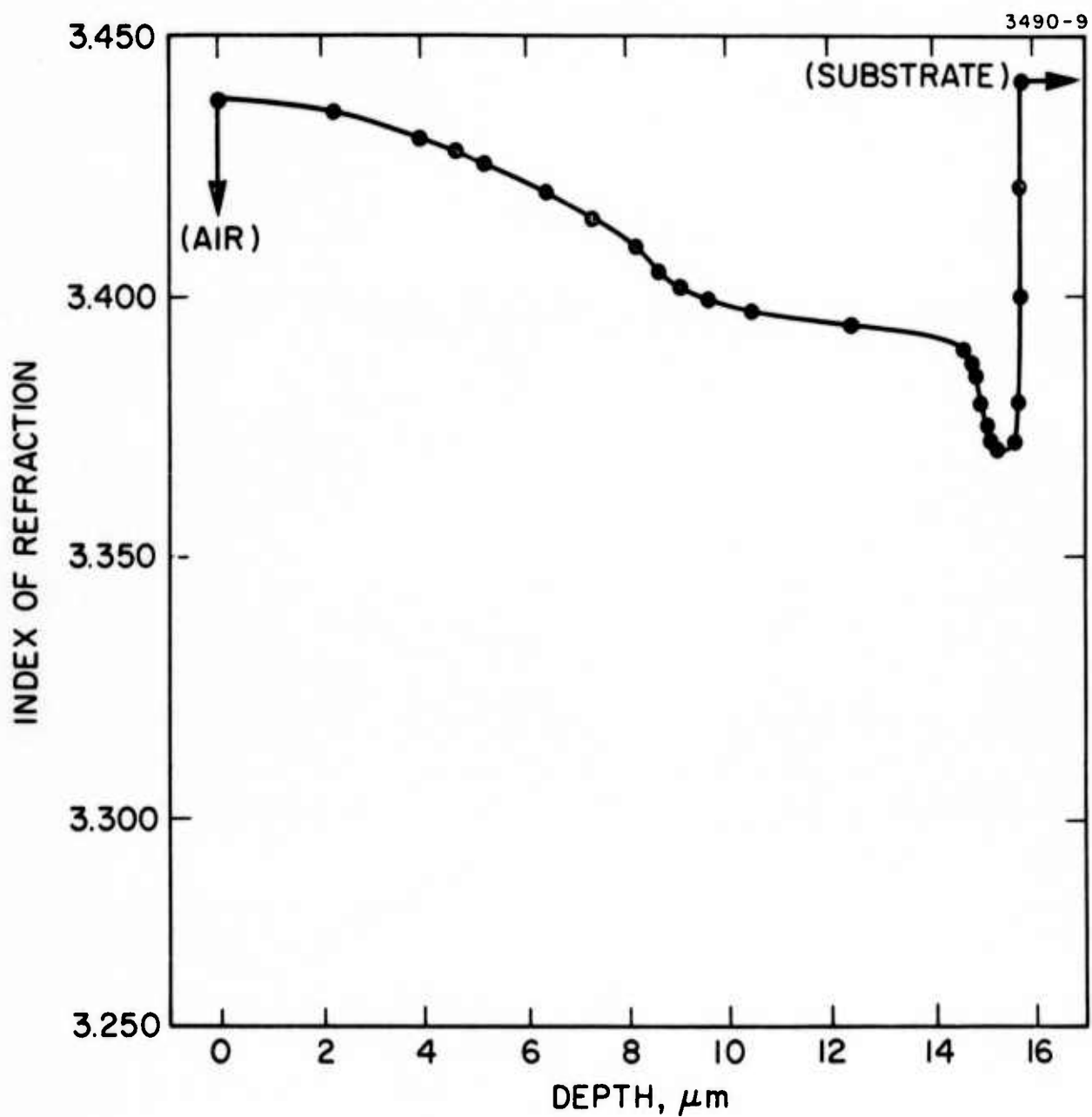


Fig. VI-6. Index of refraction in (GaAl)As waveguide, sample (0147).

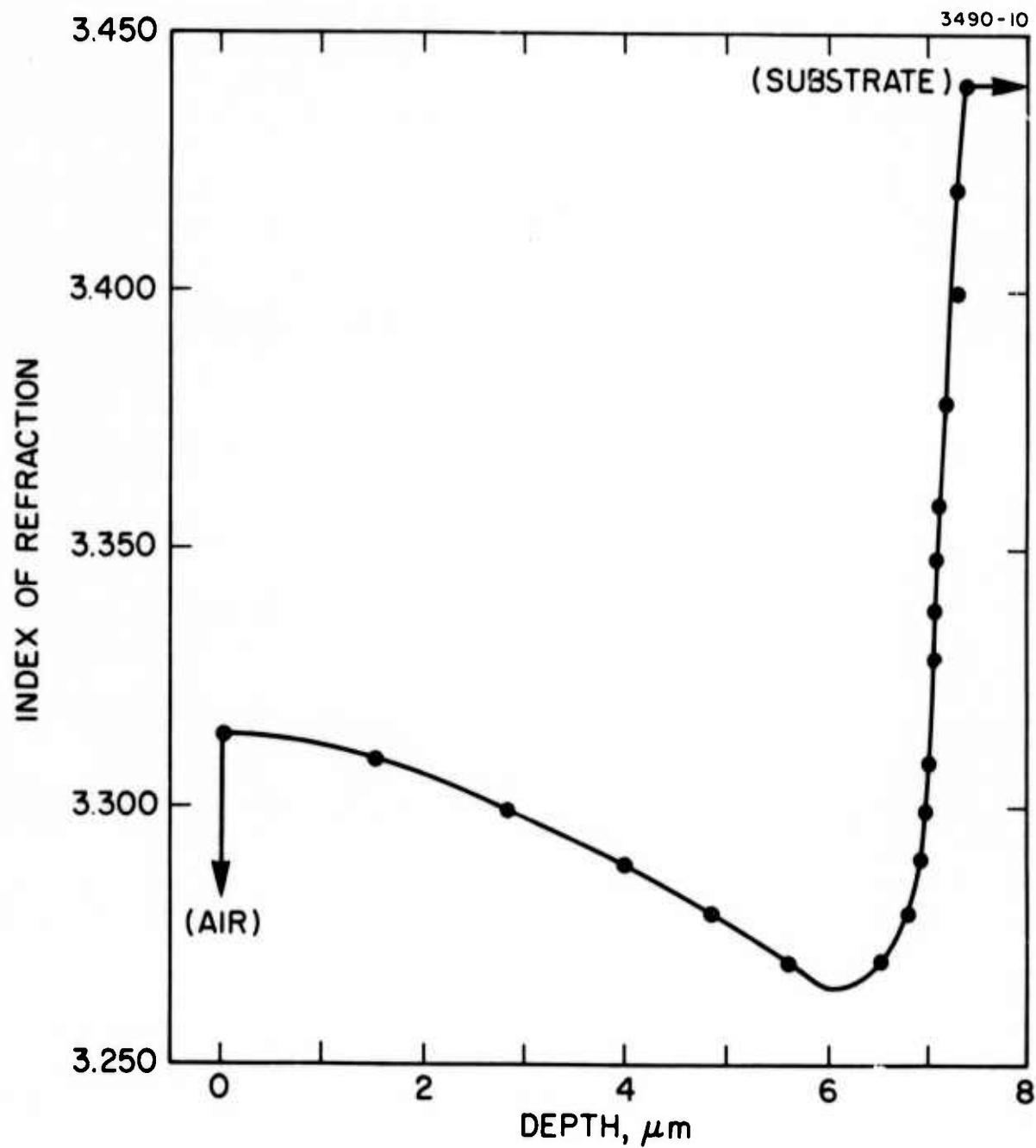


Fig. VI-7. Index of refraction in (GaAl)As waveguide, sample 0175.

expect these layers to function as waveguides. The experimentally measured mode profiles for these samples are shown in Figs. VI-8 and VI-9. In addition to determining the optical mode profile in these samples we also measured the optical attenuation coefficients. The loss coefficient in sample 0147 was

$$\alpha = 1.1 \text{ cm}^{-1},$$

while in sample 0175 we measured

$$\alpha = 0.2 \text{ cm}^{-1}.$$

(The loss measurement data for sample 0175 are shown in Fig. VI-5.)

The major reason for the greater loss in sample 0147 is that it had an overgrowth while sample 0175 did not. This overgrowth is an additional graded layer, several microns thick, caused by a fast freeze of refined melt due to insufficient wiping. Additional loss is introduced by the overgrowth layer because it reduces the index of refraction difference at the interface with the guiding layer from what it would be for air allowing light to penetrate into the rough, spotty, lossy overgrowth. The effect of the overgrowth was clearly demonstrated in the case of one sample 0151 which was only partially covered by an overgrowth. In the region which had no overgrowth losses were measured to be  $\alpha = 0.5 \text{ cm}^{-1}$  while in the region where the overgrowth was present losses were increased to  $\alpha = 5.0 \text{ cm}^{-1}$ . By eliminating the overgrowth problems and improving surface quality losses can probably be reduced very close to the limit of free carrier absorption.

A theoretical value for the free carrier absorption in these samples with  $n \leq 10^{16}/\text{cm}^3$  may be calculated by the method of Haughton and Smith<sup>7</sup> yielding a value of  $\alpha = 0.03 \text{ cm}^{-1}$ , while an estimate has

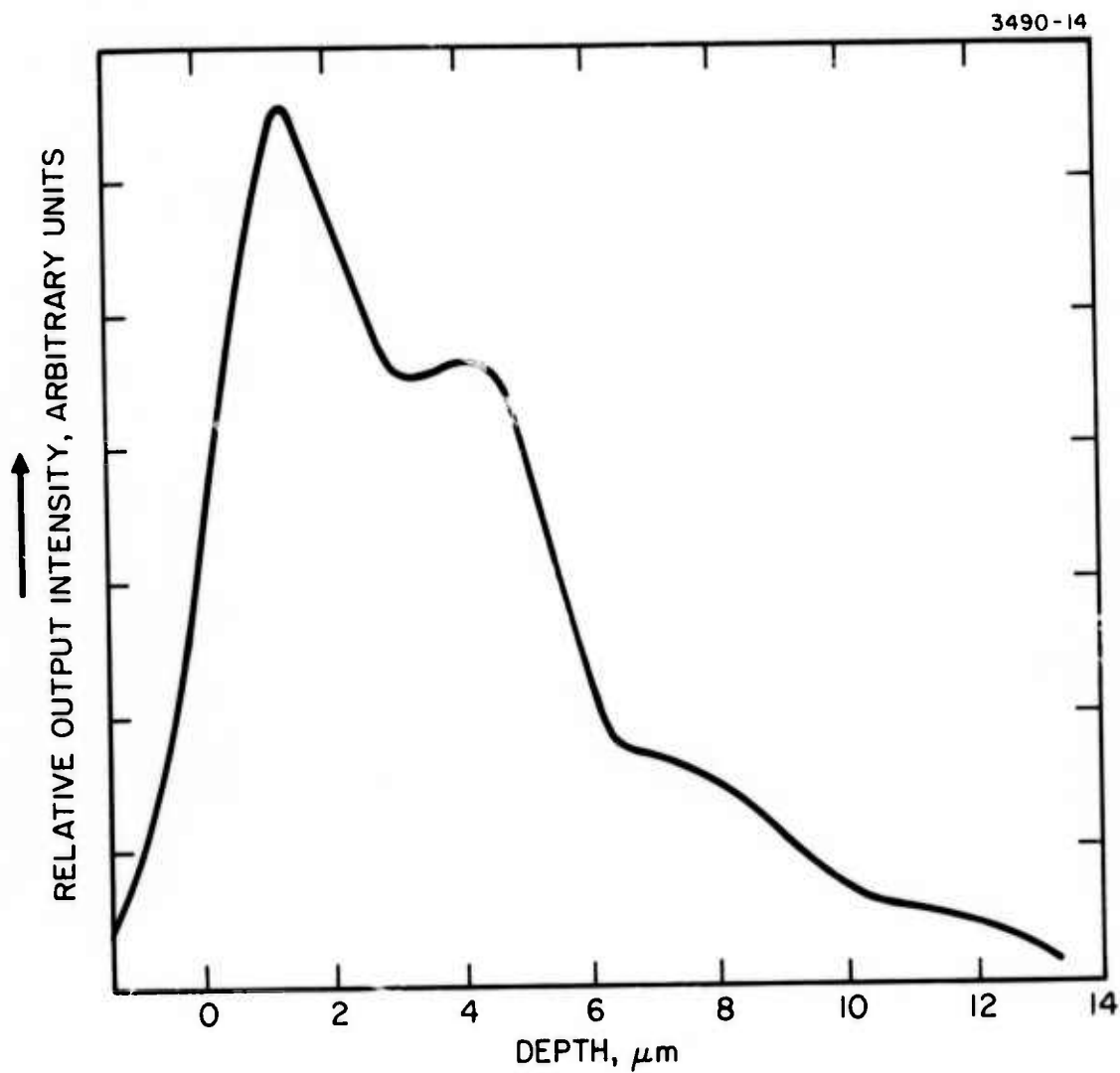


Fig. VI-8. Experimentally determined mode profile for sample 0147.

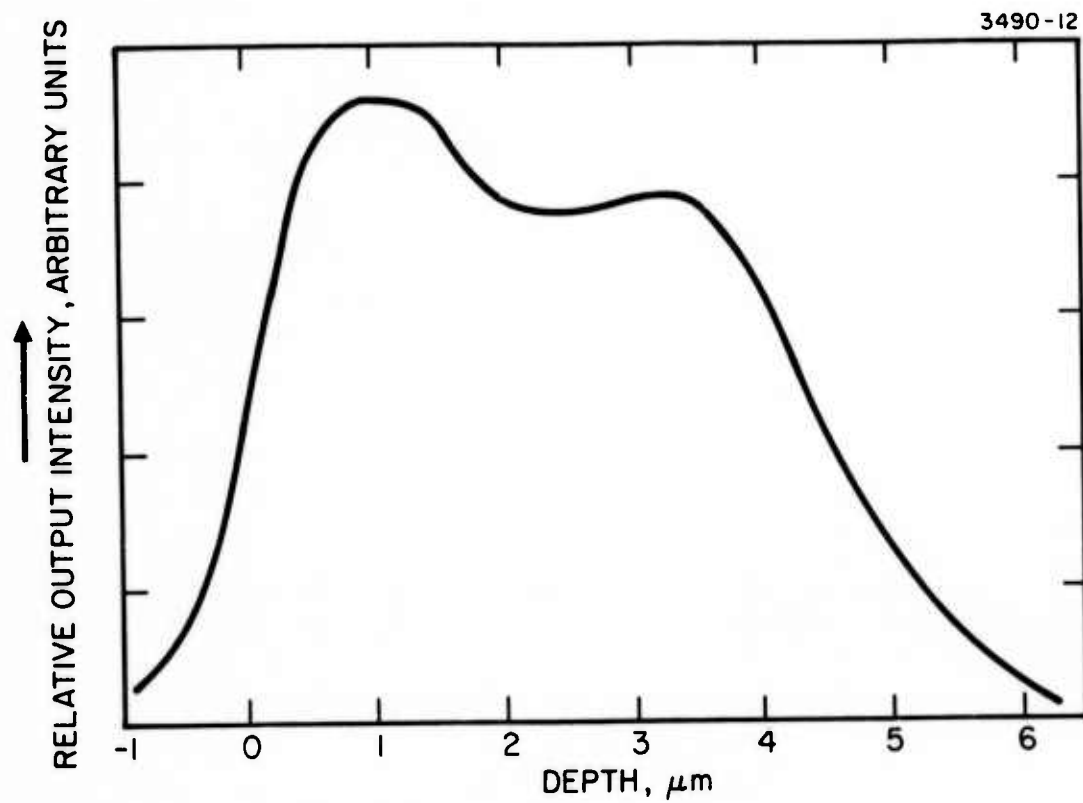


Fig. VI-9. Experimentally determined mode profile for sample 0175.

been made based on experimental data by Dumke<sup>8</sup> yielding  $\alpha \approx 0.1 \text{ cm}^{-1}$ . We have measured losses approaching this value, as can be seen by referring to the data of Table VI-1, which summarizes the loss data for the samples that have been described.

Another possible loss may be encountered because of the evanescent field being non zero in the substrate. If the field is large enough in this region light will be coupled out of the guide and be lost in the substrate. However for the low order modes of all guides which we have grown by the limited melt technique the evanescent field is completely negligible in the substrate.

One method for avoiding overgrowth problems is to grow a capping layer of (GaAl)As on top of the waveguiding layer. The Al concentration should be higher in the capping layer than in the waveguiding layer in order to confine the waveguided mode. The Al concentration profile for such a capping layer (sample 0171) is shown in Fig. V-3, and the techniques used to produce the double layer structure have been described in that section. The calculated index of

TABLE VI-1  
Optical Losses in (GaAl)As Single (Graded)  
Layer Waveguides

Sample No.	Al Concentration, Atomic %	Thickness, $\mu\text{m}$	Attenuation Coefficient, $\text{cm}^{-1}$
147	4.5	14	1.1
151	5	4	0.5 no over-growth 5.0 w/5 $\mu\text{m}$ overgrowth
175	15	7	0.17

T1503

refraction profile for sample 0171 based on the Al concentration data is shown in Fig. VI-10. This sample performed well as an optical waveguide with light being guided in the  $n \approx 3.375$  layer at 4 to 9  $\mu\text{m}$  depth. One is forced to conclude that a peak in Al concentration (dip in index of refraction) must have been present at the 9  $\mu\text{m}$  depth interface with the substrate, for otherwise optical confinement would not have occurred. However because of limited resolution of the electron beam microprobe, as explained earlier in this report, a layer of high Al concentration less than  $2500 \text{ \AA}$  thick would not be detectable.

As was described in Section V of this report, single layer GaAlAs waveguides have also been fabricated from samples with a graded Al concentration profile which were grown by the infinite melt technique. The optical mode profile for a sample of this type is shown in Fig. VI-11. It is a multimode profile, indicating that a substantial Al concentration peak must be present at the GaAs-(GaAl)As interface. These single layer (GaAl)As waveguides grown by the infinite melt method were produced late in the program. Thus loss coefficients were not measured. However, the fact that such waveguides can be made by this method is important because the infinite melt method can be used to grow uniform epitaxial layers on wafers several centimeters in diameter. Wafers of this size would be suitable for optical integrated circuit fabrication.

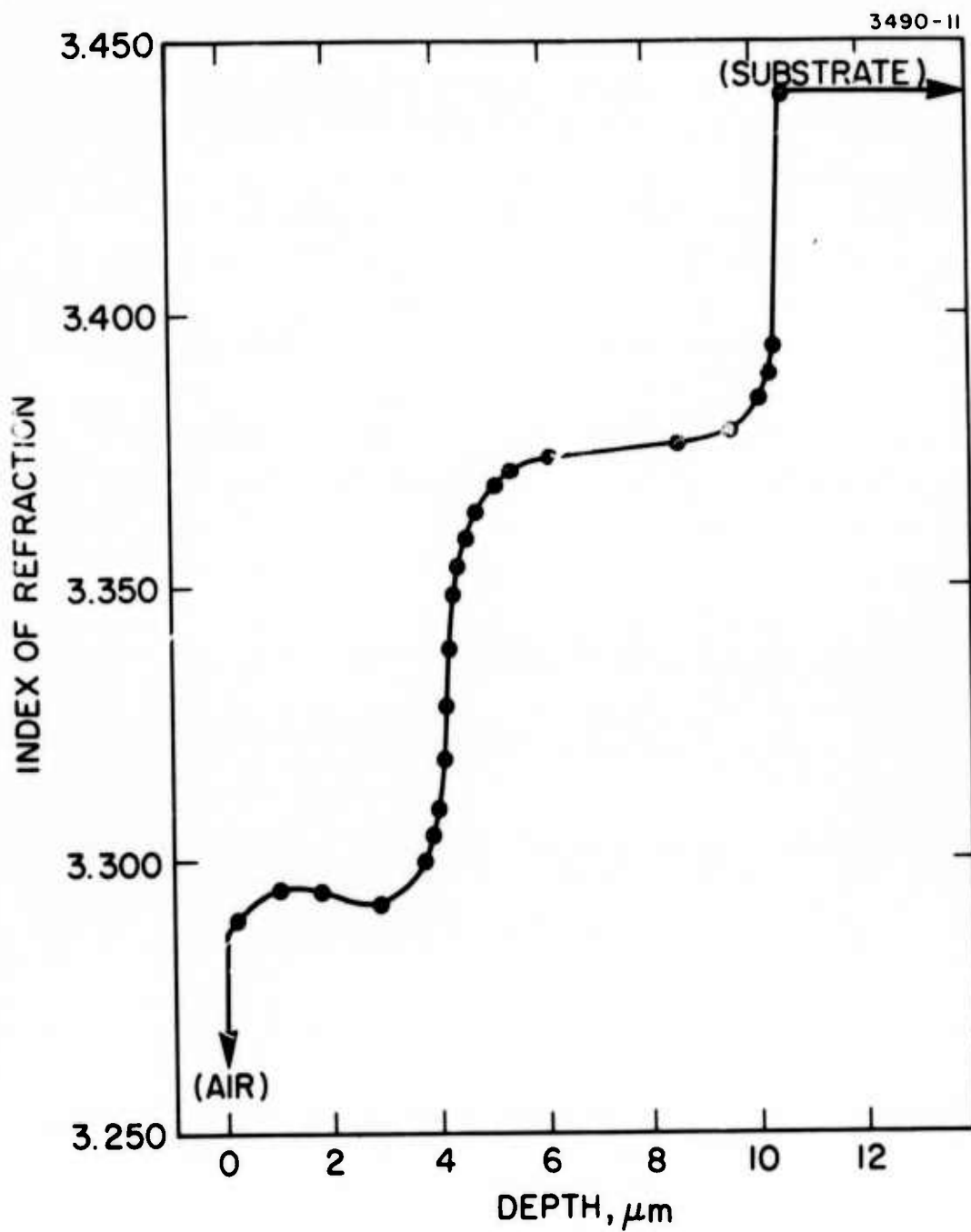


Fig. VI-10. Index of refraction in (GaAl)As waveguide, sample 0171.

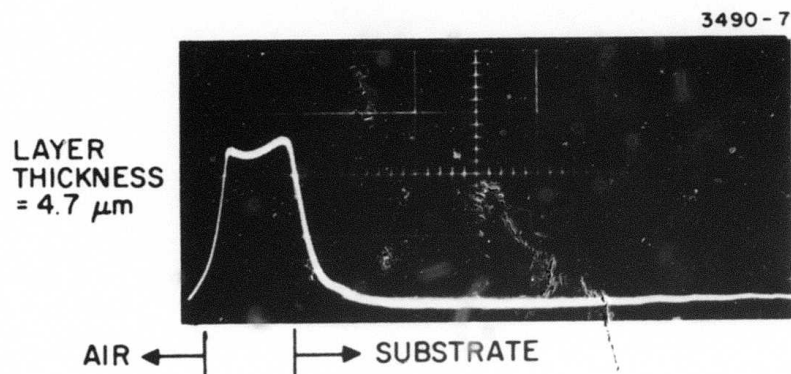


Fig. VI-11. Optical mode profile for (GaAl)As layer grown by infinite melt technique.

## VII. DEVICE ANALYSIS AND FABRICATION TECHNIQUES

### A. Proton-Implanted Waveguide Detectors in GaAs and (GaAl)As

#### 1. Analysis of Proton-Implanted Integrated Waveguide/Detector

One of the device elements of an optical integrated circuit that is of particular interest to us is the integrated waveguide/detector. A fundamental problem in the fabrication of this device is that of wavelength incompatibility. An integral detector formed in a waveguide which transmits light of a certain wavelength with low loss will generally have an extremely low quantum efficiency because the bandgap will be, of necessity, too large to allow substantial interband absorption. Under a Company-funded program we have used proton bombardment to locally shift the absorption edge of GaAs to a longer wavelength in the active volume of the detector. Thus, we have been able to fabricate integrated waveguide/detectors in GaAs. This work has recently been published and a reprint of the paper is included as Appendix B of this report. Since this technique appears useful in the case of (GaAl)As waveguides as well, we have evaluated the theoretically projected performance of a proton-implanted detector as part of the work done under this contract. Experimental data compiled in the Company-funded research program (Appendix B) were used in the evaluation. Experimental fabrication and evaluation of proton-bombarded waveguide/detectors in (GaAl)As layers grown at HRL also have been accomplished under this contract and are described in Section VI-A-2.

Figure VII-1 depicts the device geometry. In the case of the GaAs waveguide detectors the optical waveguiding structure consisted of a 3.5  $\mu\text{m}$  thick n-type (S-doped,  $n = 2.8 \times 10^{16} \text{ cm}^{-3}$ ) epitaxial film grown on a degenerate n-type substrate ( $n = 1.25 \times 10^{18} \text{ cm}^{-3}$ ). Good optical confinement for the guide thickness used resulted from the guide-substrate refractive index discontinuity generated by the plasma

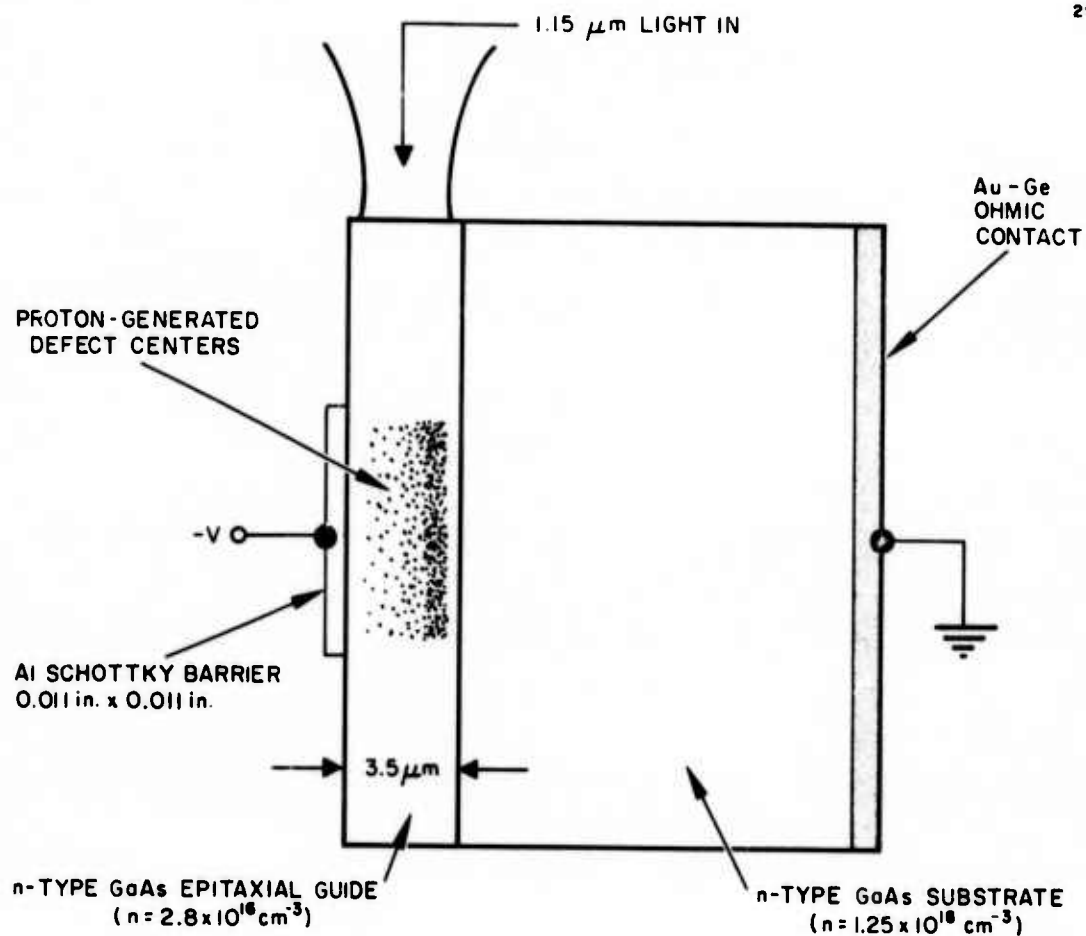


Fig. VII-1. Proton-implanted integrated optical detector device geometry.

depression effect; prior to implantation, optical attenuation at  $1.15 \mu\text{m}$  was measured to be  $1.3 \text{ cm}^{-1}$  and could be accounted for by consideration of free carrier substrate penetration losses. The aluminum Schottky barrier was 11 mil square.

The principle of operation of the detector is similar to that of conventional p-n or p-i-n junction photodetectors. Upon the application of a reverse bias to the Schottky barrier, a depletion layer is produced which, given sufficient reverse bias, extends across that high resistivity waveguiding layer to the lower resistivity substrate. Any dipole transitions made possible by radiation-produced defect levels then generate free carriers which are swept out of the depletion layer, thereby causing current to flow through an external circuit. The situation is depicted schematically in Fig. VII-2. By ensuring that the radiation-induced damage extends over most of the waveguiding layer and by choosing epitaxial material of high purity (in order to allow the widest possible depletion region), maximum detector efficiency can be obtained over a given interaction length.

When illuminated, as shown in Fig. VII-1, by a Spectra Physics model 120 He-Ne laser emitting 0.75 MW of optical power at  $1.15 \mu\text{m}$ , a particular (typical) detector generated a current of approximately  $1.5 \times 10^{-5} \text{ A}$  when biased to near reverse breakdown voltage. Hence, the number of electrons swept out of the depletion layer per second was

$$e = \frac{1.5 \times 10^{-5}}{1.602 \times 10^{-19}} = 0.935 \times 10^{14} \text{ electrons/s.}$$

In this integral waveguide/detector the waveguide was implanted with 300 keV protons, the total integrated flux of which was  $2 \times 10^{15} \text{ cm}^{-2}$ . The sample was then annealed at  $500^\circ\text{C}$  for 30 min in order to allow some optical transmission through the damaged waveguide; residual, defect-associated losses were measured to be  $\approx 15 \text{ cm}^{-1}$  based on a comparison of the optical attenuation before and after implantation and

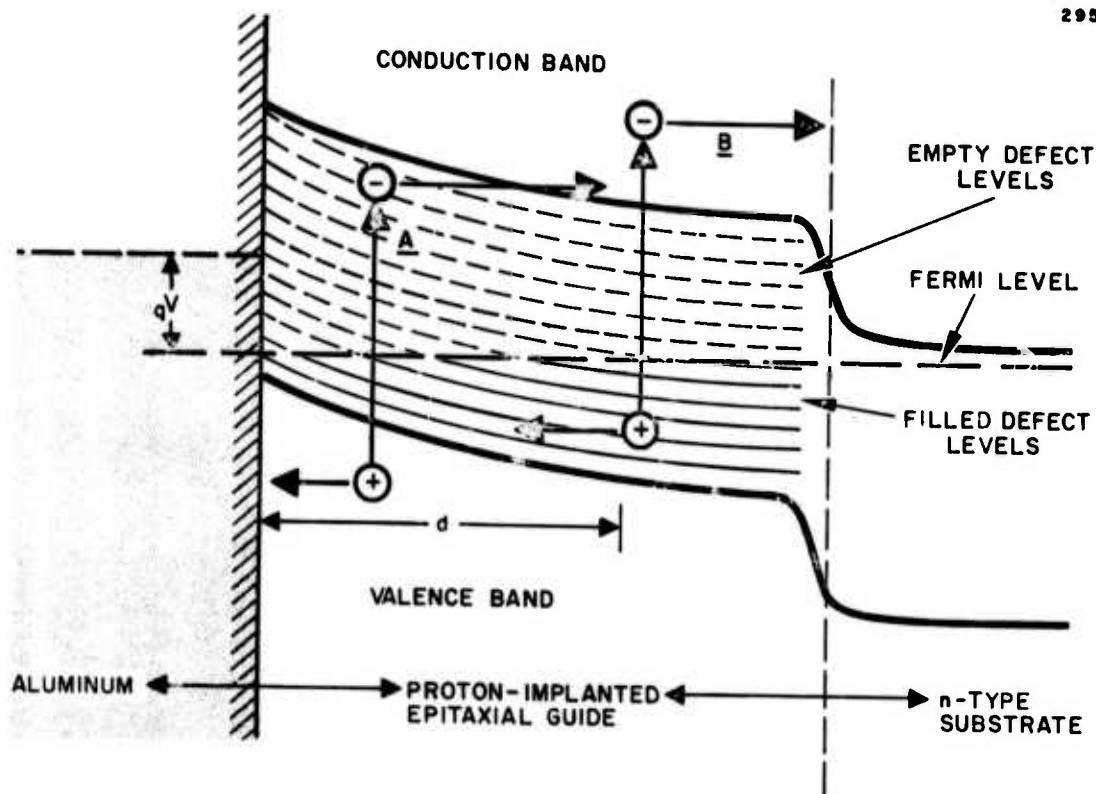


Fig. VII-2. Principle of operation of integrated optical detector: Upon the application of a reverse bias ( $V$ ) electrons liberated by transitions labeled A and B are swept out of depletion layer  $d$  resulting in the flow of current.

annealing. The Schottky barrier was 8 mil from the waveguide input face. Thus, taking the output power of the laser to be 0.75 MW and the overall waveguide insertion loss to be 50% (including both reflection at the input face, 30%, and waveguide mode coupling loss, 20%) and assuming that the entire guided beam passed under the Schottky barrier in question, the number of photons per second that were lost while traversing the detector is given by

$$P = \frac{(0.75 \times 10^{-3})(0.5) \exp(-15 \times 0.0025 \times 8) [1 - \exp(-15 \times 0.0025 \times 11)]}{(1.08)(1.602 \times 10^{-19})}$$

$$= 5.42 \times 10^{14} \text{ photons/s.}$$

The internal quantum efficiency of the detector was, therefore,

$$\left(\frac{e}{p}\right) \times 100 = 17\% .$$

Two factors probably contributed to this relatively low quantum efficiency, namely, dissipative absorption and incomplete layer depletion. Calorimetric absorption measurements made by Stein<sup>9</sup> indicate that essentially all of the optical attenuation observed in proton implanted GaAs can be attributed to absorption rather than diffuse scattering. However, Stein's measurements cannot distinguish between absorption which generates a carrier and absorption resulting from dissipative centers such as the microscopic metallic inclusions reported by McNichols in neutron bombarded GaAs.<sup>10</sup> Calculations made by Stein<sup>9</sup> indicate that possibly as much as 60% of the total bombardment induced absorption at 1.15  $\mu\text{m}$  wavelength could be attributed to dissipative absorption and scattering, with only the remaining 40% resulting in the promotion of trapped electrons to the conduction band. This effect would impose a fundamental limit to the quantum efficiency of a proton-implanted detector, but the 60% value calculated by Stein is a

"worst case" estimate and, in any case, the effect diminishes at wavelengths closer to the band edge wavelength. For example, based on Stein's calculation the dissipative absorption would be at most 45% of the total at 1.0  $\mu\text{m}$ .

A second factor action to reduce quantum efficiency is incomplete layer depletion. The residual free carrier concentration in the implanted waveguide being presently considered, as determined by the capacitance-voltage technique, was found to be  $\approx 2.8 \times 10^{16} \text{ cm}^{-3}$ , or approximately the original pre-implantation value. As a result, the width of the depletion layer (for a reverse bias of 30 V) was only 2.9  $\mu\text{m}$ , compared with the waveguide thickness of 3.5  $\mu\text{m}$ . Calculations based on optical mode shape indicate that, under these circumstances, only approximately 90% of the electrons liberated from trapping levels are exposed to the influence of the electric field generated within the depletion region. This effect can, of course, be minimized by using a thinner or more lightly doped waveguide, or altered proton dose/energy combination to achieve full depletion.

The fabrication of a proton-implanted detector integrally within a (GaAl)As waveguide can be accomplished by using the same techniques that have been applied successfully to GaAs. Probably, the most useful integral waveguide/detector combination would be one that could function satisfactorily at a wavelength of 0.9  $\mu\text{m}$ , and, hence, could be used with a GaAs LED or laser source. As discussed in Section II (summary appears in Table II-2 of that Section) this requires minimum aluminum concentrations of 7% in the waveguide and 11% in the substrate, for single-mode propagation in a guide of thickness  $t = 2.5 \mu\text{m}$  with attenuation  $= 2 \text{ cm}^{-1}$ . The region in which the detector volume is desired would be implanted with 250 keV protons in a dose  $10^{16}/\text{cm}^2$  to produce the required absorptive centers. The exact distribution of the defect-associated energy states within the bandgap of the (GaAl)As is not known. However, assuming their spacing from the band edge scales linearly with bandgap, one estimates

an absorption coefficient in the proton-implanted region of  $\alpha = 5 \times 10^3 \text{ cm}^{-1}$  at  $0.9 \text{ }\mu\text{m}$ , based on the data measured by Stein<sup>9</sup> for GaAs. This implies that the length of the detector in the direction of propagation should be at least  $15 \text{ }\mu\text{m}$  to obtain essentially total absorption. Again, based on extrapolation of Stein's GaAs data, one would project that possibly as much as 40% of the total absorption would go into dissipative processes rather than carrier generation. However, it should be emphasized that this percentage represents an estimated upper limit rather than a predicted value. Thus, if the carrier concentration in the waveguide is kept low enough ( $\leq 10^{16} \text{ electrons/cm}^3$ ) that the detector volume can be completely depleted by the reverse biased Schottky diode, all of the carriers generated will be swept out, giving an estimated internal quantum efficiency of at least 60%.

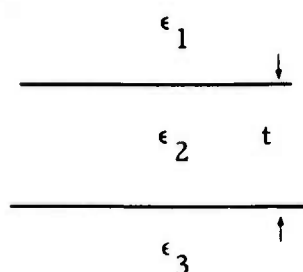
## 2. Fabrication of Proton Implanted Detectors

As part of the work done under this program the proton bombardment technique was used to produce for the first time an integrated waveguide/detector in a (GaAl)As single layer waveguide of the type described in Section VI. The waveguide was a single layer of (GaAl)As on a silicon doped GaAs substrate (sample 0135). The guiding layer was similar to that of sample 0147, having an aluminum concentration of 5% (atomic) and a thickness of  $13 \text{ }\mu\text{m}$ . Since good optical confinement was observed it is presumed that there was a peak in the Al concentration profile at the (GaAl)As-GaAs interface like that measured for sample (0147) (see Fig. V-1). However, all of sample (0135) was used for waveguide fabrication and none was left over for microprobe measurements to be made. Optical loss measurements made on waveguides cleaved from sample 0135 prior to proton bombardment indicated an absorption coefficient at  $\lambda = 1.15 \text{ }\mu\text{m}$  of  $\alpha \approx 0.2 \text{ cm}^{-1}$ . A 3 mm long waveguide cleaved from this sample was bombarded over one third of its length with a dose of  $1 \times 10^{15}/\text{cm}^2$ , 300 keV protons. This bombardment produced a factor of 10 increase in absorption ( $\alpha = 2 \text{ cm}^{-1}$  at  $1.15 \text{ }\mu\text{m}$ ) as compared to the loss observed

in the non bombarded region. This absorption coefficient is relatively low compared with those that have been observed in similarly bombarded GaAs samples ( $\sim 100 \text{ cm}^{-1}$ ). However, it must be remembered that an atomic Al concentration of 5% shifts the absorption edge in the non-bombarded material to shorten wavelength by approximately  $700 \text{ \AA}$ . Another important factor tending to limit the change in  $\alpha$  produced by bombardment in this case was that the waveguiding layer was  $13 \text{ }\mu\text{m}$  thick and the range of 300 keV protons in GaAs is only  $3 \text{ }\mu\text{m}$ . Thus only one quarter of the thickness of the waveguiding layer would be affected by the proton bombardment. To fabricate a detector structure like that shown in Fig. 1 of Appendix B a Schottky barrier contact was formed on the surface of the bombarded region. When the device was reverse biased with a dc voltage of 20 V and light from the He-Ne laser was focused onto the cleaved end face of the waveguide nearest the proton bombarded region a photocurrent  $\sim 1 \text{ }\mu\text{A}$  was produced. Since the magnitude of the coupling loss at the cleaved end face is not known it is impossible to determine a quantum efficiency for the device from these experiments. However, they have served to demonstrate that proton bombardment can be used to produce a monolithically coupled waveguide/detector in (GaAl)As as well as GaAs. Further work is required to fully characterize and optimize the device. The coupling loss, and hence the quantum efficiency, could be evaluated by first determining optical attenuation in a waveguide/detector by successively shortening the waveguide and remeasuring the loss after each step. Then the coupling loss could be determined by measuring the input and output powers and subtracting waveguide attenuation loss from the total power loss to yield the value for the coupling loss. We were prevented from making this determination of quantum efficiency merely by a lack of time; the measurement procedure is straightforward.

#### B. Analysis of Leaky Waveguides

In a conventional confined propagation waveguide the dielectric constants obey



$\epsilon_1 < \epsilon_2 > \epsilon_3$ . In some cases it may be easier to fabricate a guide where  $\epsilon_1 < \epsilon_2 < \epsilon_3$ . This would be the case, for example, if layer 3 is a GaAs substrate while 2 is  $\text{Ga}_{(1-x)}\text{Al}_x\text{As}$  (1 is air). Such a structure is inherently lossy, since no total internal reflection can take place at the 2-3 interface. We will show below that for moderate values of  $t$  the "leak" loss can be reduced to a tolerable level.

Consider the problem of propagation in the dielectric configuration of Fig. VII-3. where

$$\epsilon_3 > \epsilon_2 > \epsilon_1, \epsilon_i = \epsilon_0 n_i^2$$

If we assume solutions of the form

$$\text{Region I} \quad E_y = A \exp[i(h_1 x + \gamma z - \omega t)] \quad x \geq t$$

$$\text{Region II} \quad E_y = \{B \cos(h_2 x) + c \sin(h_2 x)\} \exp[i(\gamma z - \omega t)] \quad 0 \leq x \leq t$$

$$\text{Region III} \quad E_y = D \exp[i(-h_3 x + \gamma z - \omega t)] \quad x \leq 0$$

Then it follows from the wave equation

$$\left(\gamma^2 + \frac{\partial^2}{\partial x^2}\right) E_y + k_i^2 E_y = 0 \quad (12)$$

$$k_i^2 = \omega^2 \mu \epsilon_i = k^2 n_i^2 \quad \left(k = \frac{2\pi}{\lambda}\right).$$

2957-II

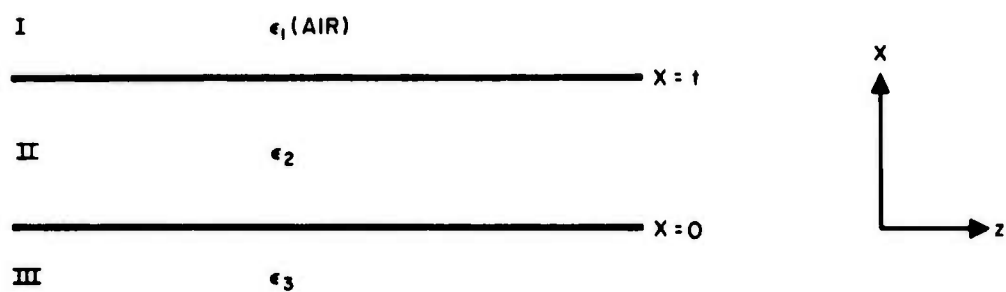


Fig. VII-3. Diagram of double layer waveguide structure.

Applying eq. (13) to regions I, II, and III gives

$$\begin{aligned} h_1^2 &= k_2^2 \left( \frac{\epsilon_1}{\epsilon_2} \right) - \gamma^2 \\ h_2^2 &= k_2^2 - \gamma^2 \\ h_3^2 &= \frac{\epsilon_3}{\epsilon_2} k_2^2 - \gamma^2 \end{aligned} \quad (13)$$

Matching  $E_y$  and  $\partial E_y / \partial x$  at  $x = 0$  and  $x = t$  gives

$$\begin{aligned} A \exp(h_1 t) - B \cos(h_2 t) - C \sin(h_2 t) &= 0 \\ h_1 A \exp(h_1 t) - i B h_2 \sin(h_2 t) + i C h_2 \cos(h_2 t) &= 0 \\ B - D &= 0 \\ i h_2 C - h_3 D &= 0. \end{aligned} \quad (14)$$

Setting the determinant of coefficients of A, B, C, and D in eq. (14) equal to zero gives

$$\tan(h_2 t) = -i(h_1 h_2 + h_3 h_2) / (-i h_2^2 + h_1 h_3). \quad (15)$$

To obtain an approximate solution we will assume that the waveguide is large so that  $k_2 a \rightarrow \infty$ . It follows from the second of eq. (13) that in the same limit  $\gamma \rightarrow k_2$  and

$$h_1 \approx i k_2 \left( 1 - \frac{\epsilon_1}{\epsilon_2} \right)^{1/2} \quad (16)$$

$$h_3 \approx k_2 \left( \frac{\epsilon_3}{\epsilon_2} - 1 \right)^{1/2}$$

so that

$$k_2, h_3, h_1 \gg h_2.$$

We can thus approximate eq. (15) by

$$h_2 t = \tan^{-1} \left[ i \left( -\frac{h_2}{h_1} - \frac{h_2}{h_3} \right) \right] + n\pi \quad n = 0, 1, 2.$$

(In view of eq. (18), the  $n = 0$  solution is discarded since  $A \sin(h_1 x) + B \cos(h_1 x) = \text{constant}$  and we only use the solution  $n = 1, 2, 3$ .)

$$\begin{aligned} &\equiv \tan^{-1} \left\{ i \left( \frac{-h_2}{ik_2 \left( 1 - \frac{\epsilon_1}{\epsilon_2} \right)^{1/2}} - \frac{h_2}{k_2 \left( \frac{\epsilon_3}{\epsilon_2} - 1 \right)^{1/2}} \right) \right\} + n\pi \\ &= \tan^{-1} \left\{ -\frac{h_2}{k_2} E_2 - i \frac{h_2}{k_2} E_3 \right\} + n\pi \end{aligned} \quad (17)$$

$$E_2 = \left( \frac{1}{1 - \frac{\epsilon_1}{\epsilon_2}} \right)^{1/2}, \quad E_3 = \left( \frac{1}{\frac{\epsilon_3}{\epsilon_2} - 1} \right)^{1/2}.$$

Since  $E_2$  and  $E_3$  are 0 (1) and  $k_2 \gg h_2$ , eq. (17) can be written as

$$h_2 t \approx -h_2 t \frac{E_2}{k_2 t} - i h_2 t \frac{E_3}{k_2 t} + n\pi$$

$$h_2 t \left( 1 + \frac{E_2}{k_2 t} + i \frac{E_3}{k_2 t} \right) = n\pi \quad n = 1, 2, 3, \dots$$

$$h_2 t \approx n\pi \left[ 1 - \frac{E_2}{k_2 t} - i \frac{E_3}{k_2 t} \right]. \quad (18)$$

Substituting eq. (18) into the second of eq. (13) given

$$\gamma_{TE} = k_2 \left[ 1 - \frac{n^2 \pi^2}{2k_2^2 t^2} \left( 1 - \frac{2E_2}{k_2 t} \right) \right] + i \frac{n^2 \pi^2 \times E_3}{2k_2 t^2 k_2 t}.$$

The exponential intensity decay coefficient is thus

$$\alpha_{TE} = 2\text{Im}\gamma_{TE} = \frac{2k_2 n^2 \pi^2 E_3}{(k_2 t)^3}, \quad n = 1, 2, 3, \dots$$

$$k_2 = \frac{2\pi}{\lambda} n_2, \quad E_3 = \frac{1}{\sqrt{\frac{\epsilon_3}{\epsilon_2} - 1}} = \frac{1}{\sqrt{\frac{n_3^2}{n_2^2} - 1}}$$

$\lambda$  = vacuum wavelength

for

$$\Delta n = n_3 - n_2 \ll n_2, n_3$$

$$\alpha_{TE} \approx \frac{1}{2\lambda \left(\frac{t}{\lambda}\right)^3 n^2 \sqrt{\frac{2\Delta n}{n}}}.$$

Calculated values for  $\alpha$  in the particular case where  $n_2 = 3.3$  and  $n_3 = 3.4$  are shown in Table VII-1.

TABLE VII-1

Calculated Values of  $\alpha$  for  $\lambda = 0.8 \mu\text{m}$ ,  $n_2 = 3.3$

$  \begin{array}{c}  n = 1 \\  \hline  n_2 = 3.3 \\  \hline  n_3 = 3.4 \\  \\  \alpha \approx \frac{1}{2\lambda \left(\frac{t}{\lambda}\right)^3 n^2 \sqrt{\frac{2\Delta n}{n}}}  \end{array}  $		
$t/\lambda$	$t, \mu\text{m}$	$\alpha, \text{cm}^{-1}$
1	0.8	2331
2	1.6	291
3	2.4	86
4	3.2	36
5	4	18
6	4.8	10.8
7	5.6	6.8
8	6.4	4.6
9	7.2	3.2
10	8	2.33
13	10.4	1.06

T1503

The data of Table VII-1 show that useful integrated optics devices can be fabricated using leaky waveguides provided the guide height is  $t \lesssim 10 \mu\text{m}$ . The losses due to leaks become  $< 1 \text{ cm}^{-1}$  for typical aluminum concentration  $x > 20\%$ .

C. Analysis of Propagation Characteristics of Periodic Dielectric Waveguides

Periodic optical structures are expected to play an important role in integrated optics. Their applications include optical filters, grating-air waveguide couplers, directional coupling, and distributed feedback lasers.

A basic understanding of the propagation characteristics of such waveguides is a prerequisite to their utilization. We have considered the problem from two points of view: (1) direct solution of Maxwell's equations, and (2) coupled mode formalism.

The first approach is important in understanding the general propagation and radiation behavior of the periodic waveguide. The second one is especially useful near the Bragg regime where the period  $\Lambda$  is some integral multiple of  $\lambda/2$  where  $\lambda$  is the wavelength in the guide. It also leads to closed-form expressions for some of the needed engineering parameters of the structure.

The periodic structure considered in our work is the corrugated dielectric waveguide.<sup>11, 12</sup> Techniques for producing such corrugations using ion milling<sup>13</sup> have been developed to the point where gratings with  $\Lambda = 0.11 \mu\text{m}$  have recently been fabricated.<sup>14</sup> The structure considered in this part of the analysis is shown in Fig. VII-4.

The model consists of a three-layered waveguide with sinusoidal corrugation. We assume no variation in the  $y$  direction and consider the propagation of a TM mode. The modification necessary to obtain the behavior of a TE mode will be described below.

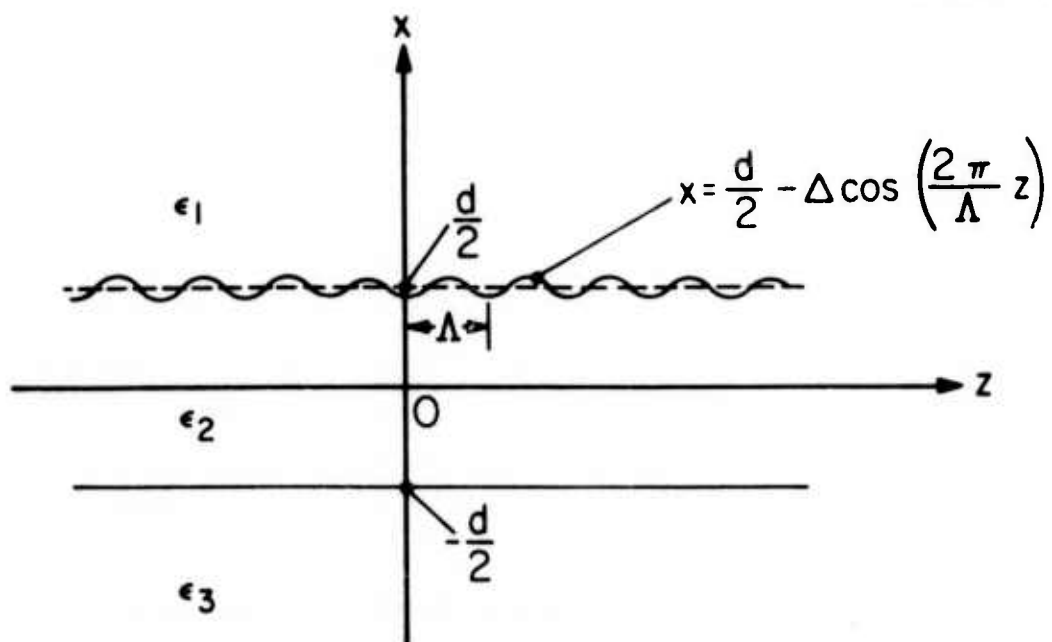


Fig. VII-4. Schematic of thin film dielectric waveguide with a sinusoidal corrugation on one side of a guide. Corrugation height  $2\Delta$ , waveguide thickness  $d$ , periodicity  $\Lambda$ .

Assuming  $\exp(-i\omega t)$  variation, we obtain from Maxwell's equations

$$\left( \nabla_t^2 + n_j^2 k_0^2 \right) H_{yj} = 0, \quad (19)$$

$$E_j = (i/\omega \epsilon_j) \nabla_t \times (H_{yj} \hat{y}), \quad (20)$$

where  $\nabla_t = \hat{x} \partial / \partial x + \hat{z} \partial / \partial z$ ,  $n_j$  is the index of refraction of layer  $j$  ( $j = 1, 2, 3$ ) and  $k_0 = \omega(\mu_0 \epsilon_0)^{1/2}$ . The propagating mode at  $\omega$  has a Floquet form and is taken as

$$H_{y1,n} = \sum_{m=-\infty}^{\infty} A_{m,n} \exp(i\beta_{m,n} z) \exp(-\gamma_{m,n} x),$$

$$x \geq d/2 - \Delta \cos(2\pi z/\Lambda); \quad (21)$$

$$H_{y2,n} = \sum_{m=-\infty}^{\infty} \exp(i\beta_{m,n} z)$$

$$\times \left[ B_{m,n} \exp(i\alpha_{m,n} x) + C_{m,n} \exp(-i\alpha_{m,n} x) \right],$$

$$-d/2 \leq x \leq d/2 - \Delta \cos(2\pi z/\Lambda); \quad (22)$$

$$H_{y3,n} = \sum_{m=-\infty}^{\infty} D_{m,n} \exp(i\beta_{m,n} z) \exp(\xi_{m,n} x),$$

$$x \leq -d/2. \quad (23)$$

$n$  refers to the mode index, while  $m$  denotes the  $m^{\text{th}}$  space harmonic of the  $n^{\text{th}}$  mode. The problem consists of solving for the space harmonic amplitudes and the propagation constants  $\gamma_{m,n}$ ,  $\alpha_{m,n}$ ,  $\xi_{m,n}$ , and  $\beta_{m,n}$ . The last four are related through the wave eq. (19) as

$$\begin{aligned}\gamma_{m,n}^2 &= \beta_{m,n}^2 - n_1^2 k_o^2, \quad \alpha_{m,n}^2 = n_2^2 k_o^2 - \beta_{m,n}^2, \\ \xi_{m,n}^2 &= \beta_{m,n}^2 - n_3^2 k_o^2,\end{aligned}\tag{24}$$

where

$$\beta_{m,n} = \beta_n + 2m\pi/L.\tag{25}$$

Note that in view of eq. (25) we need only solve for  $-\pi/L < \beta_n < \pi/L$  and the rest of the dispersion ( $\omega - \beta$ ) diagram can be obtained from eq. (25).

Applying the continuity conditions to  $E_t$  and  $H_t$  at the two interfaces leads to an infinite set of homogeneous algebraic equations for the coefficients  $A_{m,n}$ ,  $B_{m,n}$ ,  $D_{m,n}$ . Truncating the number of terms in the resulting determinantal equation and solving it numerically on a computer leads to the dispersion relations. These are drawn in Figs. VII-5, VII-6, and VII-7 for the parameters:

Corrugation height:  $2\Delta = 0.3 \mu\text{m}$

Thickness of waveguide:  $d = 3 \mu\text{m}$

Periodicity:  $\Lambda$  arbitrary

$n_2 = 3.6$

$n_3 = 3.4$

Notice the existence near  $\beta\Lambda = \pi$  of a forbidden frequency regime. In this regime, which is magnified in detail in Fig. VII-7, the propagation constants are complex. This is a result of Bragg scattering between the forward ( $\beta\Lambda = \pi$ ) and the backward ( $\beta\Lambda = -\pi$ ) traveling

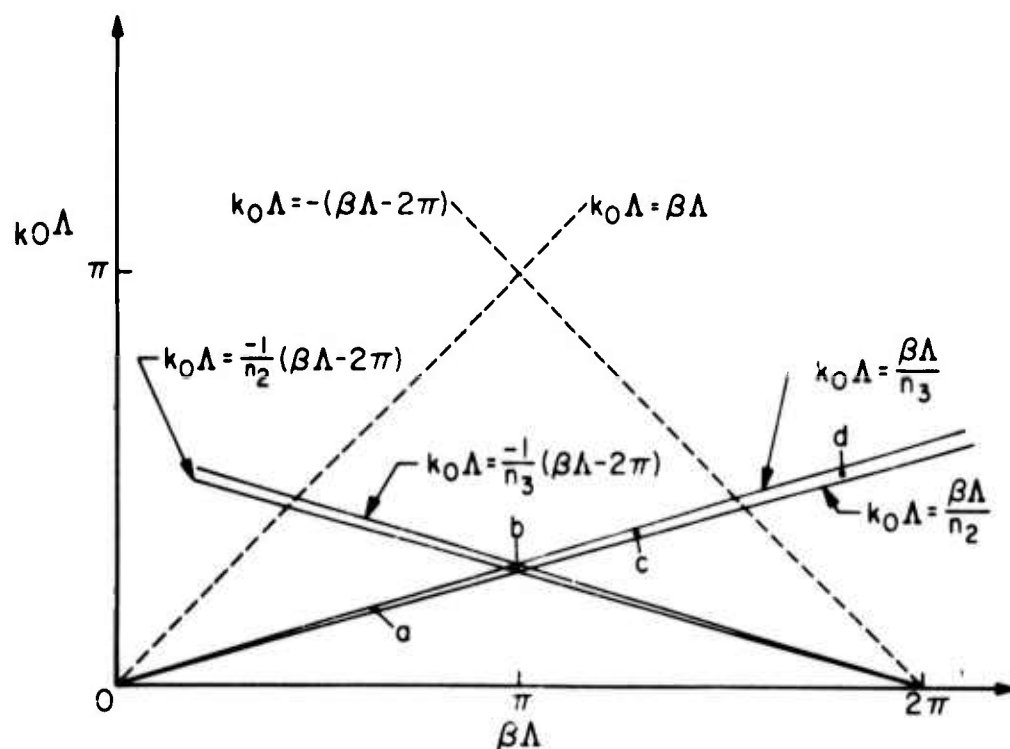


Fig. VII-5. Asymptotic lines of dispersion diagram (solid lines). If dispersion curve lies in regions a and b, the mode is confined in a guide. In region c the guided modes couple to a substrate leaky mode. In region d the guided modes couple to both air and substrate leaky modes.

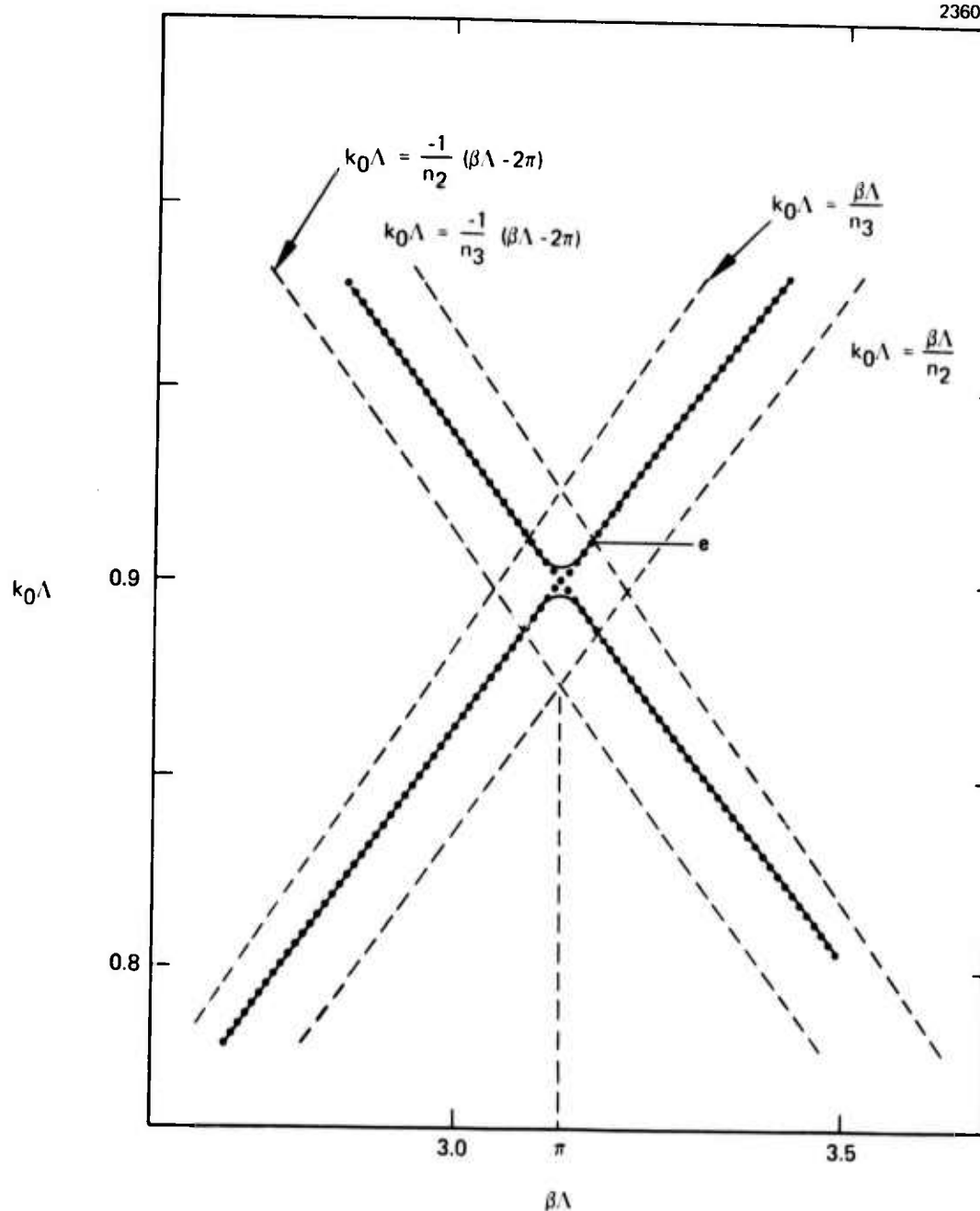


Fig. VII-6. Dispersion diagrams for a corrugated and an uncorrugated waveguide. Solid lines show the dispersion diagram for a sinusoidally corrugated waveguide. Dotted lines show the dispersion diagram for an uncorrugated waveguide (TM mode).

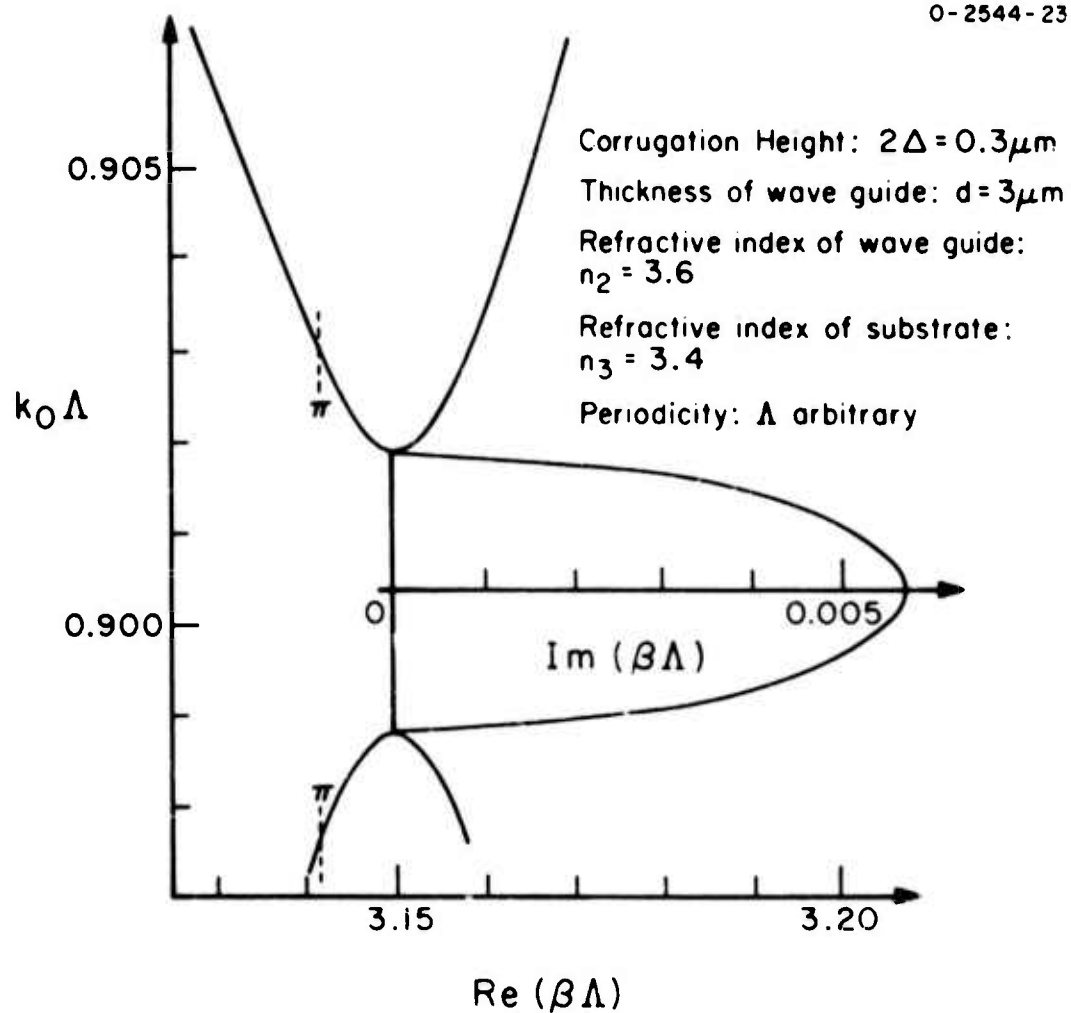


Fig. VII-7. Enlarged dispersion diagram at the vicinity of a forbidden gap (TM mode).

waves which becomes resonant when  $2\pi/\Lambda = 2\beta$ . This is the region which is most useful in distributed feedback lasers<sup>14</sup> and in optical filtering. This region can be studied by assuming that the optical propagation here is dominated by the two modes with  $\beta\Lambda = \pm\pi$ . This leads us to the coupled mode formalism developed below.<sup>15</sup>

The field component  $E_x$  of the corrugated waveguide can be expanded in the TM mode field of the smooth waveguide as

$$E_x = \sum_m \frac{\beta_m B_m(z)}{2\omega\epsilon} H_y^{(m)}(x) \exp[i(\omega t - \beta_m z)] + \text{c.c.}, \quad (26)$$

where  $B_m(z)$  is the normalized mode amplitude so defined so that  $|B_m|^2$  is the total power (per unit width in the  $y$  direction) in mode  $m$ . The field  $H_y^{(m)}(x)$  is given by

$$\begin{aligned} H_y^{(m)}(x) &= -C[(h/\bar{q}) \cos(ht) + \sin(ht)] \exp[p(x+t)], \quad x \leq -t, \\ &= C[-(h/\bar{q}) \cos(hx) + \sin(hx)], \quad -t \leq x \leq 0, \\ &= -(h/\bar{q}) C \exp(-qx), \quad x \geq 0, \end{aligned} \quad (27)$$

where, referring to Fig. VII-8, the continuity conditions at  $x = 0$  and  $x = -t$  result in the eigenvalue relation

$$\begin{aligned} \tan(ht) &= h(\bar{p} + \bar{q})/(h^2 - \bar{p}\bar{q}), \\ \bar{p} &\equiv \left(n_2^2/n_3^2\right)p, \quad \bar{q} \equiv \left(n_2^2/n_1^2\right)q. \end{aligned} \quad (28)$$

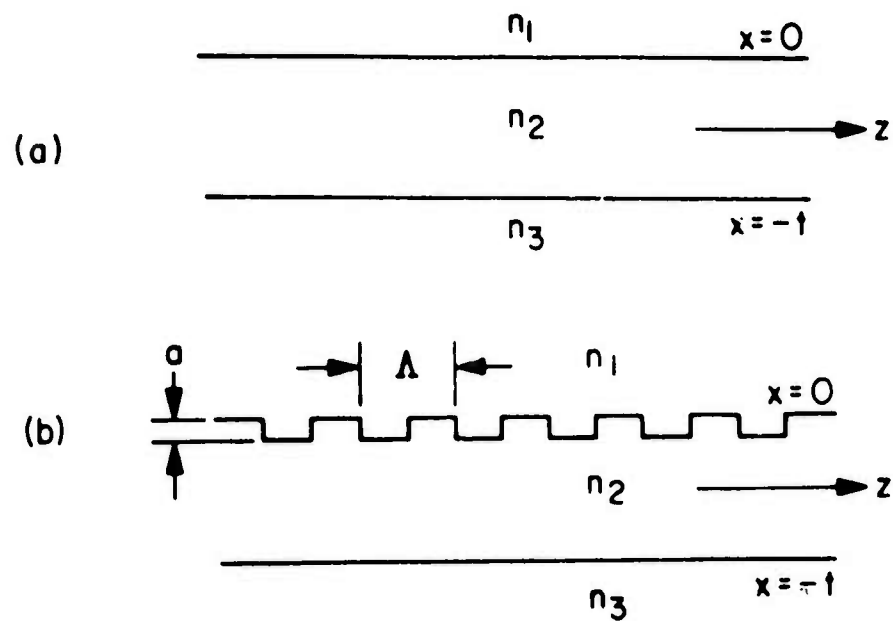


Fig. VII-8. (a) Unperturbed waveguide. (b) Waveguide with square wave perturbation.

We choose the constant  $C$  in eq. (27) so that  $|B_m|^2$  is the power per unit width ( $y$ ) in the mode. This determines  $C_m$  as

$$C_m = 2(\omega \epsilon_o / \beta_m t_{\text{eff}})^{1/2},$$

where

$$t_{\text{eff}} = \frac{\bar{q}^2 + h^2}{\bar{q}^2} \left[ \frac{t}{n_2^2} + \frac{q^2 + h^2}{\bar{q}^2 + h^2} \frac{1}{n_1^2 q} + \frac{p^2 + h^2}{\bar{p}^2 + h^2} \frac{1}{n_3^2 p} \right]. \quad (29)$$

The effect of surface corrugation is to generate a perturbation polarization wave

$$P_x = \Delta n^2(r) \epsilon_o E_x, \quad (30)$$

where  $\Delta n^2(r)$  is the deviation of  $n^2(r)$  of the corrugated structure from that of the smooth guide. Referring to Fig. VII-8(b), we have

$$\Delta n^2(r) = \Delta n^2(x) \left\{ \frac{1}{2} + (2/\pi) [\sin \eta z + \frac{1}{3} \sin 3 \eta z + \dots] \right\}$$

$$\Delta n^2(x) = n_2^2 - n_1^2, \quad -a \leq x \leq 0; \quad (31)$$

$$= 0, \quad \text{elsewhere.}$$

The polarization driving the backward mode is given by eq. (30) when  $E_x$  is the field of the forward mode and vice versa. Under these conditions, a substitution of eqs. (26) and (30) into Maxwell's equation leads to

$$dB_m^-/dz = \kappa B_m^+ \exp(-i\Delta z) ,$$

$$dB_m^+/dz = \kappa B_m^- \exp(+i\Delta z) , \quad (32)$$

where the superscripts + and - , respectively, refer to the forward and backward modes. The phase mismatch factor is defined by

$$\Delta(\omega) \equiv 2\beta(\omega) - \eta , \quad (33)$$

where  $\eta = 2\pi/\Lambda$  is the fundamental spatial frequency of the periodic modulation. The coupling constant  $\kappa$  is given by

$$\kappa = \frac{\omega\mu_0}{4\pi} \int_{-\infty}^{\infty} \frac{\Delta n^2(x)}{n^2(x)} \left[ H_y^{(m)}(x) \right]^2 dx . \quad (34)$$

We consider the case of a wave  $B_m^+$  incident on a corrugated section of length  $L$ . The appropriate boundary conditions are  $B^-(L) \equiv 0$  and  $B^+(0) \equiv B(0)$ . The solutions of eq. (32) are then

$$B^+(z) = B(0) \frac{\exp\left(+\frac{1}{2}i\Delta z\right)}{-\Delta \sinh\left(\frac{1}{2}SL\right) + iS \cosh\left(\frac{1}{2}SL\right)} \\ \times \left\{ \Delta \sinh\left[\frac{1}{2}S(z-L)\right] + iS \cosh\left[\frac{1}{2}S(z-L)\right] \right\} . \quad (35)$$

$$B^-(z) = B(0) \frac{2i\kappa \exp\left(-\frac{1}{2}i\Delta z\right)}{-\Delta \sinh\left(\frac{1}{2}SL\right) + iS \cosh\left(\frac{1}{2}SL\right)} \sinh\left[\frac{1}{2}S(z-L)\right]$$

where

$$S \equiv (4\kappa^2 - \Delta^2)^{1/2} . \quad (36)$$

A sketch of the mode power  $|B^+|^2$  and  $|B^-|^2$  is shown in Fig. VII-9. The exponential-like decay is caused by backward Bragg scattering and not, as in grating couplers, to radiation. The exponential regime of the solution exists according to eqs. (35) and (36) when

$$\Delta(\omega) \leq 2\kappa . \quad (37)$$

Since  $\Delta(\omega) \equiv 2\beta_{m_{th}}(\omega) - \eta$ , where  $\beta_m(\omega)$  is the propagation constant of the unperturbed  $m_{th}$  mode, eq. (35) depends on the frequency  $\omega$ . It is easy to show that the frequencies at which eq. (37) is satisfied are in the "forbidden" optical gap. From eqs. (26) and (35), we can write the complex propagation constant as

$$\beta' = \beta - \frac{1}{2} \Delta \pm \frac{1}{2} iS = \frac{1}{2} \eta \pm \frac{1}{2} iS . \quad (38)$$

Using the above definitions of  $\Delta$  and  $S$  we have

$$\begin{aligned} \text{Im}\beta' &= \left[ \kappa^2 - (\beta - \eta/2)^2 \right]^{1/2} \\ &\approx \left[ \kappa^2 - (n_{eff}^2/c^2)(\omega - \omega_0)^2 \right]^{1/2} \end{aligned} \quad (39)$$

where  $\omega_0$  is the midgap frequency so that  $\beta(\omega_0) = \eta/2$ . In the second equality of (39) we approximate  $\beta(\omega) \approx (\omega/c)n_{eff}$ . Thus,  $c/n_{eff}$  is the slope of the unperturbed dispersion  $(\omega - \beta)$  characteristics near  $\omega_0$ . The "height" of the energy gap is determined from eq. (39) as

$$(\Delta\omega)_{gap} \equiv \omega_u - \omega_l = 2\kappa c/n_{eff} . \quad (40)$$

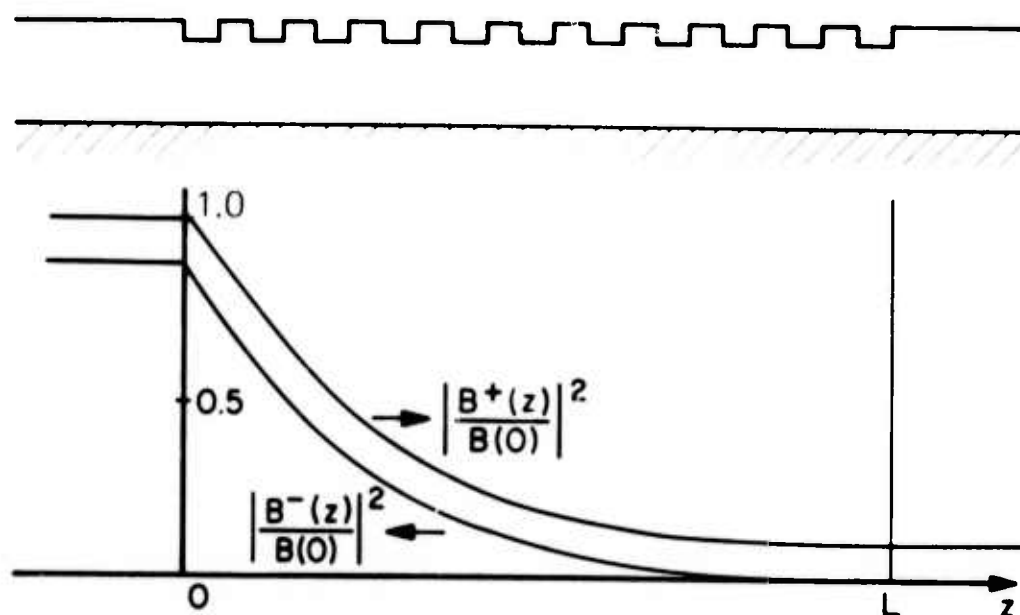


Fig. VII-9. Normalized mode power flowing in the  $+z$  direction,  $(|B^+(z)/B(0)|^2)$  and in the  $-z$  direction,  $(|B^-(z)/B(0)|^2)$ , as a function of  $z$  ( $\kappa L = 1.84$ ,  $L = 1$ ,  $\Delta = 0$ ).

For frequencies  $\omega$  outside the gap  $[\Delta(\omega)^2 > 4\kappa^2]$ ,  $(\beta - \eta/2) > \kappa$ , and  $\beta'$  is real. The shape of the  $\omega - \beta'$  curve near the upper limit of the gap ( $\omega > \omega_u$ ) is obtained from eqs. (36) and (38) as

$$\beta' = \frac{1}{2} \eta \pm \left[ \left( n_{\text{eff}}^2 / c^2 \right) (\omega - \omega_u)^2 + (2n_{\text{eff}} \kappa / c) (\omega - \omega_u) \right]^{1/2}. \quad (41)$$

Equations (39), (40), and (41) are general and apply to any spatially periodic perturbation. As a check on the above theory we applied it to the same situation considered in the first part of this section. For the case of well-confined modes, eq. (34) simplifies to

$$\kappa \approx \frac{\lambda_o a}{6n_2 t^3} \quad (42)$$

where  $a \ll \lambda_o$ . We have plotted eqs. (39) and (41) using the same data as in Fig. VII-7, i.e.,  $t = 3 \mu\text{m}$ ,  $\Lambda = 0.143 \mu\text{m}$ ,  $\lambda_o = 1 \mu\text{m}$ ,  $a = 0.3 \mu\text{m}$ ,  $n_3 = 3.4$ ,  $n_2 = 3.6$ ,  $n_1 = 1$  and took  $n_{\text{eff}} \approx n_2$ . The result is shown in Fig. VII-10. The agreement is close. At least part of the discrepancy is a result of the underestimation of  $\kappa$  which resulted from the well-confined mode approximation. The above agreement shows that we can use eqs. (35), (39), (40), and (41) in designing new Bragg filters and modulators.

The operation as modulators is based on the fact that the transmission coefficient of the device

$$\left| B^+(L)/B(0) \right|^2 = \exp \left\{ - 2 \left[ \kappa^2 - (\beta - \eta/2)^2 \right]^{1/2} L \right\}.$$

Since  $\beta \sim (\omega/c)n_2$ , the transmission depends on either  $\omega$ , as described above, or on  $n_2$ . An electro-optic (or photoelastic) variation of  $n_2$

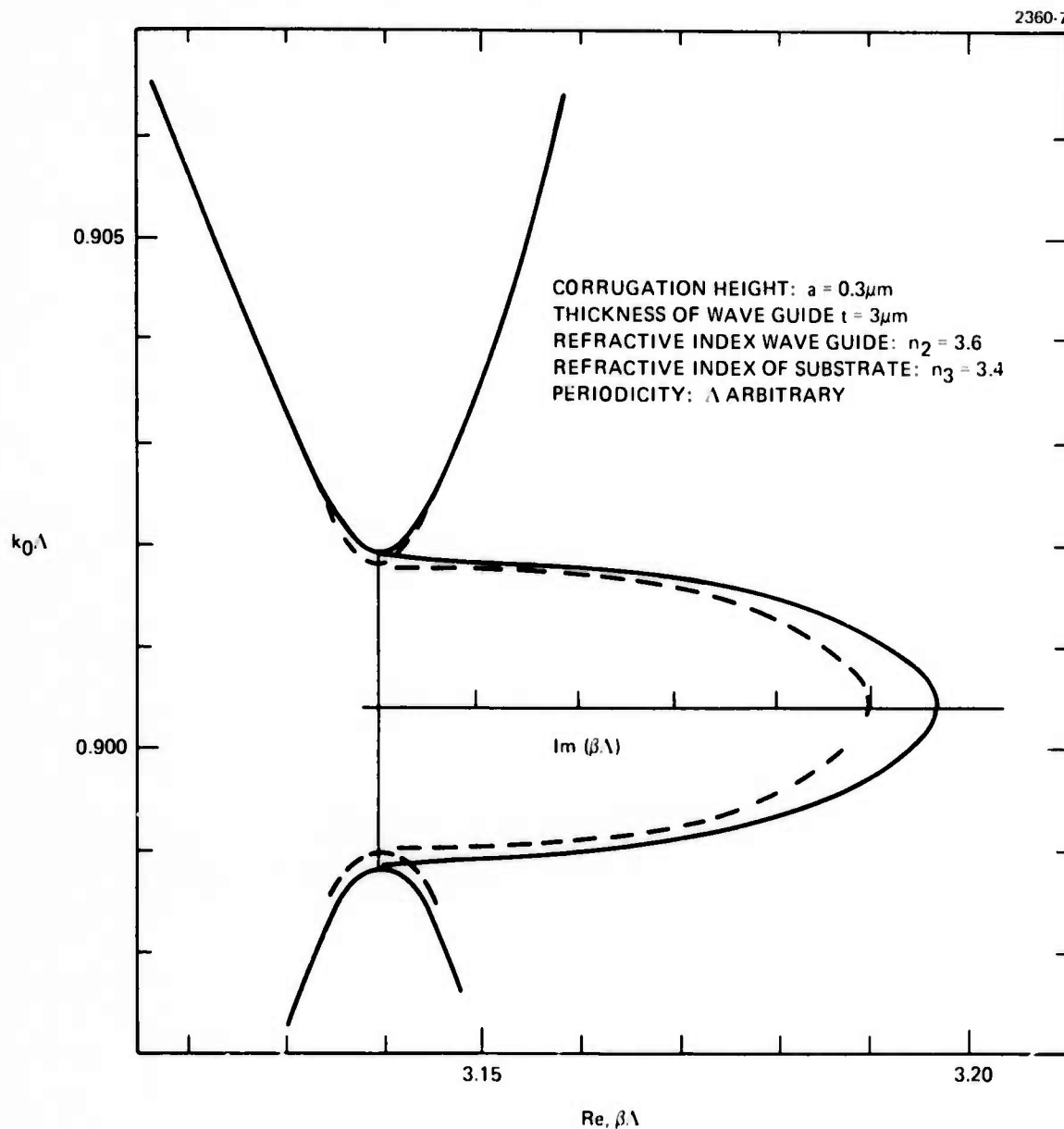


Fig. VII-10. Dispersion diagram for periodically perturbed waveguide in the region of the forbidden optical gap.

will vary the transmission. Referring to Fig. VII-10, the effect of varying  $n_2$  can be understood by fixing the frequency but moving the dispersion diagram vertically. In the limit of well confined modes the expression (eq. 42) for  $\kappa$  is also valid for TE modes. The resulting transmission and reflection characteristics are shown in Fig. VII-11 in which  $\kappa L = 1.84$ .

O-2544-26

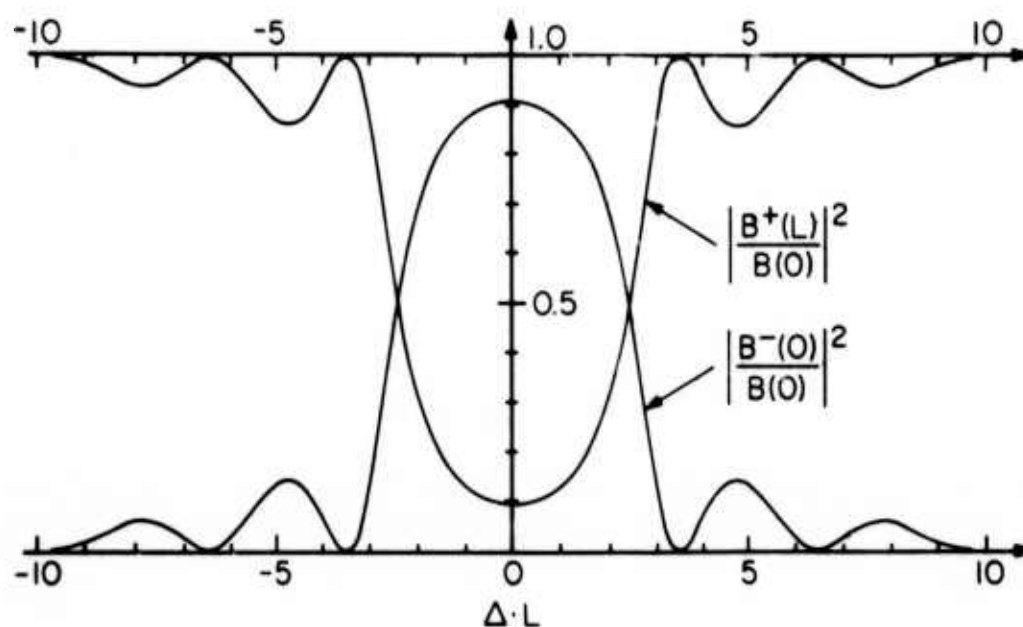


Fig. VII-11. The transmission and reflection characteristics of a corrugated section of length  $L$  as a function of  $\Delta \cdot L$  drawn for  $\kappa L = 1.84$ .

## VIII. CONCLUSIONS AND RECOMMENDATIONS

The results of this program, both theoretical and experimental, have demonstrated that  $\text{Ga}_{(1-x)}\text{Al}_x\text{As}$  optical waveguides can be epitaxially grown with acceptably low loss for use in optical integrated circuits. Loss can be reduced to less than 3 dB/cm for wavelengths in the range 1.15  $\mu\text{m}$  to 0.85  $\mu\text{m}$  by using aluminum concentrations  $0.1 \leq x \leq 0.4$  to shift the absorption edge to shorter wavelength as required, and by maintaining high purity growth conditions so that carrier concentration is  $< 10^{16}/\text{cm}^3$ . For example, we have measured losses at  $\lambda = 1.15 \mu\text{m}$  of 0.7 dB/cm in waveguides with aluminum concentration  $x = 0.3$ . It has been demonstrated that such waveguides can be fabricated by either the limited melt or the infinite melt method of liquid epitaxy. The former has the advantage of a small volume easily changed melt, whereas the latter can be used to produce large area wafers for complex optical integrated circuits. We have made waveguiding layers with area  $> 4 \text{ cm}^2$  using the infinite melt method. We have also shown that it is feasible to make monolithic device elements that are compatible with (GaAl)As waveguides. Integral waveguide detectors were fabricated in part of the (GaAl)As waveguides grown in this program, using the proton bombardment technique we had previously applied to GaAs. These results have established a basis for further research and development work, particularly in the area of fabricating compatible monolithic combinations of waveguides and other device elements, leading to fabrication of an optical integrated circuit. All of the waveguides considered under this contract have been of the planar or slab type. We feel that the next step in extending this work to produce practical waveguides for optical integrated circuits is to investigate channel waveguides in which the light is confined laterally as well as in depth. Such waveguides have been produced by ion milling<sup>13</sup> or by proton bombardment<sup>16</sup> of planar waveguiding layers like those we have grown but no comprehensive study of their characteristics has yet been made, even though it is generally recognized that channel guides will be used to interconnect the elements of an optical integrated

circuit analogous to wires in an electrical integrated circuit. Other device studies performed under this contract should also be continued and extended. Theoretical estimates of the performance characteristics of "leaky" waveguides and corrugated gratings should now be verified by fabricating the devices and experimentally evaluating them. The proton bombarded waveguide/detector should be fully characterized and evaluated since preliminary results indicate that the proton bombardment method is a convenient means of producing compatible monolithic waveguide/detector combinations. Along with the work on integral waveguide detectors it is also required that integral emitter/waveguide combinations be fabricated. The most likely candidate to perform this function is a GaAs edge emitting diode coupled monolithically to a (GaAl)As waveguide. The basic techniques for producing such a combination are presently known, but it remains to actually fabricate, evaluate, and optimize the device.

In the preceding paragraphs of this section we have stated our basic conclusions and recommendations. More specific technical conclusions that can be drawn from the results of this program are as follows. The growth of GaAs waveguides on (GaAl)As substrates by vapor phase epitaxy is greatly limited by the high reactivity of aluminum, and by the relatively high absorption of the GaAs layer for wavelengths shorter than  $1.1 \mu\text{m}$ . The level of absorption that is tolerable, of course, depends on the particular application, but absorption loss is greater than 3 dB/cm for wavelengths shorter than  $1.1 \mu\text{m}$  in GaAs (see Fig. II-6). However, the liquid epitaxial growth of  $\text{Ga}_{(1-x)}\text{Al}_x\text{As}$  waveguiding layers on GaAs substrates is a practical means of producing waveguides for use in optical integrated circuits at wavelengths in the range  $1.15 \mu\text{m}$  to  $0.85 \mu\text{m}$ . We have grown  $\text{Ga}_{(1-x)}\text{Al}_x\text{As}$  layers by both limited melt and infinite melt epitaxy and demonstrated that both methods are capable of producing layers adequate for integrated optics applications. However, each of the two methods has particular advantages in different applications. The limited melt method is convenient and economical for feasibility studies since it uses small melts that can be discarded after each growth, permitting frequent changes in melt composition. It also is convenient for the growth of multilayer structures since a slide bar with a number of wells can be used. However the large surface-to-volume ratio of the melt limits the purity of the layer to a minimum background impurity

concentration  $\approx 10^{16}/\text{cm}^3$  under practically obtainable growth conditions. Also the melt never is totally homogeneous since there is no way to stir it, and the aluminum tends to segregate into the grown layer depleting the melt immediately above it. Because of this inhomogeneity of the melt the optimum growth procedure must be empirically established for a specific system and a specific goal for reproducibility. The infinite melt system is not subject to these problems of inhomogeneity because the growth matrix can be maintained uniform with predictable properties. Thus large area wafers ( $\sim 4 \text{ cm}^2$ ) with controlled uniform characteristics can be grown conveniently. The main disadvantage of the infinite melt method is the inconvenience and expense of changing the melt composition if one desires to grow a different type of layer, or a multilayer structure. For a flexible approach to optical integrated circuit fabrication the ability to use both the limited melt and the infinite melt growth techniques in a complementary fashion is highly desirable.

One of the more significant results of this program was the demonstration of low loss waveguides in (GaAl)As with as much as 30% aluminum. The discovery that low loss waveguides could be made by growing a single epitaxial layer with a graded aluminum concentration profile also was significant. The determination of losses, measured to be as low as 0.7 dB/cm at 1.15  $\mu\text{m}$  and projected to be 2.2 dB/cm at 0.85  $\mu\text{m}$ , indicates that single layer (GaAl)As waveguides on GaAs substrates can be used for optical integrated circuits on wafers sized  $\sim 1 \text{ cm}$ . There is nothing to suggest that such low losses cannot also be obtained in double layer (GaAl)As waveguides. In either case, an important factor determining the loss when light is guided in the top-most layer of a structure is the surface quality of the air - (GaAl)As interface. This surface should be smooth and free from overgrowth regions to minimize loss. Alternatively, a capping layer of (GaAl)As can be added which has a higher aluminum concentration than that in the waveguiding layer in order to confine the guided waves. Single layer (GaAl)As waveguides with graded aluminum concentration offer convenience of fabrication as compared with conventional double layer guides and should be useful in many optical integrated circuits. However,

they lack the flexibility of double layer guides for use in more complex circuits since one does not have independent control of aluminum concentration and thickness.

In addition to the waveguides which were grown and evaluated in this program we also considered a number of compatible device elements. Theoretical analyses were made of "leaky" waveguides and of periodic waveguide structures for filters or DFB lasers. The results of these analyses indicated that useful integrated optics devices can be fabricated using leaky waveguides provided the guide height is  $\geq 10 \mu\text{m}$  for a  $\lambda \approx 0.8 \mu\text{m}$ . Another conclusion was that there is a frequency range for corrugated dielectric waveguides within which there is strong coupling between the forward and backward traveling waves. Corrugated waveguides can be used as reflectors for filters or DFB lasers near the resonance point for which  $\beta\Lambda = \pi$ , where  $\beta$  is the propagation constant and  $\Lambda$  is the period of the corrugations. In the final months of this program we fabricated and evaluated monolithic waveguide/detectors formed by proton bombardment of (GaAl)As waveguides, demonstrating that the technique is applicable to (GaAl)As as well as GaAs. Calculations predict that quantum efficiency of at least 60% should be obtainable at a wavelength  $\approx 0.9 \mu\text{m}$ .

In conclusion, the results of this program have demonstrated that (GaAl)As waveguides can be grown with the characteristics required for optical integrated circuit fabrication. However much work remains to be done, particularly in the area of fabricating compatible monolithic combinations of waveguides and other device elements.

## REFERENCES

1. J. T. Boyd, IEEE J. Quantum Electron. QE-8, 788 (1972).
2. J. Shah, B. Miller, and A. DiGiovanni, J. Appl. Phys. 43, 3436 (1972).
3. M. D. Sturge, Phys. Rev. 127, 768 (1962).
4. W. Spitzer and J. Whelan, Phys. Rev. 114, 59 (1959).
5. R. N. Hall, J. of the Electrochemical Soc., 385-388, May 1965.
6. J. M. Blum and K. K. Shin, Proc. IEEE 59, 1498, (1971).
7. J. T. Houghton and S. D. Smith, Infra-Red Physics (Oxford University Press, 1966), p. 143, eq. 4-26.
8. W. P. Dumke, Phys. Rev. 127, 1559 (1962).
9. H. J. Stein, Proc. International Conference on Ion Implantation in Semiconductors and Other Materials, Dec. 11-14, 1972, Yorktown Heights, N.Y. (Plenum Press, N.Y., 1973).
10. J. L. McNichols and W. S. Ginell, J. Appl. Phys. 38, 656 (1967).
11. K. Sakuda and A. Yariv, Opt. Commun. 8, 1 (1973).
12. H. Stoll and A. Yariv, Opt. Commun. 8, 5 (1973).
13. H. L. Garvin, E. Garmire, S. Somekh, H. Stoll, and A. Yariv, Appl. Opt. 12, 455 (1973).
14. H. Yen, M. Nakamura, E. Garmire, S. Somekh, A. Yariv, and H. L. Garvin, Opt. Commun. 9, 35 (1973).
15. A. Yariv, IEEE J. Quantum Electron., to be published.
16. S. Somekh, E. Garmire, A. Yariv, H. L. Garvin, and R. G. Hunsperger, Appl. Opt. 13, 327 (1974).

## APPENDIX A

### CALCULATION OF FREE CARRIER ABSORPTION

The equation of motion of an impurity electron can be written as

$$-\omega^2 m^* x + \frac{i\omega m^* x}{\tau} = -e E e^{i\omega t}$$

where

$m^*$  = effective mass

$\tau$  = scattering time

$E$  = electric field amplitude

From the solution of this equation we obtain

$$x = \frac{-eE/m^*}{-\omega^2 + i\omega/\tau}$$

$$D \equiv \epsilon_{\text{total}} E = \epsilon E + P_{\text{electr}} = \epsilon E + Nex$$

$$\epsilon_{\text{total}} = D/E = \epsilon - \frac{Ne^2/m^*}{\omega^2 + 1/\tau^2} - i \frac{\frac{Ne^2\omega}{m^*\tau}}{\omega^4 + \omega^2/\tau^2}$$

$$\epsilon_{\text{total}} = \epsilon_0 \left( K_r^P - \frac{Ne^2/m^* \epsilon_0}{\omega^2 + 1/\tau^2} - i \frac{Ne^2/(m^* \epsilon_0 \omega \tau)}{\omega^2 + 1/\tau^2} \right)$$

where,  $K_r^P$  is the real part of the relative dielectric constant for the material with no impurities. Therefore,

$$\text{Im}K = - \frac{Ne^2/(m^* \epsilon_0 \omega \tau)}{\omega^2 + 1/\tau^2}$$

For a wave propagating as  $\exp(i\omega t - ikz)$ , we have

$$k = \omega \sqrt{\mu_0 \epsilon_{\text{total}}}$$

$$\omega \sqrt{\mu_0 \epsilon} \left( 1 - \frac{Ne^2}{2m^* \epsilon \omega^2} - i \frac{Ne^2}{2m^* \epsilon \omega^3 \tau} \right) \quad A-1$$

where we assumed  $\omega^2 \gg 1/\tau^2$ . The power absorption coefficient, therefore is given by

$$\alpha = 2 (\text{Im}K) = \frac{k_o K_i}{\sqrt{K_r}} = \sqrt{\frac{\mu_0}{\epsilon}} \frac{Ne^2}{m^* \omega^2 \tau}.$$

## APPENDIX B

### Proton-implanted optical waveguide detectors in GaAs

H. Stoll and A. Yariv

California Institute of Technology, Pasadena, California 91109

R. G. Hunsperger and G. L. Tangonan

Hughes Research Laboratories, Malibu, California 90265

(Received 17 August 1973)

Defect levels introduced by implanting GaAs with high-energy protons give rise to optical absorption at wavelengths greater than that of the normal absorption edge at  $0.9 \mu$ . Optical waveguide detectors may be fabricated by taking advantage of this absorption mechanism in the presence of a Schottky barrier depletion layer. Detector response times less than 200 ns and external quantum efficiencies of 16% have been observed.

In a continuing program to build circuit components for integrated optics we have investigated the possibility of fabricating optical detectors by proton implantation of GaAs dielectric waveguides. The basic principle is as follows: A small volume of an epitaxial GaAs waveguide, such as the one shown in Fig. 1, is implanted with protons. Structural disorder created by the implantation process causes the previously low-loss waveguide to become highly lossy for radiation around  $1 \mu$ . One of the mechanisms responsible for this absorption is the liberation of free carriers which had become trapped at defect centers. A photodetector results when these carriers are swept through the depletion layer generated by a reverse-biased Schottky barrier which has been deposited over the implanted region as shown in Fig. 1. We report below the fabrication of integrated optical detectors based on this principle. The detectors have been found to be sensitive to light of wavelengths  $> 0.9 \mu$ , a wavelength which can be transmitted nearly unattenuated by the GaAs guides used. The optical waveguide structure consisted of a  $3.5\text{-}\mu\text{m}$ -thick  $n$ -type (S-doped,  $n \approx 10^{18}/\text{cm}^3$ ) epitaxial film grown on a degenerate  $n$ -type substrate ( $n \approx 1.25 \times 10^{19}/\text{cm}^3$ ). The guide-substrate refractive index discontinuity generated by the plasma depression effect allowed good optical confinement for the particular guide thickness used; prior to proton implantation optical attenuation at  $1.15 \mu$  was measured to be  $1.3 \text{ cm}^{-1}$  and could be accounted for by consideration of free carrier substrate penetration losses.

As shown in Fig. 1, a small volume of the waveguide

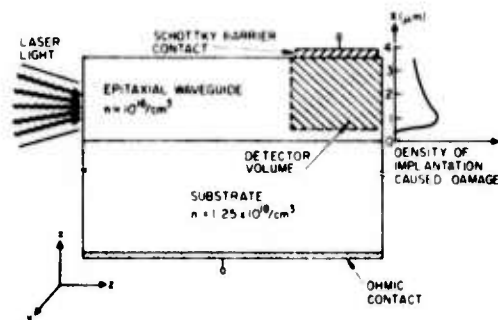


FIG. 1. Diagram of proton-implanted optical waveguide detector.

structure was proton bombarded to form the waveguide detector; 300-keV protons were used, the total integrated flux of which was  $2 \times 10^{15}/\text{cm}^2$ . The damage layer which resulted was approximately  $3 \mu\text{m}$  thick with a damage peak occurring about  $2.5 \mu\text{m}$  below the surface.

The implanted waveguide was then annealed at  $500^\circ\text{C}$  for 30 min in order to allow some optical transmission through the damaged region; residual losses in this region were measured to be  $\approx 15 \text{ cm}^{-1}$  based on a comparison of the optical attenuation before and after implantation and annealing. Finally, 11-mil-square Al Schottky barriers were evaporated in a waffle pattern over the implanted area.

The principle of the operation of this device is similar to that of conventional  $p$ - $n$  or  $p$ - $i$ - $n$  junction photodetectors.

Upon the application of a reverse bias to the Schottky barrier, a depletion layer is produced which, given sufficient reverse bias, extends across the high-resistivity waveguiding layer to the lower-resistivity substrate. Any dipole transitions made possible by radiation

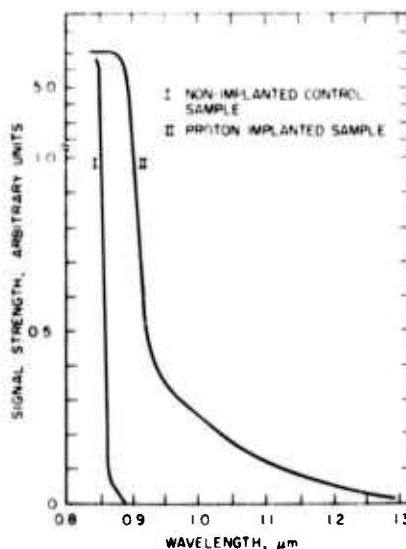


FIG. 2. Photoresponse of optical waveguide detector as a function of wavelength.

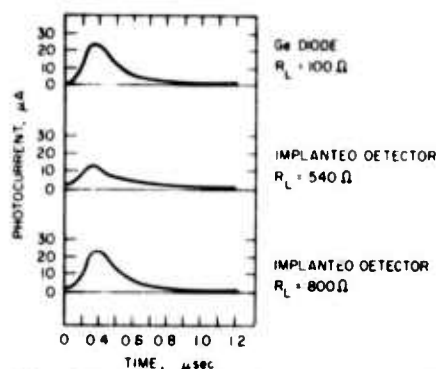


FIG. 3. Response of waveguide detector to pulsed optical signal.

tion-produced defect levels generate free carriers which are swept out of the depletion layer, thereby causing current to flow through an external circuit. By ensuring that the radiation-induced damage extends over most of the waveguiding layer and choosing epitaxial material of high purity, maximum efficiency can be obtained over a given interaction length.

Measurements of the photosensitivity of both unimplanted and implanted annealed samples are shown in Fig. 2. Transparent Au barriers, sputter deposited on the surface, were used to measure sensitivity as a function of wavelength. A monochromator-filtered incandescent light source was focused through the transparent Au layer into the active volume of the detectors. The curve for the irradiated sample reveals a defect-associated energy level distribution within the band gap, as well as a shift of the effective absorption edge to lower energies. Calorimetric measurements<sup>2</sup> made on proton-irradiated GaAs at 1.06  $\mu\text{m}$  indicate that substantially all of the implantation-induced optical attenuation in the 1- $\mu\text{m}$ -wavelength region can be attributed to absorption as opposed to diffuse scattering. The origin of this absorption is thought to be disorder-induced band tailing. The possibility that it is due, at least in part, to the excitation of electrons from energy levels associated with As (or Ga) vacancy complexes is strong, particularly in view of the fact that free carrier compensation by proton implantation appears to be Fermi-level dependent.<sup>3,4</sup>

An attempt was made to measure detector rise and fall times at 1.06  $\mu\text{m}$  using an acoustically Q-switched Nd:YAG laser focused into a cleaved face of the waveguide structure of Fig. 1. The pulse response of the implanted detector is compared to that of a commercial Ge (Philco L4521) detector in Fig. 3. In both cases the

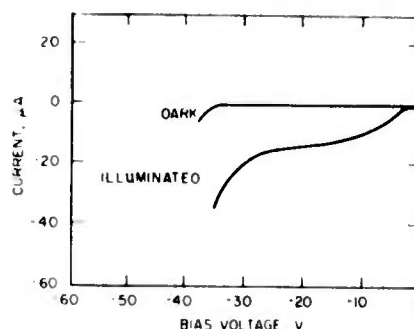


FIG. 4. Reverse bias current-voltage characteristics of waveguide detector.

rise and fall times appeared to be  $\sim 200$  and  $\sim 400$  ns, respectively. Reducing the size of the load resistors used merely decreased the signal strength; the pulse shapes remained the same. Since the Ge detector response is in the GHz range, it was concluded that the rise and fall times measured were a function of the Q-switched laser and did not represent limits of the implanted detector.

Figure 4 shows  $I$ - $V$  curves for a reverse-biased implanted detector under dark and 1.15- $\mu\text{m}$  illumination conditions. The measured external quantum efficiency at 1.15  $\mu\text{m}$ , 294°K, and a reverse bias of 20 V was about 16%. This number should increase as optimal proton damage profile and heat treatment conditions are approached for a given waveguiding configuration.

In conclusion we have demonstrated a simple technique for fabricating integrated optical detectors sensitive at wavelengths  $> 0.9 \mu\text{m}$  using proton implantation. Device performance is promising and should improve as implantation and heat treatment procedures are refined.

The authors would like to thank Dr. W. C. Holton of Texas Instruments for providing the epitaxial GaAs material.

<sup>1</sup>D. Hall, A. Yariv, and E. Garmire, *Appl. Phys. Lett.* 17, 127 (1970).

<sup>2</sup>H. J. Stein, *Proceedings of the International Conference on Ion Implantation in Semiconductors and Other Materials*, Yorktown Heights, 1972 (Plenum, New York, 1973).

<sup>3</sup>H. Sioli, E. Garmire, A. Yariv, and R. G. Hunsperger (unpublished).

<sup>4</sup>K. Wohlenben and W. Beck, *Z. Naturforsch.* 219, 1057 (1966).